Theory article

Shifting epigenetic contexts influence regulatory variation and disease risk

Daniel Richard[1], Terence D. Capellini[1,2]

[1]Department of Human Evolutionary Biology, Harvard University, Cambridge, MA 02138, USA
[2]Broad Institute of MIT and Harvard, Cambridge, MA 02142, USA

Correspondence to: Terence D. Capellini; **email:** tcapellini@fas.harvard.edu
Keywords: development, aging, evolution, GWAS, disease
Received: April 8, 2021 **Accepted:** June 1, 2021 **Published:** June 16, 2021

ABSTRACT

Epigenetic shifts are a hallmark of aging that impact transcriptional networks at regulatory level. These shifts may modify the effects of genetic regulatory variants during aging and contribute to disease pathomechanism. However, these shifts occur on the backdrop of epigenetic changes experienced throughout an individual's development into adulthood; thus, the phenotypic, and ultimately fitness, effects of regulatory variants subject to developmental- versus aging-related epigenetic shifts may differ considerably. Natural selection therefore may act differently on variants depending on their changing epigenetic context, which we propose as a novel lens through which to consider regulatory sequence evolution and phenotypic effects. Here, we define genomic regions subjected to altered chromatin accessibility as tissues transition from their fetal to adult forms, and subsequently from early to late adulthood. Based on these epigenomic datasets, we examine patterns of evolutionary constraint and potential functional impacts of sequence variation (e.g., genetic disease risk associations). We find that while the signals observed with developmental epigenetic changes are consistent with stronger fitness consequences (i.e., negative selection pressures), they tend to have weaker effects on genetic risk associations for aging-related diseases. Conversely, we see stronger effects of variants with increased local accessibility in adult tissues, strongest in young adult when compared to old. We propose a model for how epigenetic status of a region may influence the effects of evolutionary relevant sequence variation, and suggest that such a perspective on gene regulatory networks may elucidate our understanding of aging biology.

INTRODUCTION

It has been suggested that the process of aging, and the concomitant manifestation of aging-related disease, is subject to both genetic and non-genetic factors impacting the regulatory networks (and subsequent behaviors) of aging cells [1, 2]. Nongenetic regulation of aging refers to epigenetics; chemical changes to the genome (e.g., at the chromatin level) that impact transcriptional programs [1], and which have been shown to accumulate with age [3–5]. The epigenetic state of chromatin can be broadly classified into activating or repressing modifications [6], referring, in part, to the increased/decreased accessibility of DNA to gene-regulatory machinery (e.g., transcription factors), and is established, maintained, and reset to switch between states [6]. Ample evidence suggests a causal relationship between changes in epigenetic state with age and hallmarks of aging in cells [3, 5]. Much recent work has focused on elucidating this relationship and how, ultimately, this contributes to age-related tissue decline and adult diseases [7].

As aging can also be considered a continuation of development [8], the epigenetic changes that are retained from early-life development may have important

consequences for the adult epigenome – establishing the context within which epigenetic aging occurs [9]. A 'fetal programming' model has been suggested whereby early epigenetic plasticity in response to environmental and nutritional stimuli, while being adaptive and beneficial to fetal and early post-natal growth, has deleterious consequences later in life by contributing to adult disease risk [9–12]. This serves as one possible mechanism for the theorized consequences of selection favoring early-life development at the cost of late-life function [9, 13, 14]. Evidence supporting this model has been largely limited to DNA methylation [9, 15–17], though replication of important loci findings has been difficult [18].

Epigenetic marks established during development can persist into adulthood [9], but they do so in the context of shifts in epigenetic states (see below) as tissues transition into their adult forms and functions. This transition process has been characterized with respect to DNA methylation, chromatin state, and gene expression across multiple tissues [19–21]. Furthermore, these fetal to adult epigenetic shifts can be compounded by additional modifications through aging-associated epigenetic changes. Such epigenetically-regulated biological pathways involved in development, such as Wnt signalling, subsequently take on a role in tissue homeostasis in adults and are implicated in age-related tissue decline [22, 23] – suggesting a molecular link between processes mediating growth and aging [8, 24]. Thus, an important component of understanding the contributions of fetal programming as well as epigenetic aging to disease biology and risk is characterizing the epigenetic changes between fetal and adult tissues and how these might interact with subsequent aging-associated modifications.

While epigenomes vary between cell types [25, 26] and changes to epigenetic state with age may be expected to manifest differently, similar aging epigenetic have been repeatedly observed across tissues epigenetic shifts have been repeatedly observed across tissues [1, 5, 20, 27, 28]. Similarly, while age-related expression changes do exhibit tissue-specificity, there is evidence of potential synchronized changes across different sets of tissues [29], particularly for certain sets of genes and pathways [29, 30], and these changes may integrate at multiple different epigenetic levels [31]. Together, these findings suggest that a central trajectory for epigenetic state that reflects innate aging processes may exist [20], upon which extrinsic and cell-type effects are layered. Similarly, studies between fetal and adult tissues have found that, while epigenetic change is observed within individual tissues, there are also common trends of development (e.g., chromatin restriction, particularly at loci involved in early development) [21, 32, 33].

Importantly, the epigenetic state of genetic variants (e.g., single nucleotide polymorphisms) influences their regulatory effects, and subsequent association with heritable disease risk [34]. Thus, general epigenetic trends across early development and later aging may influence the phenotypic effects of regulatory mutations, albeit the extent to which this occurs is unknown. These phenotypes, if impacting an individual's fitness, may be acted upon by natural selection. Evolutionary theories have been proposed which suggest that mutations contributing to aging pathologies are 'allowed' to accumulate due to the reduced fitness consequences of disease in older, post-reproductive individuals [35], or that beneficial mutations selected for early development become deleterious with age [36–38]. Studying the added dimension of epigenetic context may provide a fresh perspective on theories of aging and selection. For example, deleterious mutations that change epigenetic context later in life may have different regulatory effects, and thus different fitness consequences, which alter the selective pressures acting on them.

In the present study, we seek to characterize common epigenetic trends between fetal and adult tissues, and subsequently examine the potential interaction of these developmental changes with later changes associated with epigenetic aging in adult tissues. We utilize our findings to propose a model for how evolutionary forces may have acted at these loci in humans, and how these forces in turn influence the distribution of mutations conferring heritable disease risk across a number of age-associated pathologies.

RESULTS

Defining chromatin accessibility change, its genomic context, and loci subject to change

To investigate epigenetic changes occurring over the course of post-natal development and aging, we focused on chromatin accessibility, as it reflects the regulatory potential of a genetic locus and can be considered a property of the epigenome which integrates a number of possible epigenetic phenomena (e.g., regulatory factor binding, chromatin remodelling, etc.) [39]. We thus consider regions with altered chromatin accessibility as being indicative of epigenetic modifications or 'shifts' in context. As a read-out of accessibility we analyzed DNase-I hypersensitivity datasets acquired from primary human tissue, and obtained fetal/adult sample pairs for eight distinct primary tissues (spleen, lung, muscle, stomach, kidney, brain, heart, and skin; see Supplementary Table 1) [6, 40]. For each tissue at each time-point, called accessible or "open" chromatin regions were consolidated across biological replicates,

then further aggregated by tissue and stage (see Supplementary Methods).

We first identified chromatin regions exhibiting recurrent accessibility changes between fetal and adult samples across tissue types (see Supplementary Methods, Figure 1A, 1B and Supplementary Figures 1, 2). We define regions as 'adult-biased' if they exhibit increased differential accessibility in adults compared to in fetuses. Conversely, we define regions as 'fetal-biased' if they exhibited decreased differential accessibility in adults compared to in fetuses. These 'pan-tissue' altered regions were compared to those defined in individual tissue comparisons, showing substantial but not complete overlap (Figure 1C) – suggesting that our approach captures cross-tissue signals of broader developmental changes and not tissue-specific effects. We next explored possible signals of epigenetic aging occurring in the context of fetal to adult changes, by further dividing our adult tissue samples into 'younger' and 'older' age categories (Methods, Supplementary Figure 3). We then assessed accessibility change between young and old occurring within the 'adult-biased' and 'fetal-biased' regions defined above (Figure 1D). This approach identified regions for which young-old differences mirrored fetal-adult differences, as well as regions where aging changes appear to counter developmental patterns. We observed a tendency for shared directionality in gains or losses of accessibility; i.e., adult-biased regions tended to also have increased accessibility in older adult samples, while regions losing accessibility in adult samples (i.e., are fetal-biased) continued this trend in older samples (chi-sq

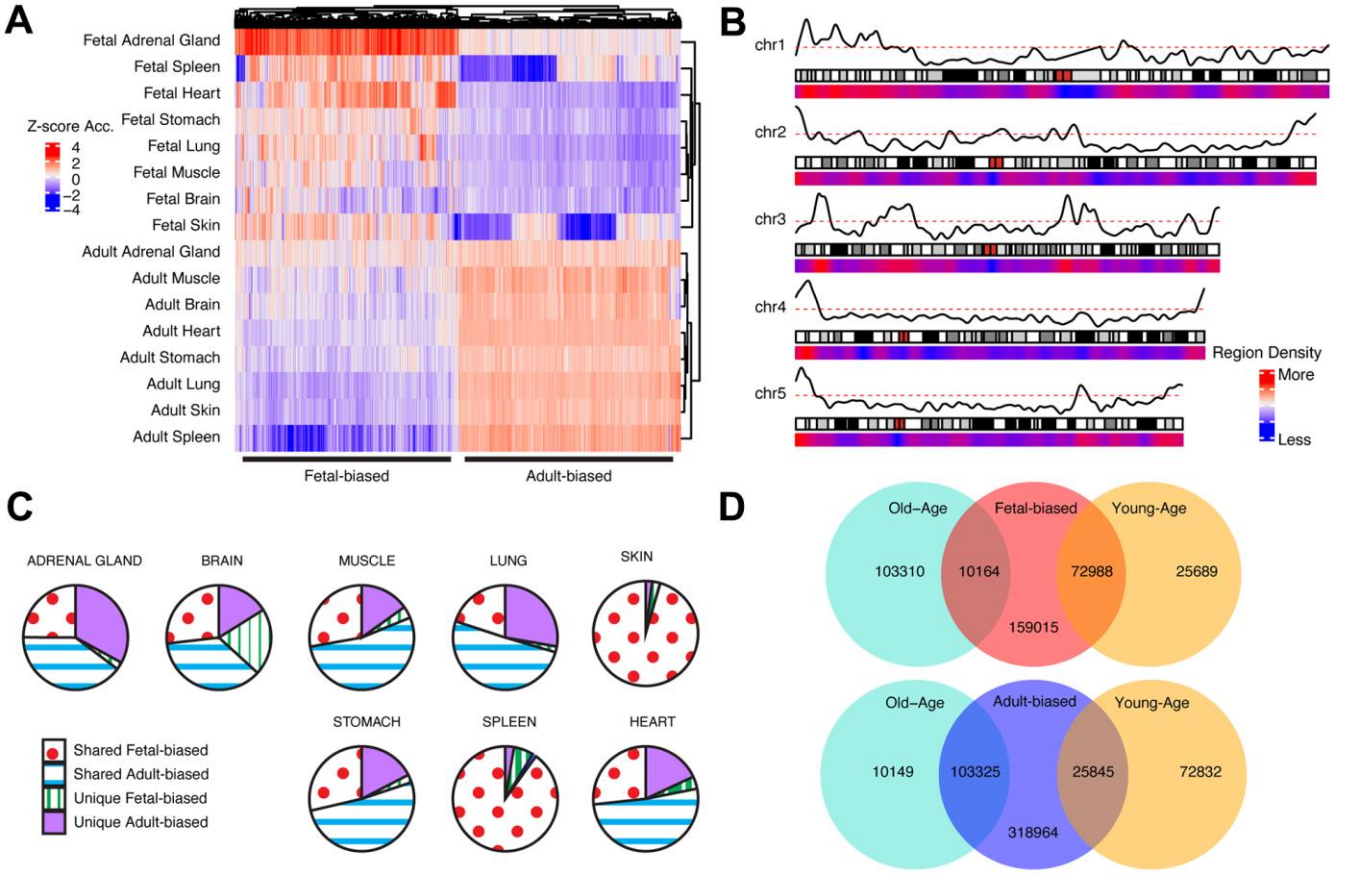

Figure 1. Cross-tissue accessibility. (**A**) Representative heatmap of Dnase-I accessibility for regions significantly different between fetal/adult tissues. Color scale indicates magnitude of chromatin accessibility signal (see Supplementary Methods). Horizontal lines denote defined fetal-biased (left) and adult-biased regions. (**B**) Genomic distribution of regions changing accessibility in fetal and adult comparison. Red/blue: density of defined differentially-accessible regions. Solid black line: relative proportion of regions more accessible in adult (top) or fetal (bottom) tissues. First five autosomes shown (see Supplementary Figure 2). (**C**) The proportion of defined altered-accessibility regions between adult and fetal samples for indicated tissues which are unique to that tissue, or captured in the pan-tissue set. (**D**) Overlaps between regions defined as differentially-accessible in fetal/adult comparison and those defined in the young/old-age comparison. Directionality in accessibility change is significantly shared (see Supplementary Table 1). Related content can be found in Supplementary Information, Supplementary Figures 1–6 and Supplementary Tables 1, 2.

test, $p < 0.05$, Supplementary Table 1). In this text, we therefore refer to regions with greater accessibility in older samples as 'old-biased' and regions with lower accessibility in older samples as 'young-biased'. As described in the Supplementary Information, we considered histone mark and DNA methylation changes, key features of developmental [21, 26, 33] and aging epigenetic changes [3, 20] as additional means to validate the behavior of these region sets (see also Supplementary Table 1).

To gain insights into the roles these region sets have in transcriptional regulation, we next characterized the genomic distribution of our adult-biased and fetal-biased region sets using adult tissue epigenetic states [26] (Supplementary Methods). We found that our region sets preferentially fell within different epigenetic states (e.g., enhancers, heterochromatin) depending on the nature of their accessibility shift (e.g., adult-biased, old-biased), suggesting that these shifts may be associated with altered regulatory biology at different loci, and that the interaction between fetal and adult shifts as well as young and old-age shifts heavily favors developmental changes to accessibility (see Supplementary Figures 4, 5, Supplementary Information).

As accessible chromatin regions often serve to regulate gene expression [39] by acting as *cis*-regulatory sequences, we next sought to identify the potential role of our regions in regulatory changes occurring during development and aging. We did this by considering promoter-level accessibility (see Methods, Supplementary Figure 6), promoter-capture (Hi-C) interactions [41], and regulatory-domain annotations [42] for genes which may be subject to control by these regulatory regions. We found a general pattern for enrichment of immune-related gene sets with the adult-biased set, while development-related (e.g., cellular proliferation) terms were enriched with fetal-biased regions, patterns echoed when considering old-biased and young-biased region sets, respectively (see Supplementary Information, Supplementary Table 2).

We next incorporated tissue expression datasets looking for general gene expression trends between fetal and adult tissues (see Methods). We observe similar enrichment terms as well as significant overlaps with gene sets defined on the regulatory level (see Supplementary Information, Supplementary Table 2). Similarly, we utilized GTEx (gene tissue expression) datasets [43] to look for corresponding shifts in gene expression with age, similar to previous work [44] (see Methods)(Supplementary Table 2). While we did not observe significant overlaps between these aging-expression gene sets and those defined using aging-accessibility changes, we did see significant overlaps with the fetal/adult expression comparisons, along with enriched gene sets with relevance to aging biology (see Supplementary Information, Supplementary Table 2).

As development and aging are phenomena subjected to the actions of random and directed evolutionary forces [13, 45, 46], we next develop expectations for how these epigenetically-altered regions may have evolved over time.

Sequence evolution of epigenetically-altered regions

Development and aging are simultaneously very ancient and variable [45, 47] biological processes and are particularly divergent in key species [48]. Thus, it may be the case that both development and age-associated regions have been shaped by a mix of evolutionary forces acting to either maintain or modify genetic sequences (e.g., regulatory enhancers). To address this possibility, we examined patterns of sequence conservation in our epigenetic datasets using phyloP [49], a measure of nucleotide conservation and/or acceleration across species (Figure 2A). Across primates, we observed that fetal-biased regions tended to have greater sequence conservation than adult-biased regions, and furthermore that both sets differed significantly from those regions not defined as developmentally-altered (Supplementary Table 3). These patterns were similarly observed when comparing age-associated regions (Supplementary Table 3). These findings of conservation differences between sets suggests that the greater regulatory and developmental role associated with fetal-biased and young-biased regions (e.g., enriched for enhancer elements) exerts functional sequence constraint while adult-biased and old-biased regions (e.g., enriched for repressed segments) are less conserved across species.

Within this broader context of species diversity and evolution, humans and chimpanzees display marked and obvious differences in development and longevity [45, 50]. This relatively recent divergence is thought to be driven largely by non-coding changes to cis-regulation [51]. We therefore next looked for evidence of regulatory modifications to biological processes that may contribute to these human/chimp differences. To do this, we intersected our regions sets with sequences demonstrating significant divergence along the human lineage (e.g., 'human accelerated regions' [52]). We found that fetal-biased regions were enriched for signals of acceleration while adult-biased regions were depleted (Figure 2B). Similar patterns were seen for young versus old-biased regions (Figure 2B and Supplementary Table 3). We found a number of genes involved in development and aging processes with putative nearby regulatory elements intersecting accelerated regions, two examples of which are shown

in Supplementary Figure 7 (see also Supplementary Information).

To gauge the evolutionary interaction between sequence constraint across species and within-species variation, we next assessed modern-day human diversity within region sets (Methods). We found that genetic diversity in fetal-biased regions was markedly reduced (i.e., constrained) compared to genomic backgrounds, as well as to intronic and promoter-TSS elements (Figure 2C and Supplementary Table 3). Conversely, adult-biased regions were enriched for sequence diversity, at the level of annotated repeat elements. These patterns were accentuated when examining young- and old-biased region datasets, and comparing region sets directly (Supplementary Table 3, Supplementary Information). Importantly, when we considered sequence diversity within other ape species, we also observed a decrease in fetal-biased, and young-biased sequence diversity (relative to adult-biased and old-biased, respectively). This latter finding further suggests that fetal-biased regions are associated with conserved regulatory

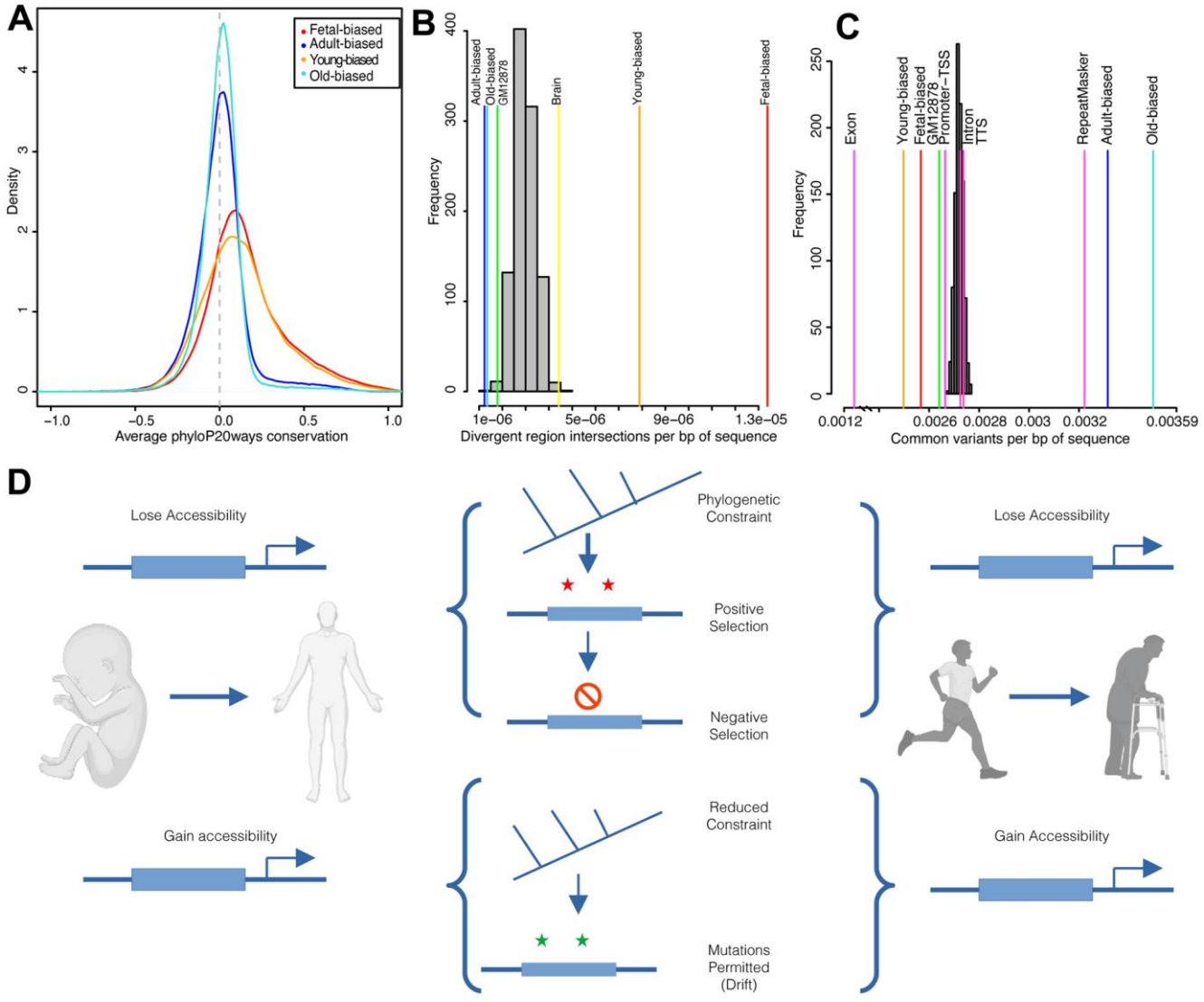

Figure 2. Sequence evolution of age-altered regions. (**A**) Distribution of average per-region sequence conservation (phyloP20ways) in differentially-accessible regions (see color legend). (**B**) Overlaps of developmental and age-related region sets and human acceleration regions. Overlaps shown relative to set size (per bp of sequence) for background (gray) and target (colored) sets; labels correspond to Supplementary Table 3. (**C**) Intersections of common human variants (per bp of sequence) for target (colored) and randomized (grey) region sets; labels correspond to results in Supplementary Table 3. (**D**) Diagram summarizing results of evolutionary sequence analyses. Accessible regions, here diagrammed as an upstream enhancer element (thick blue box), which either gain or lose accessibility over development (left) or ageing (right) exhibit different patterns of evolutionary sequence behavior. Created with BioRender.com. See also Supplementary Figures 7, 8.

function that discourages mutation and/or drift (Supplementary Figure 8 and Supplementary Table 3).

Overall, natural selection appears to have acted upon regions subject to accessibility shifts in development and aging, modifying some loci (i.e., accelerated divergence indicative of ancient positive selection) while protecting others (i.e., reduced variation indicative of more recent negative selection) (Figure 2D).

Importantly, selective forces, both positive and negative, manifest phenotypically through the effects of random genetic mutations, which act to modify gene regulatory networks to varying degrees. We next examine this relationship.

Epigenetic shifts in age-associated trait associations

In our above analyses, the observed signals of consistent inter- and intra-species conservation in regions most associated with early development (i.e., the fetal-biased set) follows with the expectation that variants negatively impacting early-life would be subject to stronger purifying selection [9, 53, 54]. Conversely, variants with later-manifesting effects, i.e., those within regions increasing in local accessibility with age (i.e., the adult-biased set), would be subjected to substantially weaker selection and may therefore be 'tolerated' [55, 56]. To test expectations of the possible deleterious effects of variants subject to accessibility change over development and aging, we utilized GWAS datasets available from the UK Biobank [57]. We extracted summary-statistics for a collection of 127 complex diseases/pathologies falling into aging-related categories [58], including metabolic disorders, cancers, cardiovascular disease, and musculoskeletal impairment (Supplementary Table 4, Methods). We similarly analyzed a set of developmental trait GWAS to act as a control for our fetal/adult accessibility comparisons, and finally considered longevity GWAS data (Supplementary Table 4, see Supplementary Information).

It has been suggested that the highly polygenic nature of complex traits and diseases reflects cumulative regulatory modification to a 'core' set of genes which functions most proximately in relevant biology [59]. Across age-associated diseases, this may reflect general aging processes, and regulatory variants impacting these would be expected to contribute to heritable aging-disease risk broadly. Given this rationale, we first considered the behavior of individual SNPs nearby accessibility-altered regions across diseases, and subsequently these behaviors at the gene-locus level (below). We aggregated per-SNP associations across diseases as a singular cross-set metric of risk association (Supplementary Methods). We confirmed that ClinVar variants, variants for which possible clinical significance have been described [60], tended to be more risk-associated by this metric, as we would expect (Supplementary Table 4). Additionally, across all diseases we individually performed enrichment tests for strongly-associated variants nearby our region sets, which corroborated the cross-disease results described below (Figure 3A, see Supplementary Information).

As variants in accessible non-coding regions likely have regulatory impacts generally [39], we confirmed that variants within or nearby regions not classified as strictly developmental nor age-altered tended to have greater association than non-accessible variants. However, this control set had significantly less association than variants nearby sets of both developmentally- and age-altered regions (i.e., fetal/adult-biased, and young/old-biased regions) (Supplementary Table 4).

Considering first developmental change, we found that variants in regions gaining nearby accessibility in adults (i.e., adult-biased) have greater association with disease than those in regions losing nearby accessibility (i.e., fetal-biased) (Figure 3B). Unexpectedly, when looking at aging accessibility changes, we observed that variants in regions gaining nearby accessibility in older-samples actually have lower cross-disease associations than those in regions becoming more accessible in younger samples (Figure 3B and Supplementary Table 4). Furthermore, we found that for intersections of development and age-altered regions that the increased disease association with adult-biased regions was abrogated when intersected with old-biased regions. The magnitude of region-set differences in disease associations was also greater in the young/old-biased comparisons (see Figure 3B, Supplementary Information).

Taken together, these results would suggest that those variants most accessible in younger adults stand to have the greatest impact (in terms of association p-value) on late-life disease risk – a finding that may have important implications for understanding the development of disease over adulthood (see Figure 3C, Discussion).

We next considered these disease-association patterns at the gene-locus level. Briefly, for a given disease we assign the most significant nearby SNP to all genes, and subsequently rank genes based on their assigned GWAS signal. Gene ranks are then aggregated across diseases, looking for genes consistently ranked higher across sets (Supplementary Methods). To confirm the behavior of this gene-ranking method, we compared the cross-set ranking of genes associated with homeostatic processes (based on GO annotations) to randomized gene sets,

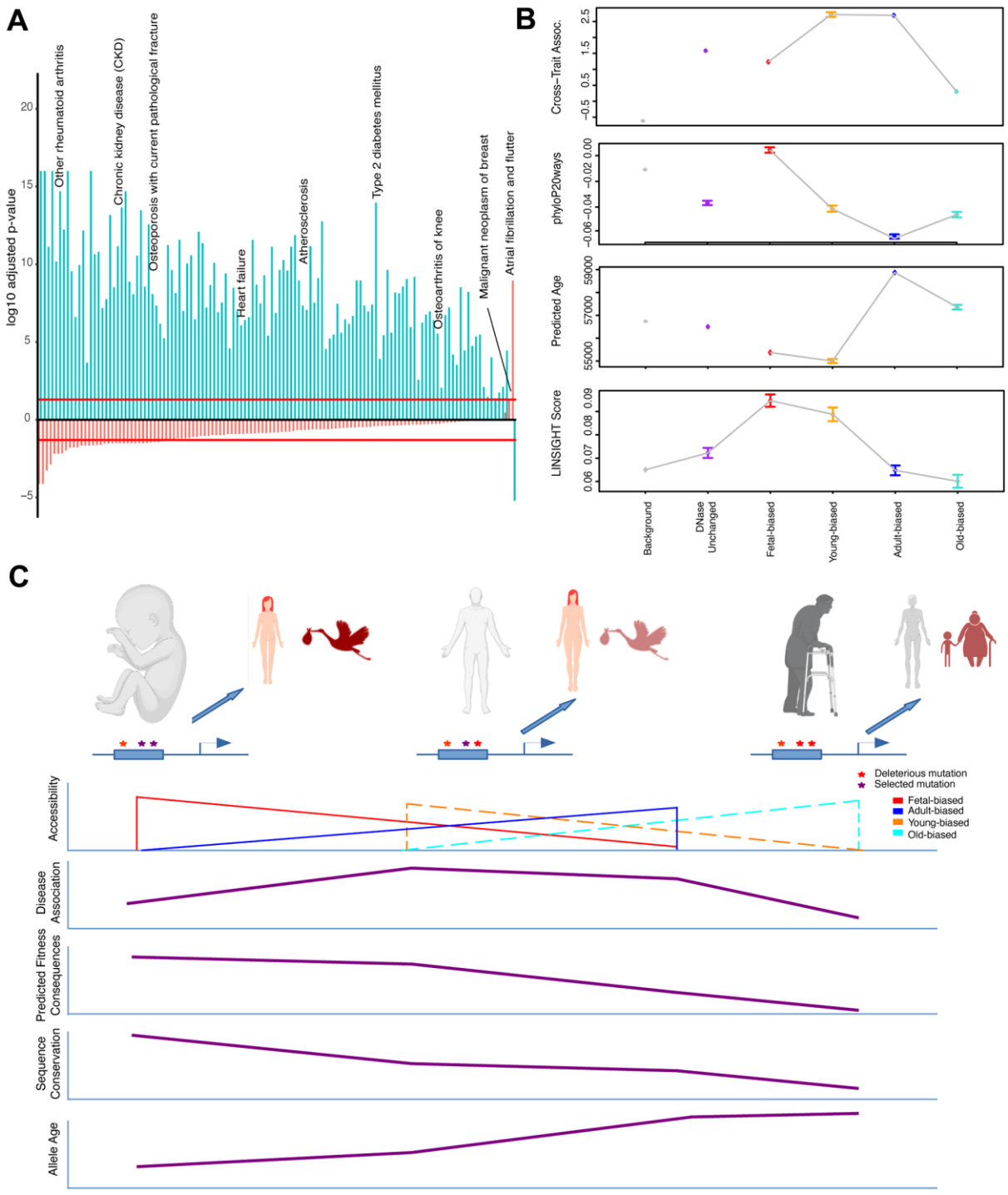

Figure 3. Epigenetic context and heritable disease associations. (**A**) Adjusted p-values for hypergeometric tests showing enrichment/depletion (positive/negative) for GWAS variants nearby regions increasing (blue) or decreasing (red) accessibility across adult tissues for a number of age-associated diseases (see Supplementary Table 4). (**B**) Cross-set disease associations, and additional per-SNP metrics, for variants nearby developmental and age-altered region sets along with unaltered DNase sites and variants not nearby accessible regions. See Supplementary Table 4 and Methods. (**C**) Model for the effects of epigenetic context on disease association and sequence evolution. (Top): Example enhancer elements more accessible in fetal, adult, and old-adult tissues (left-right) which have been modified by mutations. (Left): Deleterious mutations disrupting regulation in development stand to have the biggest impact on fitness, while having a moderate effect on tissue homeostasis. (Middle): Mutations disrupting regulation in young-adult tissues have a moderate impact on fitness, but a larger effect on tissue homeostasis (particularly over adulthood). (Right): Mutations disrupting regulation in old-adult tissues have weak impacts on fitness, and a weak effect on tissue homeostasis (which has already deteriorated with age). (Bottom): Illustrating patterns of accessibility, disease association, sequence constraint and variant allele age for these sets of regions changing accessibility over time.

finding that these gene loci tend to harbor stronger genetic variants across a larger number of diseases than expected (compared to randomized sets), but not so for genes involved in reproductive organ development (see Supplementary Information, Supplementary Table 4).

We applied this method to the sets of development and age-associated genes we defined above and asked whether they tended to have more or less cross-disease GWAS signals than expected. Our sets defined by accessibility-region contacts supported our earlier findings on strong GWAS signals nearby development and age-altered regions – namely, loci of both adult-biased and young-biased gene sets were enriched for strong GWAS signals across diseases, while fetal-biased and old-biased gene sets were associated with relatively weaker GWAS signals (Supplementary Table 4). Sets defined by RNA-seq data showed more of a mix of enriched/depleted GWAS signals across developmental and age comparisons, reflecting the possibility that a mixture of genes increasing and decreasing expression over time may additively contribute to aging disease biology (see Supplementary Information).

Given our results, found at both genome-wide and gene-locus set levels, we finally sought to take an unbiased approach to identify relevant 'core' aging-related genes solely on the basis of aggregate GWAS signals (see Supplementary Methods, Supplementary Information). Overall, we had limited success in defining a set of genes with clear, pan-tissue biological relevance, suggesting that, if such a core does exist, that it may be too broad, or the per-locus signals too moderate, for our method to robustly detect. However, since our results suggest the importance of altered epigenetics in modifying GWAS associations, we performed a similar gene-prioritization analysis using variants occurring nearby altered-accessibility regions (Supplementary Methods). This yielded markedly different enrichments for terms relating to immune processes and gene regulation (see Supplementary Information, Supplementary Table 4). One particular set of genes, involved in histone deacetylation, has repeatedly been linked to aging and epigenetics [61, 62] and was identified using our set of young-age regions (see Figure 4). We explore this set in more detail below.

Sequence evolution and disease association

Our previous analyses found that patterns of inter- and intra-species sequence conservation depended on epigenetic status (i.e., degree of accessibility) of regulatory elements. Subsequently, we found that the risk association of variants across a number of age-associated diseases also varied based on accessibility change in the vicinity of the variant. Much work has been done on understanding the relationship between sequence conservation and disease risk [63–66]. For example, a transcription factor (TF) binding site may be subjected to negative selection to conserve its sequence and hence function. Mutations that occur within this site would more likely impact *cis*-regulatory biology, and therefore manifest an association with disease. If this disease impacts fitness, then over time, such mutations will be eliminated, so that genetically 'older' mutations are less prevalent [65, 67]. Given our interest in the evolution of development and aging processes, we wanted to investigate the role that epigenetics has on this disease-evolution relationship - and whether this holds with our data. By comparing the cross-trait associations of variants falling within and outside primate-conserved sequences (phastCons) [68] (Supplementary Methods), we found that variants within conserved sequences tend to have greater disease associations, along with younger estimated allele age (Supplementary Table 4). These patterns also hold true for phastCons sequences within age- and developmentally-altered regions (Supplementary Table 4), and follow with previously observed enrichments for GWAS associations of conserved, younger (allele age) variants [65, 67, 69].

We next considered primate conservation, estimated allele age, and cross-set association of variants, looking for the effects of nearby accessibility change on these metrics (Supplementary Methods). As an additional metric for predicted fitness consequences, particularly of non-coding variants, we also included per-bp LINSIGHT scores [70], which integrates data on chromatin accessibility, TF binding motifs, and comparative genomics.

First, we found that variants falling near fetal-biased regions were more conserved, younger, and had lower cross-set association, while variants near adult-biased regions behaved oppositely (Figure 3B and Supplementary Table 4). We also found that the predicted functional consequences associated with fetal-biased regions were greater than with adult-biased regions, despite the lower cross-set association with aging-associated diseases (Figure 3C, see Discussion). Variants falling near old-biased regions were less conserved, had older allele age, and had lower cross-set association than their young-biased counterparts (Supplementary Table 4). These old-biased regions were also associated with the lowest predicted functional consequences (in aggregate) of any set, while the set of young-biased regions had the second-highest average. To compare these behaviors with variants of annotated clinical significance we independently examined ClinVar variants, which while demonstrating

increased cross-set association, tended to also be more conserved, younger, and have stronger predicted fitness consequences (Supplementary Table 4).

Collectively, our results indicate that variants stratified by nearby accessibility change violate the expected relationship between sequence conservation and disease association (behaviors instead observed for ClinVar variants). Namely, those regions exhibiting the highest sequence constraint (Figure 3C, left) do not also exhibit the strongest aging-disease associations, nor do those regions exhibiting the weakest constraint, as might be expected in a 'mutation accumulation' theory of aging [35]. However, when considering predicted functional consequences (LINSIGHT), which are not defined based on aging demographic data, this pattern is reversed (i.e., the most constrained set, fetal-biased regions, had the strongest predicted consequences despite weaker aging-disease associations). This unexpected behavior may have important implications for evolutionary models of late-onset complex disease genetics. Based on our results, we propose such a model suggesting the outsized impact of regulatory sequences active in early adulthood on genetic contributions to aging-associated disease risk (see Figure 3C, Discussion).

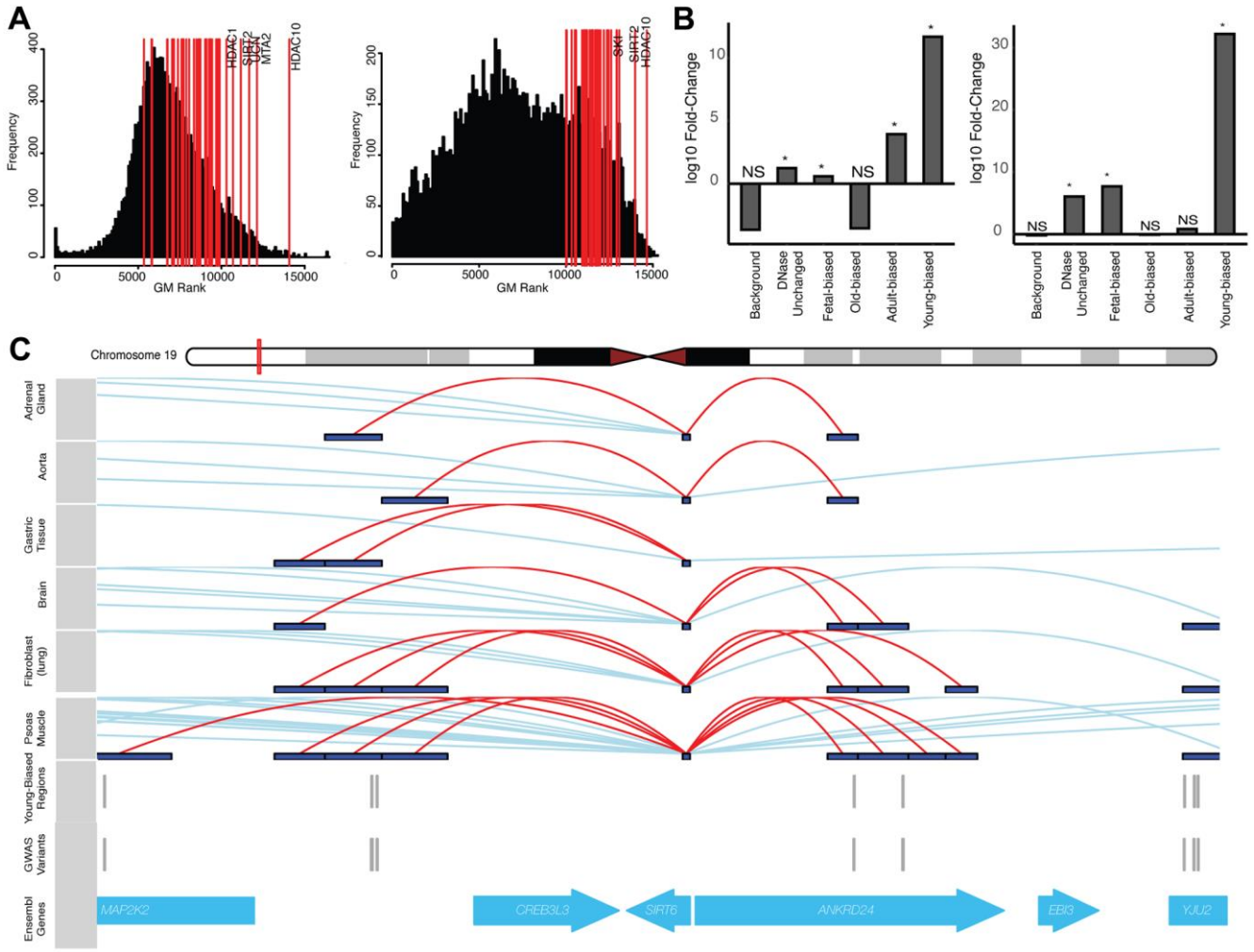

Figure 4. Altered-accessibility regions identify relevant aging biology. (**A**) (Left) Distribution of cross-disease ranks for all protein-coding genes, when ranking by local variants independent of accessibility data (see Supplementary Methods). Red lines indicate genes within the 'histone deacetylation' (HDAC) GO term; top ranked genes (by geometric mean) are indicated. (Right) Similar distribution of cross-disease ranks, ranking genes with variants nearby young-biased regions. Red lines indicate top HDAC genes by rank. (**B**) (Left) Fold-change of normal cumulative distribution function (CDF) p-values of variants within HDAC gene loci associated with different region sets, relative to CDF test performed using all variants, for cross-disease Z-score metric (see Supplementary Methods). (Right) Similar plot for per-variant LINSIGHT scores. See Supplementary Table 4. (**C**) Variants directly intersecting young-biased regions which interact with the *SIRT6* promoter. (Top) Visualized promoter-capture data [41] across multiple cell-types. (Bottom) Tracks indicating variants which overlap young-biased regions within the *SIRT6* gene locus.

Our proposed model suggests that focusing on disease risk loci containing such putative regulatory sequences (i.e., young-biased regions), should implicate sets of genes involved in aging biological processes. Our gene-level GWAS analyses using young-biased regions identified genes involved with histone deacetylation as being more consistently associated with aging-disease GWAS signal, a pattern which was diminished when considering gene-level associations in the absence of this epigenetic information (Figure 4A), and when using other region sets (e.g., old-biased regions) (Figure 4B). Histone deacetylation enzymes have known impacts on epigenetic aging biology [7, 61, 62] and aging diseases [71]. Within our young-biased enriched gene set we identified *SIRT6* and *SIRT7* as having multiple variants falling nearby young-biased regions which contacted their respective gene promoters (Figure 4C). Both these enzymes have been associated with maintaining heterochromatin during aging [72–74]; *SIRT7* decreases expression with age, and antagonizes hMSC epigenetic aging [73], while *SIRT6* loss manifests an aging-like state [75]. It may be possible that decreased accessibility of regulatory regions controlling the expression of these genes are involved in decreases in sirtuin expression and heterochromatin [72].

DISCUSSION

In this study we sought to describe how changing epigenetic context, defined here as changes to chromatin accessibility over both development and subsequent aging, influences the behavior of evolutionary forces and genetic disease risk at the sequence level. To address this question, we defined genomic regions whose chromatin accessibility consistently shift over the course of development and aging. Our approach to identify epigenetic shifts relies on the observation that chromatin accessibility broadly reflects the regulatory capacity at a given locus [39], though we acknowledge that more subtle epigenetic changes (e.g., post-translational modifications, CpG methylation) may not be well captured by this accessibility-based definition of epigenetic context.

We performed several analyses suggesting that these regions reflect developmental and aging signatures from previous literature, including genomic features (e.g., repeat elements, CpG sites), epigenetic states (e.g., euchromatin/heterochromatin) and histone mark data. Gene sets associated with developmentally-altered regions were enriched for immune system function and cellular proliferation terms, echoing an earlier study of fetal to adult epigenetic changes [21]. Furthermore, we found correspondence between these gene sets and genes whose RNA-seq expression generally shifted between fetal and adult tissues. Incorporating an independent RNA-seq dataset of adult age-stratified tissues we did not observe the same level of correspondence with age-altered regions – it is possible that some aspects of epigenetic aging (e.g., global de-repression [3, 5, 76]) may account for this disconnect, whereby local accessibility changes are less-directly linked to local expression changes. Interestingly, comparing patterns of expression change in our fetal-adult and young-old comparisons, we saw similar gene-set enrichments (i.e., cell-cycling biased towards fetal and younger-age samples, immune responses biasing towards adult and older-age samples), suggesting that the continuation of epigenetic shifts we observed across development and aging (Figure 1D) may be mirrored at the expression level.

Given that epigenetic state impacts the potential regulatory effects of deleterious variants [34], we looked to see if local development and/or ageing changes to epigenetic context impacts the strength of association between variants and aging-associated diseases. While it is possible that a number of these aging diseases share genetic correlations [77], that these variants are associated with multiple age-associated diseases is also a key expectation for the functional relevance of age-altered regions. In other words, it is the change in epigenetic context that modifies the regulatory potential of these variants, and this has direct impacts on individual associations with multiple diseases.

According to the fetal programming model, we would expect that regulatory regions most active during early development, both dictating developmental processes as well as responding to environmental perturbations [9], would have an out-sized impact on the manifestation of adult-onset diseases. This would be evident in the increased associations of nearby variants with heritable risk for these diseases. However, we found that such fetal-biased regions were not those having the greatest impact with regards to aging disease associations, despite having greater predicted fitness consequences – finding instead that fetal-biased regions are depleted for aging disease GWAS signals, and associated more with developmental diseases/traits (Supplementary Table 4). A recent study of fetal chromatin accessibility at the single-cell level similarly found genetic associations with developmental traits (e.g., height) using regions accessible in different cell-types [78]. We suggest that the 'fetal programming' of epigenetic status during early development, genome-wide, has a more moderate impact on aging disease biology than has been previously suggested – though we note that certain developmental loci (e.g., Wnt genes) can and do play a role in aging [8, 24].

According to a model wherein epigenetic aging influences the phenotypic effects of regulatory mutations, we would expect that mutations with increased local accessibility in adult tissues, particularly aged adult tissues, would have stronger impacts on aging disease biology in these tissues (reflected in increased association with heritable disease risk). Here, we found that variants gaining nearby accessibility (i.e., adult-biased regions) have stronger associations across a number of aging-related diseases including several kinds of neoplasms, arthritis, and atherosclerosis. This finding suggests that the regulatory effects of deleterious variants may become 'uncovered' as tissues mature and follows with proposed links between development and ageing processes [8, 20, 24]. However, we also found that regions most accessible later in life, when these diseases manifest, are actually associated with weaker GWAS variants. This young/old bias in aging-disease GWAS signal was far stronger than the fetal/adult bias (i.e., the young-biased set was more strongly enriched than adult-biased, and vice-versa). Taken together, these results suggest that (1) accessibility changes in aging tissues have a greater effect on aging tissue diseases, but (2) that variants more accessible earlier in adult life play a bigger regulatory role in contributing to disease risk than do those which gain accessibility later on. Disruptions to regulation in younger tissues may act to set tissues down a path of increasing dysfunction and decline, especially if deleterious variants are able to (cumulatively) contribute to dysfunction as they gradually lose activity with age. In other words, by the time an individual reaches old-age their tissues have had sufficient time to accumulate these dysfunctional effects, 'setting the stage' for disease manifestation. Variants more active in old-age, by contrast, have less of an impact on disease manifestation, as their regulatory effects have had less time to integrate. It may be that the time at which disease prevention and/or intervention would be most effective is, perhaps non-intuitively, early in adult life rather than once phenotypes manifest.

We cannot rule out the effects of cell-type specific epigenetic (accessibility) shifts influencing the phenotypic impacts of regulatory sequence modifications on aging-associated disease risk. Similarly, it has been suggested that a facet of aging is 'epigenetic drift' – the accumulation of epigenomic aberrations that contribute to mis-regulation of gene regulatory networks, a component of which is tissue-specific [79, 80]. However, the pan-signals which we do observe with respect to evolutionary forces, disease associations, and sets of implicated gene loci indicates the relevance of our approach in understanding the broader components of development and aging-accessibility changes, which may be complemented with future research focusing on those more tissue-specific components.

Regulation of general aging-related mechanisms, as well as increases in heritable disease risk, represent phenotypes upon which evolutionary forces may act to modify aging and mortality rates. We found that young-biased regions were enriched for signals of positive selection, a number of which implicated relevant aging-associated genes, and exhibited increased phylogenetic and within-human sequence constraint. Given that these behaviors are intermediate between those observed with regions more accessible in fetal and older-adult tissues, we suggest the following model (Figure 3D).

Regulatory sequences most active during development are subjected to strong negative selection, both to maintain human-derived functional sequences and discourage subsequent modifications, as dysregulation of development would have the largest fitness consequences. Similarly, sequences most active during early adulthood are subjected to negative selection to maintain proper tissue maintenance and discourage disease. However, the strength of this selection is reduced, as we expect fitness benefits/costs to diminish with age as individuals reproduce less frequently [53–55]. Thus, despite the fact that mutations within or nearby these functional sequences stand to have the greatest impact on disease risk (as noted above) they are less efficiently purged, and are allowed to accumulate over generations [35]. Finally, sequences most active in older adults are under relaxed selective pressures and allowed to drift – mutations are permitted and retained, particularly due to the reduced associations that these mutations have with heritable disease risk. Overall, this model suggests that considering the changing epigenetic context of disease-associated variants may help in prioritizing GWAS signals to loci involved in disease biology (e.g., as we saw for histone deacetylases) and, ultimately, the aging processes driving tissue decline and eventual manifestation of aging-associated disease.

MATERIALS AND METHODS

Accessibility datasets

DNase-I hypersensitivity datasets were obtained from ENCODE [40] for eight different fetal and adult tissues (adrenal gland, brain, heart, lung, muscle, skin, spleen and stomach) (see Supplementary Table 1 for accessions and metadata). Raw data was processed as described in the Supplementary Methods, with called open-chromatin regions consolidated across replicates and tissues in order to define a final set of reproducible regions. This aggregated set of peaks was then used to

assess both pan-tissue, as well as per-tissue, accessibility changes between fetal and adult datasets using the limma package (version 3.46) in R [81, 82]. Differentially-accessible regions were defined using a Benjamini-Hochberg FDR [83] cutoff of < 0.05.

Adult DNase samples were further stratified in order to define age-altered chromatin regions, splitting samples used in the above analysis into those individuals younger than 50 ('young-adult') and those older than 50 ('old-adult'), this age representing a roughly equal split of sample numbers. Not all tissues used in the initial fetal/adult comparison were represented in these age-stratified sets – thus we restricted the tissue comparisons to brain, heart, lung, muscle and stomach tissues. A similar computational method as that used in defining fetal- and adult-biased regions was applied here (see Supplementary Methods). We compared accessibility changes between young and old-adult samples within those regions exhibiting fetal/adult biases, defining young-biased and old-biased regions (again, using an FDR cutoff of < 0.05).

Promoter accessibility change

All hg19 Refseq gene TSS were obtained from the UCSC Genome Browser [84] and padded 1kb up/downstream to define promoter regions. For each promoter region, DNase read coverage was compared between adult and fetal samples, with resulting data processed using a similar differential-accessibility method as that used above (see Supplementary Methods). Significantly differentially-accessible promoters were defined using an FDR cut-off of 0.05. As an additional, more stringent analysis, we also defined differentially-accessible promoters based on intersections with the above defined region sets (see Supplementary Methods).

Promoter capture datasets: Promoter-capture data was obtained from Jung et al., 2019 [41]; this dataset was generated from promoter-capture assays across a number of different tissues and cell-types. Given our pan-tissue approach, we considered all data (with the exception of OV2, as we excluded sex-specific tissues from all previous obtained datasets). To generate a set of genomic regions which show evidence of contacting gene promoters, we filtered interacting regions to those which contacted their respective promoters in at least two different tissues/cell-types. This moderate filter was used to exclude those regions for which interactions appear to be exclusive to one dataset, while allowing for regions that do not show such exclusivity.

Gene-set enrichment analyses: Gene sets generated in our analyses were tested for enrichment in different GO Biological Process terms using the 'enrichGO' function from the clusterProfiler [85] package version 3.16.1, with semantically-similar GO terms collapsed and significantly-enriched terms defined as adjusted p-value < 0.05.

ENCODE RNA-seq datasets: Processed per-gene quantification files, as generated by the ENCODE pipeline were obtained from the ENCODE web portal [40] (see Supplementary Table 2 for file accessions and metadata). Given the limited availability of adult tissue samples for use in differential-expression analysis, we instead defined a less-stringent method to identify broad changes in gene expression which demonstrate consistency across tissues (see Supplementary Methods).

GTEx RNA-seq processing: Processed RNA-seq quantification files were obtained from the GTEx web portal [43] for the following tissues (matching the above young/old-age accessibility comparison): brain (Brain - Cerebellum), heart (Heart – Left Ventricle), lung (Lung), muscle (Muscle - Skeletal) and stomach (Stomach). Similar to the processing performed in Benayoun et al [44], we applied quality filters to remove lowly-expressed and non-coding genes, and subsequently used the same definitions of 'young-age' and 'old-age' (as in the above analyses) to calculate differential expression using limma-voom (see Supplementary Methods).

Human sequence variation datasets: Variation data from the 1000 Genomes Project phase 3 (1KGP) [86] (n = 2504 individuals) in .vcf.gz format was obtained and intersected with our region sets using tabix [87] (version 1.9) to obtain variants occurring within these altered-accessibility regions. Common variants were defined using a minor allele frequency (MAF) threshold of >= 0.05. These sets of intersected variants were subsequently used to compare sequence variation across region sets, as well as comparing region-intersected variation to genomic backgrounds and feature sets (see Supplementary Methods).

GWAS summary statistics data: To define a set of aging-associated diseases for use in our analyses, we first used broadly-defined categories as described in Chang et al., 2019 [58]. This study described 92 age-related diseases grouped into broader disease categories based on analyses of large-scale demographic datasets. We took these classifications and manually extracted relevant GWAS phenotypes assessed by the UK Biobanks study [57], obtaining pre-processed summary statistics for these phenotypes provided by the Neale lab [77] (https://nealelab.github.io/UKBB_ldsc/downloads.html). These data were subsequently utilized

across several bioinformatic analyses (see Supplementary Methods).

Additional computational methods, including implementations of statistical tests described in the Results, are described in detail in the Supplementary Methods document. The datasets supporting the findings of this study are publicly-available – accession codes and URLs are provided in the Supplementary Methods and Tables. Computational code for processing these datasets is available upon reasonable request from the Lead Contact.

AUTHOR CONTRIBUTIONS

DR: Conceptualization, Data curation, Formal analysis, Investigation, Visualization, Methodology, Manuscript Writing; TDC: Conceptualization, Supervision, Funding acquisition, Investigation, Manuscript Writing, Project administration.

ACKNOWLEDGMENTS

We thank Dr. Anne Brunet for meaningful discussions relating to concepts of aging, development and epigenetics. We thank three anonymous reviewers for their excellent insights into our work.

CONFLICTS OF INTEREST

The authors declare that they have no conflicts of interest.

FUNDING

Research reported in this publication was supported by The American School of Prehistoric Research, Harvard University.

REFERENCES

1. Brunet A, Berger SL. Epigenetics of aging and aging-related disease. J Gerontol A Biol Sci Med Sci. 2014 (Suppl 1); 69:S17–20. https://doi.org/10.1093/gerona/glu042 PMID:24833581

2. Rodríguez-Rodero S, Fernández-Morera JL, Menéndez-Torre E, Calvanese V, Fernández AF, Fraga MF. Aging genetics and aging. Aging Dis. 2011; 2:186–95. PMID:22396873

3. Booth LN, Brunet A. The Aging Epigenome. Mol Cell. 2016; 62:728–44. https://doi.org/10.1016/j.molcel.2016.05.013 PMID:27259204

4. Criscione SW, Teo YV, Neretti N. The Chromatin Landscape of Cellular Senescence. Trends Genet. 2016; 32:751–61. https://doi.org/10.1016/j.tig.2016.09.005 PMID:27692431

5. López-Otín C, Blasco MA, Partridge L, Serrano M, Kroemer G. The hallmarks of aging. Cell. 2013; 153:1194–217. https://doi.org/10.1016/j.cell.2013.05.039 PMID:23746838

6. ENCODE Project Consortium. An integrated encyclopedia of DNA elements in the human genome. Nature. 2012; 489:57–74. https://doi.org/10.1038/nature11247 PMID:22955616

7. Zhang W, Qu J, Liu GH, Belmonte JC. The ageing epigenome and its rejuvenation. Nat Rev Mol Cell Biol. 2020; 21:137–50. https://doi.org/10.1038/s41580-019-0204-5 PMID:32020082

8. Blagosklonny MV, Hall MN. Growth and aging: a common molecular mechanism. Aging (Albany NY). 2009; 1:357–62. https://doi.org/10.18632/aging.100040 PMID:20157523

9. Hanson M, Godfrey KM, Lillycrop KA, Burdge GC, Gluckman PD. Developmental plasticity and developmental origins of non-communicable disease: theoretical considerations and epigenetic mechanisms. Prog Biophys Mol Biol. 2011; 106:272–80. https://doi.org/10.1016/j.pbiomolbio.2010.12.008 PMID:21219925

10. Gicquel C, El-Osta A, Le Bouc Y. Epigenetic regulation and fetal programming. Best Pract Res Clin Endocrinol Metab. 2008; 22:1–16. https://doi.org/10.1016/j.beem.2007.07.009 PMID:18279777

11. Godfrey KM, Lillycrop KA, Burdge GC, Gluckman PD, Hanson MA. Non-imprinted epigenetics in fetal and postnatal development and growth. Nestle Nutr Inst Workshop Ser. 2013; 71:57–63. https://doi.org/10.1159/000342552 PMID:23502139

12. Rinaudo P, Wang E. Fetal programming and metabolic syndrome. Annu Rev Physiol. 2012; 74:107–30. https://doi.org/10.1146/annurev-physiol-020911-153245 PMID:21910625

13. Kirkwood TB. Understanding ageing from an evolutionary perspective. J Intern Med. 2008; 263:117–27. https://doi.org/10.1111/j.1365-2796.2007.01901.x PMID:18226090

14. Kirkwood TB. Evolution of ageing. Mech Ageing Dev. 2002; 123:737–45. https://doi.org/10.1016/s0047-6374(01)00419-5 PMID:11869731

15. Conradt E, Adkins DE, Crowell SE, Raby KL, Diamond LM, Ellis B. Incorporating epigenetic mechanisms to advance fetal programming theories. Dev Psychopathol. 2018; 30:807–24. https://doi.org/10.1017/S0954579418000469 PMID:30068415

16. Fraga MF, Ballestar E, Paz MF, Ropero S, Setien F, Ballestar ML, Heine-Suñer D, Cigudosa JC, Urioste M, Benitez J, Boix-Chornet M, Sanchez-Aguilera A, Ling C, et al. Epigenetic differences arise during the lifetime of monozygotic twins. Proc Natl Acad Sci USA. 2005; 102:10604–09. https://doi.org/10.1073/pnas.0500398102 PMID:16009939

17. Ollikainen M, Smith KR, Joo EJ, Ng HK, Andronikos R, Novakovic B, Abdul Aziz NK, Carlin JB, Morley R, Saffery R, Craig JM. DNA methylation analysis of multiple tissues from newborn twins reveals both genetic and intrauterine components to variation in the human neonatal epigenome. Hum Mol Genet. 2010; 19:4176–88. https://doi.org/10.1093/hmg/ddq336 PMID:20699328

18. Saffery R, Novakovic B. Epigenetics as the mediator of fetal programming of adult onset disease: what is the evidence? Acta Obstet Gynecol Scand. 2014; 93:1090–98. https://doi.org/10.1111/aogs.12431 PMID:24835110

19. Aagaard-Tillery KM, Grove K, Bishop J, Ke X, Fu Q, McKnight R, Lane RH. Developmental origins of disease and determinants of chromatin structure: maternal diet modifies the primate fetal epigenome. J Mol Endocrinol. 2008; 41:91–102. https://doi.org/10.1677/JME-08-0025 PMID:18515302

20. Horvath S, Raj K. DNA methylation-based biomarkers and the epigenetic clock theory of ageing. Nat Rev Genet. 2018; 19:371–84. https://doi.org/10.1038/s41576-018-0004-3 PMID:29643443

21. Yan L, Guo H, Hu B, Li R, Yong J, Zhao Y, Zhi X, Fan X, Guo F, Wang X, Wang W, Wei Y, Wang Y, et al. Epigenomic Landscape of Human Fetal Brain, Heart, and Liver. J Biol Chem. 2016; 291:4386–98. https://doi.org/10.1074/jbc.M115.672931 PMID:26719341

22. Maiese K, Li F, Chong ZZ, Shang YC. The Wnt signaling pathway: aging gracefully as a protectionist? Pharmacol Ther. 2008; 118:58–81. https://doi.org/10.1016/j.pharmthera.2008.01.004 PMID:18313758

23. Salminen A, Kaarniranta K. Insulin/IGF-1 paradox of aging: regulation via AKT/IKK/NF-kappaB signaling. Cell Signal. 2010; 22:573–77. https://doi.org/10.1016/j.cellsig.2009.10.006 PMID:19861158

24. de Magalhães JP. Programmatic features of aging originating in development: aging mechanisms beyond molecular damage? FASEB J. 2012; 26:4821–26. https://doi.org/10.1096/fj.12-210872 PMID:22964300

25. Rivera CM, Ren B. Mapping human epigenomes. Cell. 2013; 155:39–55. https://doi.org/10.1016/j.cell.2013.09.011 PMID:24074860

26. Kundaje A, Meuleman W, Ernst J, Bilenky M, Yen A, Heravi-Moussavi A, Kheradpour P, Zhang Z, Wang J, Ziller MJ, Amin V, Whitaker JW, Schultz MD, et al, and Roadmap Epigenomics Consortium. Integrative analysis of 111 reference human epigenomes. Nature. 2015; 518:317–30. https://doi.org/10.1038/nature14248 PMID:25693563

27. Day K, Waite LL, Thalacker-Mercer A, West A, Bamman MM, Brooks JD, Myers RM, Absher D. Differential DNA methylation with age displays both common and dynamic features across human tissues that are influenced by CpG landscape. Genome Biol. 2013; 14:R102. https://doi.org/10.1186/gb-2013-14-9-r102 PMID:24034465

28. Kubben N, Misteli T. Shared molecular and cellular mechanisms of premature ageing and ageing-associated diseases. Nat Rev Mol Cell Biol. 2017; 18:595–609. https://doi.org/10.1038/nrm.2017.68 PMID:28792007

29. Yang J, Huang T, Petralia F, Long Q, Zhang B, Argmann C, Zhao Y, Mobbs CV, Schadt EE, Zhu J, Tu Z, and GTEx Consortium. Synchronized age-related gene expression changes across multiple tissues in human and the link to complex diseases. Sci Rep. 2015; 5:15145. https://doi.org/10.1038/srep15145 PMID:26477495

30. Frenk S, Houseley J. Gene expression hallmarks of cellular ageing. Biogerontology. 2018; 19:547–66. https://doi.org/10.1007/s10522-018-9750-z PMID:29492790

31. Bou Sleiman M, Jha P, Houtkooper R, Williams RW, Wang X, Auwerx J. The Gene-Regulatory Footprint of Aging Highlights Conserved Central Regulators. Cell Rep. 2020; 32:108203. https://doi.org/10.1016/j.celrep.2020.108203 PMID:32997995

32. Yuen RK, Neumann SM, Fok AK, Peñaherrera MS, McFadden DE, Robinson WP, Kobor MS. Extensive epigenetic reprogramming in human somatic tissues between fetus and adult. Epigenetics Chromatin. 2011; 4:7. https://doi.org/10.1186/1756-8935-4-7 PMID:21545704

33. Zhu J, Adli M, Zou JY, Verstappen G, Coyne M, Zhang X, Durham T, Miri M, Deshpande V, De Jager PL, Bennett DA, Houmard JA, Muoio DM, et al. Genome-wide chromatin state transitions associated with developmental and environmental cues. Cell. 2013; 152:642–54. https://doi.org/10.1016/j.cell.2012.12.033 PMID:23333102

34. Boyle AP, Hong EL, Hariharan M, Cheng Y, Schaub MA, Kasowski M, Karczewski KJ, Park J, Hitz BC, Weng S, Cherry JM, Snyder M. Annotation of functional variation in personal genomes using RegulomeDB. Genome Res. 2012; 22:1790–97. https://doi.org/10.1101/gr.137323.112 PMID:22955989

35. Charlesworth B. Patterns of age-specific means and genetic variances of mortality rates predicted by the mutation-accumulation theory of ageing. J Theor Biol. 2001; 210:47–65. https://doi.org/10.1006/jtbi.2001.2296 PMID:11343430

36. Kirkwood TB, Rose MR. Evolution of senescence: late survival sacrificed for reproduction. Philos Trans R Soc Lond B Biol Sci. 1991; 332:15–24. https://doi.org/10.1098/rstb.1991.0028 PMID:1677205

37. Richard D, Liu Z, Cao J, Kiapour AM, Willen J, Yarlagadda S, Jagoda E, Kolachalama VB, Sieker JT, Chang GH, Muthuirulan P, Young M, Masson A, et al. Evolutionary Selection and Constraint on Human Knee Chondrocyte Regulation Impacts Osteoarthritis Risk. Cell. 2020; 181:362–81.e28. https://doi.org/10.1016/j.cell.2020.02.057 PMID:32220312

38. Rodríguez JA, Marigorta UM, Hughes DA, Spataro N, Bosch E, Navarro A. Antagonistic pleiotropy and mutation accumulation influence human senescence and disease. Nat Ecol Evol. 2017; 1:55. https://doi.org/10.1038/s41559-016-0055 PMID:28812720

39. Klemm SL, Shipony Z, Greenleaf WJ. Chromatin accessibility and the regulatory epigenome. Nat Rev Genet. 2019; 20:207–20. https://doi.org/10.1038/s41576-018-0089-8 PMID:30675018

40. Davis CA, Hitz BC, Sloan CA, Chan ET, Davidson JM, Gabdank I, Hilton JA, Jain K, Baymuradov UK, Narayanan AK, Onate KC, Graham K, Miyasato SR, et al. The Encyclopedia of DNA elements (ENCODE): data portal update. Nucleic Acids Res. 2018; 46:D794–801. https://doi.org/10.1093/nar/gkx1081 PMID:29126249

41. Jung I, Schmitt A, Diao Y, Lee AJ, Liu T, Yang D, Tan C, Eom J, Chan M, Chee S, Chiang Z, Kim C, Masliah E, et al. A compendium of promoter-centered long-range chromatin interactions in the human genome. Nat Genet. 2019; 51:1442–49. https://doi.org/10.1038/s41588-019-0494-8 PMID:31501517

42. McLean CY, Bristor D, Hiller M, Clarke SL, Schaar BT, Lowe CB, Wenger AM, Bejerano G. GREAT improves functional interpretation of cis-regulatory regions. Nat Biotechnol. 2010; 28:495–501. https://doi.org/10.1038/nbt.1630 PMID:20436461

43. GTEx Consortium. The Genotype-Tissue Expression (GTEx) project. Nat Genet. 2013; 45:580–85. https://doi.org/10.1038/ng.2653 PMID:23715323

44. Benayoun BA, Pollina EA, Singh PP, Mahmoudi S, Harel I, Casey KM, Dulken BW, Kundaje A, Brunet A. Remodeling of epigenome and transcriptome landscapes with aging in mice reveals widespread induction of inflammatory responses. Genome Res. 2019; 29:697–709. https://doi.org/10.1101/gr.240093.118 PMID:30858345

45. Carroll SB. Evo-devo and an expanding evolutionary synthesis: a genetic theory of morphological evolution. Cell. 2008; 134:25–36. https://doi.org/10.1016/j.cell.2008.06.030 PMID:18614008

46. Kirkwood TB, Holliday R. The evolution of ageing and longevity. Proc R Soc Lond B Biol Sci. 1979; 205: 531–46. https://doi.org/10.1098/rspb.1979.0083 PMID:42059

47. Jones OR, Scheuerlein A, Salguero-Gómez R, Camarda CG, Schaible R, Casper BB, Dahlgren JP, Ehrlén J, García MB, Menges ES, Quintana-Ascencio PF, Caswell H, Baudisch A, Vaupel JW. Diversity of ageing across the tree of life. Nature. 2014; 505:169–73. https://doi.org/10.1038/nature12789 PMID:24317695

48. Ferris E, Abegglen LM, Schiffman JD, Gregg C. Accelerated Evolution in Distinctive Species Reveals Candidate Elements for Clinically Relevant Traits, Including Mutation and Cancer Resistance. Cell Rep. 2018; 22:2742–55. https://doi.org/10.1016/j.celrep.2018.02.008 PMID:29514101

49. Pollard KS, Hubisz MJ, Rosenbloom KR, Siepel A. Detection of nonneutral substitution rates on mammalian phylogenies. Genome Res. 2010; 20:110–21. https://doi.org/10.1101/gr.097857.109 PMID:19858363

50. Kirkwood TB. The origins of human ageing. Philos Trans R Soc Lond B Biol Sci. 1997; 352:1765–72. https://doi.org/10.1098/rstb.1997.0160 PMID:9460059

51. Varki A, Altheide TK. Comparing the human and chimpanzee genomes: searching for needles in a haystack. Genome Res. 2005; 15:1746–58. https://doi.org/10.1101/gr.3737405 PMID:16339373

52. Hubisz MJ, Pollard KS. Exploring the genesis and functions of Human Accelerated Regions sheds light on their role in human evolution. Curr Opin Genet Dev. 2014; 29:15–21. https://doi.org/10.1016/j.gde.2014.07.005 PMID:25156517

53. Carnes BA, Olshansky SJ. Evolutionary Perspectives on Human Senescence. Popul Dev Rev. 1993; 19:793. https://doi.org/10.2307/2938414

54. Ricklefs RE. The evolution of senescence from a comparative perspective. Funct Ecol. 2008; 22:379–92. https://doi.org/10.1111/j.1365-2435.2008.01420.x

55. Williams GC. Pleiotropy, natural selection, and the evolution of senescence. Evolution. 1957; 11:398–411. http://doi.wiley.com/10.1111/j.1558-5646.1957.tb02911.x

56. Wright A, Charlesworth B, Rudan I, Carothers A, Campbell H. A polygenic basis for late-onset disease. Trends Genet. 2003; 19:97–106. https://doi.org/10.1016/s0168-9525(02)00033-1 PMID:12547519

57. Sudlow C, Gallacher J, Allen N, Beral V, Burton P, Danesh J, Downey P, Elliott P, Green J, Landray M, Liu B, Matthews P, Ong G, et al. UK biobank: an open access resource for identifying the causes of a wide range of complex diseases of middle and old age. PLoS Med. 2015; 12:e1001779. https://doi.org/10.1371/journal.pmed.1001779 PMID:25826379

58. Chang AY, Skirbekk VF, Tyrovolas S, Kassebaum NJ, Dieleman JL. Measuring population ageing: an analysis of the Global Burden of Disease Study 2017. Lancet Public Health. 2019; 4:e159–67. https://doi.org/10.1016/S2468-2667(19)30019-2 PMID:30851869

59. Boyle EA, Li YI, Pritchard JK. An Expanded View of Complex Traits: From Polygenic to Omnigenic. Cell. 2017; 169:1177–86. https://doi.org/10.1016/j.cell.2017.05.038 PMID:28622505

60. Landrum MJ, Lee JM, Benson M, Brown GR, Chao C, Chitipiralla S, Gu B, Hart J, Hoffman D, Jang W, Karapetyan K, Katz K, Liu C, et al. ClinVar: improving access to variant interpretations and supporting evidence. Nucleic Acids Res. 2018; 46:D1062–67. https://doi.org/10.1093/nar/gkx1153 PMID:29165669

61. Hall JA, Dominy JE, Lee Y, Puigserver P. The sirtuin family's role in aging and age-associated pathologies. J Clin Invest. 2013; 123:973–79. https://doi.org/10.1172/JCI64094 PMID:23454760

62. Sen P, Shah PP, Nativio R, Berger SL. Epigenetic Mechanisms of Longevity and Aging. Cell. 2016; 166:822–39. https://doi.org/10.1016/j.cell.2016.07.050 PMID:27518561

63. Cooper GM, Goode DL, Ng SB, Sidow A, Bamshad MJ, Shendure J, Nickerson DA. Single-nucleotide evolutionary constraint scores highlight disease-causing mutations. Nat Methods. 2010; 7:250–51. https://doi.org/10.1038/nmeth0410-250 PMID:20354513

64. Cooper GM, Shendure J. Needles in stacks of needles: finding disease-causal variants in a wealth of genomic data. Nat Rev Genet. 2011; 12:628–40. https://doi.org/10.1038/nrg3046 PMID:21850043

65. Hujoel ML, Gazal S, Hormozdiari F, van de Geijn B, Price AL. Disease Heritability Enrichment of Regulatory Elements Is Concentrated in Elements with Ancient Sequence Age and Conserved Function across Species. Am J Hum Genet. 2019; 104:611–24. https://doi.org/10.1016/j.ajhg.2019.02.008 PMID:30905396

66. MacArthur DG, Manolio TA, Dimmock DP, Rehm HL, Shendure J, Abecasis GR, Adams DR, Altman RB, Antonarakis SE, Ashley EA, Barrett JC, Biesecker LG, Conrad DF, et al. Guidelines for investigating causality of sequence variants in human disease. Nature. 2014; 508:469–76. https://doi.org/10.1038/nature13127 PMID:24759409

67. Gazal S, Finucane HK, Furlotte NA, Loh PR, Palamara PF, Liu X, Schoech A, Bulik-Sullivan B, Neale BM, Gusev A, Price AL. Linkage disequilibrium-dependent architecture of human complex traits shows action of negative selection. Nat Genet. 2017; 49:1421–27. https://doi.org/10.1038/ng.3954 PMID:28892061

68. Siepel A, Bejerano G, Pedersen JS, Hinrichs AS, Hou M, Rosenbloom K, Clawson H, Spieth J, Hillier LW, Richards

S, Weinstock GM, Wilson RK, Gibbs RA, et al. Evolutionarily conserved elements in vertebrate, insect, worm, and yeast genomes. Genome Res. 2005; 15:1034–50. https://doi.org/10.1101/gr.3715005 PMID:16024819

69. Finucane HK, Bulik-Sullivan B, Gusev A, Trynka G, Reshef Y, Loh PR, Anttila V, Xu H, Zang C, Farh K, Ripke S, Day FR, Purcell S, et al, and ReproGen Consortium, Schizophrenia Working Group of the Psychiatric Genomics Consortium, and RACI Consortium. Partitioning heritability by functional annotation using genome-wide association summary statistics. Nat Genet. 2015; 47:1228–35. https://doi.org/10.1038/ng.3404 PMID:26414678

70. Huang YF, Gulko B, Siepel A. Fast, scalable prediction of deleterious noncoding variants from functional and population genomic data. Nat Genet. 2017; 49:618–24. https://doi.org/10.1038/ng.3810 PMID:28288115

71. Tang J, Yan H, Zhuang S. Histone deacetylases as targets for treatment of multiple diseases. Clin Sci (Lond). 2013; 124:651–62. https://doi.org/10.1042/CS20120504 PMID:23414309

72. Benayoun BA, Pollina EA, Brunet A. Epigenetic regulation of ageing: linking environmental inputs to genomic stability. Nat Rev Mol Cell Biol. 2015; 16:593–610. https://doi.org/10.1038/nrm4048 PMID:26373265

73. Bi S, Liu Z, Wu Z, Wang Z, Liu X, Wang S, Ren J, Yao Y, Zhang W, Song M, Liu GH, Qu J. SIRT7 antagonizes human stem cell aging as a heterochromatin stabilizer. Protein Cell. 2020; 11:483–504. https://doi.org/10.1007/s13238-020-00728-4 PMID:32504224

74. Tasselli L, Zheng W, Chua KF. SIRT6: Novel Mechanisms and Links to Aging and Disease. Trends Endocrinol Metab. 2017; 28:168–85. https://doi.org/10.1016/j.tem.2016.10.002 PMID:27836583

75. Mostoslavsky R, Chua KF, Lombard DB, Pang WW, Fischer MR, Gellon L, Liu P, Mostoslavsky G, Franco S, Murphy MM, Mills KD, Patel P, Hsu JT, et al. Genomic instability and aging-like phenotype in the absence of mammalian SIRT6. Cell. 2006; 124:315–29. https://doi.org/10.1016/j.cell.2005.11.044 PMID:16439206

76. Tsurumi A, Li WX. Global heterochromatin loss: a unifying theory of aging? Epigenetics. 2012; 7:680–88. https://doi.org/10.4161/epi.20540 PMID:22647267

77. Bulik-Sullivan B, Finucane HK, Anttila V, Gusev A, Day FR, Loh PR, Duncan L, Perry JR, Patterson N, Robinson EB, Daly MJ, Price AL, Neale BM, and ReproGen Consortium, and Psychiatric Genomics Consortium, and Genetic Consortium for Anorexia Nervosa of the Wellcome Trust Case Control Consortium 3. An atlas of genetic correlations across human diseases and traits. Nat Genet. 2015; 47:1236–41. https://doi.org/10.1038/ng.3406 PMID:26414676

78. Domcke S, Hill AJ, Daza RM, Cao J, O'Day DR, Pliner HA, Aldinger KA, Pokholok D, Zhang F, Milbank JH, Zager MA, Glass IA, Steemers FJ, et al. A human cell atlas of fetal chromatin accessibility. Science. 2020; 370:eaba7612. https://doi.org/10.1126/science.aba7612 PMID:33184180

79. Teschendorff AE, West J, Beck S. Age-associated epigenetic drift: implications, and a case of epigenetic thrift? Hum Mol Genet. 2013; 22:R7–15. https://doi.org/10.1093/hmg/ddt375 PMID:23918660

80. Zampieri M, Ciccarone F, Calabrese R, Franceschi C, Bürkle A, Caiafa P. Reconfiguration of DNA methylation in aging. Mech Ageing Dev. 2015; 151:60–70. https://doi.org/10.1016/j.mad.2015.02.002 PMID:25708826

81. R Development Core Team. R: A Language and Environment for Statistical Computing. Vienna, Austria; 2008. http://www.r-project.org

82. Ritchie ME, Phipson B, Wu D, Hu Y, Law CW, Shi W, Smyth GK. limma powers differential expression analyses for RNA-sequencing and microarray studies. Nucleic Acids Res. 2015; 43:e47. https://doi.org/10.1093/nar/gkv007 PMID:25605792

83. Benjamini Y, Hochberg Y. Controlling the false discovery rate: a practical and powerful approach to multiple testing. J R Stat Soc Ser B (Methodological). 1957; 57:289–300. http://www.jstor.org/stable/2346101

84. Karolchik D, Hinrichs AS, Furey TS, Roskin KM, Sugnet CW, Haussler D, Kent WJ. The UCSC Table Browser data retrieval tool. Nucleic Acids Res. 2004; 32:D493–96. https://doi.org/10.1093/nar/gkh103 PMID:14681465

85. Yu G, Wang LG, Han Y, He QY. clusterProfiler: an R package for comparing biological themes among gene clusters. OMICS. 2012; 16:284–87. https://doi.org/10.1089/omi.2011.0118 PMID:22455463

86. Auton A, Brooks LD, Durbin RM, Garrison EP, Kang HM, Korbel JO, Marchini JL, McCarthy S, McVean GA, Abecasis GR, and 1000 Genomes Project Consortium. A global reference for human genetic variation. Nature.

2015; 526:68–74.
https://doi.org/10.1038/nature15393
PMID:26432245

87. Li H. Tabix: fast retrieval of sequence features from generic TAB-delimited files. Bioinformatics. 2011; 27:718–19.
https://doi.org/10.1093/bioinformatics/btq671
PMID:21208982

SUPPLEMENTARY MATERIALS

Supplementary Information (SI) Text

Comparing altered accessibility regions to genomic annotations, epigenetic states, and additional epigenetic datasets

As past studies have found that altered distribution of certain histone marks (e.g., H3K27ac) are a key feature of fetal to adult epigenetic changes [1–3] as well as epigenetic aging [4], the changes in chromatin accessibility we observe likely also reflects, in part, histone mark modification.

To define the epigenetic context within which our development- and age-altered regions fall, we utilized genome-wide assignments of epigenetic state as defined by the Roadmap Epigenomics Project Consortium [3], which employs a Hidden Markov Model to assign one of several possible epigenetic annotations to 200bp segments of the genome, integrating both chromatin-modification and accessibility datasets to define state probabilities, for different epigenomes (e.g., skin, brain tissues, etc.). Given that our altered regions were defined using a pan-tissue approach, for each 200bp segment we subset those epigenetic states defined for adult tissue samples, and took the state definition recurrent in the majority of samples as an 'adult-majority' assignment (see Supplementary Methods). We next intersected our region sets with these assigned segments, comparing the distribution of regions falling within different epigenetic states to the genome-wide distribution of these states to look for biases (Supplementary Figure 4). Adult-biased regions were enriched for epigenetic states associated with transcription, heterochromatin, and repressed Polycomb regions (Supplementary Table 1). Conversely, fetal-biased regions were enriched for states associated with enhancers, promoters, and 'primary DNase', while also showing a more moderate enrichment for repressed Polycomb regions. Likewise, old-biased regions were enriched for heterochromatin and quiescent states, while young-biased regions were enriched for all other states (Supplementary Table 1). By intersecting the fetal and adult as well as young and old-biased regions, we saw that the enrichments for different fetal and adult sets - i.e., adult-biased with heterochromatic states, fetal-biased with euchromatic states - overrode the young-biased and old-biased enrichment patterns (Supplementary Figure 4). Utilizing publicly-available epigenetic datasets and annotations through the LOLA [5] software (see Supplementary Methods), we again saw overlaps of the adult-biased region set for genomic annotations of 'repressed segments' and repeat sequences in this set, similar to the Roadmap epigenetic state results above (Supplementary Figure 4). Considering fetal-biased regions, we observed enrichments for TSS segments, Promoter/enhancer segments, and Vista enhancers, along with annotated CpG islands. We also saw similar enrichments for young- and old-biased sets (relative to their Roadmap enrichment results), and again saw the overriding fetal and adult patterns of enrichments in intersection sets (Supplementary Figure 5).

We next sought to validate the expected correspondence between development-associated chromatin accessibility and histone modifications, first using an independent dataset of fetal ChIP-seq experiments [1]. This study defined fetal bivalent promoter regions, which are thought to poise expression of developmental genes for rapid induction upon appropriate signaling [6]. Bivalent promoters tended to not be intersected by adult-biased regions, while fetal-biased regions were enriched in these sets ($p < 1e\text{-}16$, hypergeometric test, see Supplementary Methods). That these marked promoters responding to developmental signals lose accessibility in adult tissues would be expected [6], suggesting that our approach is capturing signals of epigenetic change in development. As additional validation of correspondence between development-, and potentially age-, associated chromatin accessibility and regions subject to histone modification, we again used LOLA enrichments, along with histone-mark ChIP-seq datasets acquired from primary tissues samples processed by ENCODE [7, 8].

ChIP-seq analyses

Given our use of DNA accessibility datasets, which should reflect the state of local chromatin with respect to chemical modifications increasing/decreasing accessibility, there is an expected concordance between open-chromatin regions defined by DNase-I hypersensitivity and the presence of nearby marks for histone post-translational modifications (i.e., histone ChIP-seq data). To first confirm this expected behavior in our accessibility data obtained from ENCODE, we further obtained ChIP-seq datasets from fetal and adult tissues matching those used in our accessibility analyses (see Supplementary Table 1 for accessions and metadata). Datasets included H3K27ac (an active, euchromatin mark), H3K27me3 and H3K9me3 (facultative and constitutive heterochromatin marks, respectively). Replicable open-chromatin regions in fetal and adult tissues were compared to their respective called ChIP-seq peak datasets looking for adjacency between accessibility and chromatin marks (within 1kb, see Supplementary Methods). For H3K27ac marks in

adult tissues, between 33-82% of replicable DNase peaks in a given tissue had adjacent ChIP-seq peak calls. For H3K27ac in fetal tissues, between 37-71% of replicable DNase peaks had adjacent ChIP-seq peak calls. For H3K27me3 in adult tissues, between 0.6-10% of replicable DNase peaks in a given tissue had adjacent ChIP-seq peak calls. For H3K27me3 in fetal tissues, between 4-27% of replicable DNase peaks had adjacent ChIP-seq peak calls. For H3K9me3 in adult tissues, between 0.05-4% of replicable DNase peaks in a given tissue had adjacent ChIP-seq peak calls. For H3K9me3 in fetal tissues, between 0.19-22% of replicable DNase peaks had adjacent ChIP-seq peak calls. The increased adjacency of DNase regions with H3K27ac (an active mark) compared to H3K27me3 and H3K9me3 (repressive marks) may be expected, given that DNase hypersensitivity should denote more accessible, active regions of chromatin.

We next asked whether the patterns of accessibility change we observed between fetal and adult tissue samples were also evident at the level of histone modifications. We thus applied a similar pipeline to that used in defining altered accessibility to define altered signals for histone marks (using ChIP-seq read coverage as an approximate, continuous metric) (see Supplementary Methods). This resulted in sets of H3K27ac, H3K27me3, and H3K9me3 peaks whose ChIP-seq signal significantly changed across tissues in comparing fetal and adult samples. Conditioning on the above DNase/ChIP-seq adjacency, we first asked whether significantly-DA DNase peaks tended to be adjacent to altered H3K27ac ChIP-seq peaks, above the general expectation for DNase peaks nearby H3K27ac peaks. We observed a 1.21 fold-change (FC) increase in the adjacency of altered DNase and ChIP-seq peaks (hypergeometric test p-value < 1e-16). Given this, we next asked whether, for these adjacent pairs, directionality was shared (i.e., DNase peaks gaining accessibility are adjacent to H3K27ac peaks gaining signal). We found that, of these adjacent pairs, those sharing direction (i.e., adult-biased DNase, adult-biased H3K27ac ChIP-seq) pairs were significantly over-represented (1.72 FC and 1.19 FC for adult/adult-biased and fetal/fetal-biased, respectively, hypergeometric tests comparing overlaps of sets, adjusted p-values < 1e-16).

We similarly checked this adjacency with H3K9me3 peaks changing signal across fetal/adult tissues. We did see a significantly-greater adjacency between significantly-DA DNase peaks and these altered H3K9me3 peaks, above general DNase/H3K9me3 adjacency (1.13 FC increase, hypergeometric test p-value < 1e-16). Of these adjacent pairs, those sharing direction (i.e., adult-biased DNase, adult-biased H3K9me3 ChIP-seq) were significantly under-represented, while those opposing direction were over-represented (1.152 FC and 1.212 FC for adult-biased DNase/fetal-biased H3K9me3 and fetal-biased DNase/adult-biased H3K9me3, respectively, hypergeometric tests comparing overlaps of sets, adjusted p-value < 1e-16). This follows with an expectation that regions gaining constitutive heterochromatic marks should lose local DNA accessibility, and vice-versa.

Next, we considered the adjacency of H3K27me3 changing signal across fetal/adult tissues. We did observe a slight, but significant, increased adjacency between significantly-DA DNase peaks and altered H3K27me3 peaks, above general DNase/H3K27me3 adjacency (1.03 FC increase, hypergeometric test p-value < 1e-16). Of these, those sharing direction (i.e., adult-biased DNase, adult-biased H3K27me3 ChIP-seq) were significantly over-represented (1.20 FC and 1.38 FC for adult/adult-biased and fetal/fetal-biased, respectively, hypergeometric tests comparing overlaps of sets, adjusted p-values < 1e-16).

Finally, we compared adjacent/overlapping (i.e., within 1 kb) developmentally-altered histone signals across different marks. For a given developmentally-altered H3K27ac peak, adjacent H3K27me3 peaks tended to also change (1.24 FC enrichment, hypergeometric test p-value < 1e-16), with regions gaining H3K27ac signal tending to lose adjacent H3K27me3 signal over development and vice-versa (1.59 FC and 1.09 FC for adult-biased H3K27ac/fetal-biased H3K27me3 and fetal-biased H3K27ac/adult-biased H3K27me3, respectively, adjusted p-values < 1e-16 and 1.9e-6, respectively). Comparing adjacent H3K27me3 and H3K9me3 developmentally-altered peaks, we observed opposing patterns, which may reflect their associations with predominantly facultative and constitutive heterochromatin, respectively. Altered H3K27ac and H3K9me3 peaks showed a small but significant degree of adjacency (~3%, 1.19 FC enrichment, hypergeometric test p-value < 1e-16), though the direction change of adjacent peaks were not consistently biased between adult/adult-biased, fetal/fetal-biased, etc., which may reflect the limited number of adjacent pairs (data not shown).

We also considered the LOLA enrichments for external histone-mark datasets, observing that adult-biased regions showed strong enrichments with ChIP-seq datasets for repressive histone modifications H3K36me3, H3K9me3, and H3K27me3 (see Supplementary Figure 5). Conversely, fetal-biased regions showed enrichments for both active (including H3K4me2/3, H3K9ac) and repressive (including H3K9me3 and H3K27me3) histone modifications.

Clock sites analysis

Given the substantial literature on changes in DNA-level methylation across both development and aging, and the observed enrichments for annotated CpG sites in the above LOLA analyses, we next looked for correspondence between our development- and age-altered region sets and CpG sites. In particular, we considered so-called 'clock sites' capable of predicting age across the entire lifespan [9–11]. Firstly, we re-confirmed the enrichment of CpG sites within developmental and age-altered DNase regions using UCSC annotated CpG sites (see Supplementary Methods), then confirmed that this enrichment held for clock sites, observing a small but significant capturing of these sites by developmentally-altered regions (40 of 353 clock sites, p-value < 1e-3 against 1000 randomized region sets). Of these regions, we saw that the fetal-biased set were enriched for overlaps with both clock sites losing methylation with age (hypo-methylated sites) and those gaining methylation with age (hyper-methylated sites), while the adult-biased set was not enriched for either set. We also saw a significant enrichment for clock sites by age-altered regions (16 of 353 clock sites, p-value < 1e-3 against 1000 randomized region sets). Of these, young-biased regions were enriched for overlaps of both hyper- and hypo-methylated clock sites, while we found no overlaps for clock sites with old-biased regions. Finally, we looked for overlaps between clock sites and our region sets at the gene-locus level – clock sites tied with particular genes (e.g., due to falling within promoter or gene-body regions) which overlap gene loci we associated with our region sets (see Supplementary Methods). This yielded significant overlaps for genes associated with developmentally-altered regions (58 genes, hypergeometric p-value = 0.005), though not those associated with age-altered regions (12 genes, hypergeometric p-value = 0.19), and we observed no significant biases in direction sharing (e.g., old-age-associated genes and hypo-methylated regions – chi-sq test p-value > 0.05) (see Supplementary Table 1).

Promoter capture datasets

To better identify biological process whose *cis*-regulatory activity are subject to change we made use of a compendium of promoter-capture Hi-C interactions [12] (see Supplementary Methods) to identify possible promoter contacts made by our region sets. We also sought to incorporate accessibility information for gene promoters (in addition to the regions contacting them), and did this by [1] intersecting gene promoters with adult- or fetal-biased regions, or [2] similar to our treatment of region accessibility changes we also assessed promoter accessibility using DNase-seq read coverage across tissue samples (Supplementary Figure 6, Supplementary Methods). Genome-wide, adult-biased regions tended to have more putative promoter contacts than fetal-biased regions, while old-biased regions tended to have less putative contacts than young-biased regions (zero-hurdle modeling, p-value << 1e-16). Gene promoters gaining accessibility are preferentially contacted by adult-biased regions, with those losing accessibility contacted by more fetal-biased regions than expected (chi-sq test, p < 1e-16), patterns which held when considering young- and old-age accessibility (chi-sq test, p < 1e-16). This bias was also true when considering gene promoter accessibility defined by intersection with our development- and age-altered region sets (see Supplementary Methods). In the context of enhancer-promoter interaction, we observed enrichments in the adult-biased set for gene-ontology terms associated with immune response, sensory perception, and keratinization (Supplementary Table 2). Conversely, fetal-biased sets were enriched for many developmental terms, as well as terms relating to cellular proliferation and TGF-B signaling (Supplementary Table 2). Echoing the fetal-biased enrichments, we found that old-biased regions were weakly enriched (adjusted p-value = 0.037) for chemokine-response terms, as well as sensory perception. However, no significant term enrichments were observed for young-biased regions and promoters.

As an additional means to consider the sets of genomic loci in which our development- and age-altered sets are distributed, we used the GREAT genome-ontology tool (see description of GREAT in Supplementary Methods). Fetal-biased regions were located near genes associated with several developmentally-related terms, such as 'animal organ morphogenesis' and 'embryo development' (Supplementary Table 2). The adult-biased region set yielded enrichments relating to immune processes, such as 'innate immune response' and 'immune effector process', as well as terms related to keratinization (Supplementary Table 2). Young-biased regions were enriched for terms relating to cell-cycling, such as 'mitotic cell cycle process'. Enrichments for old-biased regions were associated with immune processes such as 'regulation of defense response', while also hitting terms related to DNA break repair and 'negative regulation of telomere maintenance' (Supplementary Table 2). Interestingly, when intersecting the fetal/adult and young/old-biased regions we saw a number of additional GREAT terms, while many signals persisted in intersect sets (Supplementary Table 2). For example, adult-biased regions which were also more accessible in older-adult samples were enriched for the 'positive regulation of immune response' term; a signal of post-natal development of immune function would be expected

[13] and that this signal persists into old-age might suggest that we also capture signals of inappropriate immune system behavior (so-called 'inflammaging' [14]).

RNA-seq expression datasets

Given the biological signals we observed by associating our region sets with gene loci, we next looked to see if similar signals are evident with tissue expression datasets. We utilized ENCODE RNA-seq datasets [8] for fetal and adult tissues – however, given the limited availability of adult tissue samples we performed a less-stringent method for identifying genes whose expression changes over development (see Supplementary Methods). These broad sets of genes yielded similar enrichments to those seen previously on the regulatory level, with genes generally less-expressed in adult tissues enriched for terms involved in growth (e.g., cell-cycling) and chromatin regulation, while those generally more-expressed in adult tissues enriched for terms relating to immune response (e.g., 'humoral immune response'), sensory perception and keratinization (Supplementary Table 2). These gene sets significantly overlapped those genes associated with adult-biased and fetal-biased regions (all genes – 1.11 FC enrichment, hypergeometric p-value = 6.73e-10) and tended to share directionality (chi-sq test, p-value < 1e-16).

We performed a similar expression analysis using adult tissue samples, stratified by the same age categories used in our accessibility analyses, for those adult tissues available from the GTEx dataset [15] which overlapped our adult-tissue accessibility datasets (brain, heart, lung, muscle and stomach) (see Supplementary Methods). Genes generally less-expressed in older samples were enriched for terms relating to growth, including cell-cycling, mitochondrial function, and protein synthesis/turnover (Supplementary Table 2).

Conversely, genes generally more-expressed in older samples were enriched for terms relating to development, including terms such as 'ECM organization', 'ossification' and 'angiogenesis'. Whether or not this follows with the suggested role for aberrant mysregulation of developmental pathways in aging biology [16, 17] signalling pathways, is unclear however. Comparing these aging accessibility and expression-defined gene sets we did not observe significant overlaps (hypergeometric test, 1.04 FC, p-value = 0.19); this may be the result of a disconnect between epigenetic dysregulation and expression changes with aging at particular loci.

Finally, we looked for overlaps between gene expression in our fetal/adult and young/old-adult comparisons, finding that genes broadly less-expressed in adult tissues (relative to fetal) are also less expressed in older adult tissues (hypergeometric, p = < 1e-16). While we did not see significant overlap in the adult-biased/old-age-biased expression sets, those genes which did overlap were enriched for immune response terms similar to those seen in the adult-biased set (data not shown).

Divergent sequence intersection enrichments

We took an aggregated set of sequences showing increased divergence along the human lineage [18–23] and intersected these with our region sets. Subsequently, we assigned each intersection to the nearest annotated gene, and asked whether these elements are actually contacted by these nearby genes via the promoter-capture datasets we had previously integrated with our region sets. These intersections, as well as whether the nearest annotated gene shows some contact data for the indicated region, are presented in Supplementary Table 3. We highlight two example loci, one associated with the fetal-biased region set, the other with the young-biased region set (both of these sets showing general enrichments for overlaps with our aggregated sequence-divergence set, see Figure 2B and Supplementary Figure 7 and Supplementary Table 3).

A region losing accessibility in adult tissues (i.e., a 'fetal-biased' region) intersects a human-accelerated region [20] intronic to *FGF1*, a fibroblast growth factor associated with numerous developmental processes as well as tissue repair [24]; this region also has promoter-capture data to suggest contact with the *FGF1* promoter. A region losing accessibility in old-adult tissue intersects a human-accelerated region [20] intronic to the *PKNOX2* gene, and which also has promoter-capture data to suggest contact with the *PKNOX2* promoter. This region lies downstream of the variant rs590211, which has previously been identified in a GWAS of extreme longevity [25, 26].

Comparing sequence diversity between region sets

Given the patterns of our different region sets in terms of the presence of common human sequence variation (relative to genomic backgrounds and other features, see Figure 2C), we directly compared the occurrence of common variants in different sets to one another in humans, chimps and gorillas (Supplementary Table 3). Within humans, fetal-biased regions tended to have far lower variation when compared to every other set, with the exception of young-biased regions (for which the difference was insignificant). Conversely, adult-biased regions had greater variation when compared to every other set, with the exception of old-biased regions

(which had higher variation). Accordingly, old-biased regions tended to have greater variation when compared to young-biased regions. Within both chimpanzees and gorillas these differences between accessibility-altered region sets were similarly observed (Supplementary Table 3).

Developmental trait GWAS

Considering our region sets comparing fetal/adult accessibility changes, we would expect that regions (which may potentially act as regulatory elements) more accessible in fetal tissues may have more of an impact on developmental processes than those regions less accessible in fetal tissues, and vice-versa when considering processes such as tissue homeostasis (e.g., in adult tissues). Therefore, in addition to our focus on aging-associated diseases/traits, we similarly collected a set of developmental traits/disease GWAS to confirm this expected behavior with regards to developmental processes.

We observed that fetal-biased regions trended towards having greater numbers of nearby significance-thresholded SNPs (reported association p-value < 1e-6) compared to a general DNase background set across almost all traits used (with the exception of childhood epilepsy). Significant enrichments (hypergeometric test, adjusted p-value < 0.05) were limited to birthweight [27] and height [28], though this may be due to the larger number of SNPs nearby target/background sets observed with these traits (see Supplementary Table 4). Conversely, adult-biased regions trended towards having decreased numbers of nearby significance-thresholded SNPs across almost all traits used (with the exception of childhood epilepsy). Significant (hypergeometric test, adjusted p-value < 0.05) depletions were observed for birth length, maternal-effect birth weight, childhood BMI, fetal-effect birth weight, gestational-duration and height (Supplementary Table 4).

Longevity GWAS

Given the patterns of association with our altered-accessibility region sets and aging-associated diseases, we also considered four different GWAS summary-statistics datasets for parental lifespan [29, 30]. Compared to DNase regions generally, we observed that fetal-biased regions were not enriched for nearby significance-thresholded longevity SNPs (and trended slightly towards depletion). By contrast, adult-biased regions were significantly enriched for the nearby presence of such variants (hypergeometric test, adjusted p-value < 0.05). Similar to adult-biased regions, young-biased regions were significantly-enriched for two of the four longevity datasets, trending slightly with a third. Old-biased regions were neither significantly enriched nor depleted for longevity GWAS signals, unlike what was seen for aging-associated diseases in general.

Effect-size distributions

In addition to determining whether or not a given variant can act to significantly impact disease heritability, the epigenetic state of a region may also determine the magnitude of this impact. For those variants falling nearby developmentally-altered regions, we also considered the reported effect size for their respective diseases. We observed 40 diseases for which variants nearby adult-biased regions had significantly greater absolute effect sizes, compared to only 3 diseases for which nearby variants had significantly reduced effect sizes (Supplementary Table 4). Given that lowering significance thresholds can increase the amount of heritable variation explained for a given trait, we also considered the effect size distribution of all variants falling near our region sets. Nearly all diseases had biased distributions, with the majority (106 of 127) having larger absolute effect sizes for adult-biased regions (Supplementary Table 4).

Per-disease enrichment testing

For each GWAS set, we defined single nucleotide polymorphisms (SNPs) with strong association signals (p-value < 1e-6) and looked for the presence of nearby epigenetically-altered regions (Supplementary Methods). We observed that, generally, our accessibility data were enriched for nearby variants (Supplementary Table 4), which is expected given that these data will capture non-coding regulatory elements which are concentrated for GWAS signal [31]. First considering accessibility change between fetal and adult tissues, we found that of this general enrichment adult-biased regions associate with a significant proportion of variants across a majority of diseases, while fetal-biased regions associated with significantly less variants than expected (Supplementary Table 4).

We next considered the effects of age-associated accessibility changes on age-related disease GWAS signals. Unexpectedly, we observed that old-biased regions, unlike adult-biased regions, are actually depleted of nearby strong variants across the majority of age-related diseases, while young-biased regions are enriched for such signals (Supplementary Table 4). Furthermore, we found that for intersections of development and age-altered regions that this age-associated behavior outweighs the earlier development behavior. Of the general enrichment in adult-biased regions, a significant portion of this can be attested to

adult-biased regions which lose accessibility in old-age (i.e., young-biased regions), while adult-biased regions which gain accessibility in old-age are actually depleted for such signals (Supplementary Table 4). Conversely, of the general depletion in fetal-biased regions, an insignificant portion of this can be attested to fetal-biased, old-biased region intersects (hypergeometric test adjusted p-value > 0.05), while those strong variants which do fall nearby fetal-biased regions tend to be concentrated near those regions also considered young-biased (Supplementary Table 4).

Gene set ranking tests

To confirm the behavior of our within-disease gene ranking strategy (see Supplementary Methods), we defined a positive-control gene set which would be expected to be strongly-associated with aging diseases using the GO term 'homeostatic process' (GO:0042592). When compared to randomly-sampled gene sets this set had significantly-increased cross-disease gene rankings (Supplementary Table 4). As a negative control, we took a gene set which would not be expected to be strongly associated with aging diseases, those involved in the development of reproductive structures (GO:0003006). This set did not have significantly-increased cross-disease gene rankings.

When looking at gene sets defined by RNA-seq data, we found that genes generally less expressed in adult tissues (fetal-biased) were enriched for cross-disease GWAS signals, while genes more expressed in adults were actually significantly depleted for such signals (Supplementary Table 4). Gene loci with increased expression in older adult tissues were enriched for GWAS signals, as were loci with decreased older-adult expression – suggesting the possibility that a mixture of genes increasing and decreasing expression over time may additively contribute to aging disease biology. It is worth noting that the fetal-biased (expression) genes significantly overlap with young-biased genes (defined by expression), possibly explaining the shared enrichment for GWAS signals, while adult-biased and old-biased genes (by expression) did not significantly overlap - though this overlap set itself, containing a number of immune-related genes, was enriched for GWAS signals (data not shown).

Cross-disease gene ranking genome-wide

It has been suggested that the highly polygenic nature of complex traits and diseases reflects cumulative regulatory modification to a 'core' set of genes who functions most proximately in relevant biology (i.e., the 'Omnigenic model') [32]. If this is indeed the case, we would expect that, for age-associated diseases across multiple tissues, those genes most involved with general pan-tissue aging processes would represent a 'core' set of genes whose dysregulation contribute to heritable risk across aging-associated diseases. We took an unbiased approach to relevant gene discovery, identifying a putative set of 'core' aging-related genes solely on the basis of aggregate GWAS signals genome-wide (without considering accessibility change) (Supplementary Methods). The resulting set of genes was enriched for terms relating to keratinization, sensory perception of smell, and neuron-related terms (e.g., glutamate receptor signaling) (Supplementary Table 4). We previously observed the former two terms in our region-association analyses, which may suggest that the effects of gene clustering (e.g., clustering of keratin genes, olfactory receptors) may bias our locus ranking method. We note that similar enrichments for these terms in our fetal/adult RNA-seq analyses were observed (Supplementary Table 2), though whether this GWAS signal – expression - accessibility concordance is due to broad changes in accessibility and subsequent transcription in gene clusters is unclear. The fact that we observe consistent enrichments for keratinization and smell perception using the RRA-based method may indicate that this method is particularly sensitive to gene-clustering effects.

Our per-disease GWAS analyses suggested the importance of altered epigenetic state, particularly that which occurs between young/old adult tissues, in considering the risk association of variants with aging-associated diseases. Therefore, we looked for consistent cross-set ranking using variants occurring nearby age-association regions (Supplementary Methods). Again, applying an RRA-based method to different accessibility region sets yielded broadly similar terms relating to keratinization and smell perception. However, when applying a functional gene-set enrichment analysis (FGSEA)-based method, we saw greater differentiation in enrichment results. Ranking genes based on variants nearby fetal-biased regions yielded terms relating to developmental processes (e.g., embryonic development, skeletal system morphogenesis), while considering adult-biased regions again yielded enrichments for keratinization. Young-biased regions yielded enrichments for 'histone deacetylation' (discussed in more detail in main text), as well as terms relating to viral infection (e.g., 'viral gene expression'). Finally, old-biased regions yielded the previously-seen enrichments for smell perception and keratinization, though also including enrichments for immune processes (e.g., 'antibacterial humoral response') and DNA methylation.

Intersection set comparisons

We compared our developmentally-associated and age-associated regions directly, here explicitly comparing

age-associated regions with developmental regions not changing with age as a more stringent contrast (Supplementary Methods). Here we also saw the much-stronger biasing of young/old-biased regions; old-biased regions associating with significantly less cross-trait heritability than fetal-biased, while young-biased regions associated with significantly more heritability than all other sets (Supplementary Table 4). Comparing development and age-altered intersection sets, we found that the strong disparity in GWAS associations between the young -and old-biased region sets outweighed the differences between the fetal- and adult-biased region sets. For example, the young-biased /fetal-biased set had the second-highest average cross-trait association, despite fetal-biased regions generally being associated with weaker GWAS signals in the previous fetal/adult comparison. Conversely, the weaker GWAS signals associated with the old-biased region set outweighed the generally-higher signals of the adult-biased region set, actually having a lower average cross-trait association than fetal-biased regions not significantly changing accessibility in the young/old accessibility analysis (see Supplementary Table 4).

Supplementary Methods

Processing accessibility datasets

DNase-I hypersensitivity datasets were obtained from ENCODE [33] for eight different fetal and adult tissues (adrenal gland, brain, heart, lung, muscle, skin, spleen and stomach), retrieving sorted, duplicate-filtered mapped read files (.bam) via the ENCODE web portal [8] in hg19 format. ENCODE file accession codes and metadata for individual samples are provided in Supplementary Table 1. To define reproducible hypersensitivity sites within each tissue, we applied the IDR statistical test [34] (version 2.0.3). Briefly, the IDR method identifies overlaps in peak calls across pairs of sample replicates by comparing ranked peak lists (using MACS2 q-value) to define a reproducibility score curve. These paired peaks are then assigned a pointwise score based on this curve. Peaks are sorted, with those falling below an "irreproducible discovery rate" (IDR) threshold (here defined as 0.05) are taken as the final reproducible peak set across replicates. For each sample, peaks were called with MACS2 [35] (version 2.1.1.2) using the following parameters: '-f BAMPE --nolambda' and '-f BAM --no-model --shift -100 --extsize 200' for paired-end and single-end experiments, respectively. An IDR threshold of 0.05 was applied, with resulting filtered peaksets combined using the 'bedtools merge' function from bedtools [36] version 2.29.1 in those instances where both single-end and paired-end experiments for a given tissue were obtained and processed separately with MACS2/IDR. Peak sets were pooled across individual tissues for a given set of samples (e.g., fetal IDR peak calls) and subsequently pooled using 'bedtools merge -c 1 -o count', filtering for peaks which were overlapped at least twice (i.e., called in at least two different tissues). Finally, peaks were fixed to a constant size by padding 75bp from the centre of each peak (150bp regions), this size based on the average size of called peaks across different sets. These tissue-consolidated peak sets, defined for adult and fetal samples, were then pooled and merged with 'bedtools merge', fixing the final set of peaks to a constant size of 150bp. DNase read-coverage was then quantified within this peak set using the 'bedcov' function of samtools [37] (version 1.5) for each mapped .bam file initially obtained, resulting in a final matrix of read coverages for all peaks across all tissue samples.

Read coverages were imported into R [38] version 4.0.2 via the limma [39] package version 3.46; coverages were subsequently normalized using the TMM method using the 'calcNormFactors' function from edgeR [40] version 3.32.1. Two different models for comparing differential-accessibility across adult/ fetal samples were used. Firstly, we considered within-tissue differences in accessibility with time (i.e., the interaction between tissue*time). Secondly, we considered across-tissue differences in accessibility with time to by accounting for all tissues simultaneously (i.e., using a model of tissue + time). For both models, we performed a standard limma-based analysis using the functions 'voomWithQualityWeights' (setting normalized = 'none', all others left to defaults), 'lmFit', 'makeContrasts', 'contrasts.fit' and finally 'eBayes'. The final sets of statistics comparing differential-accessibility across all peaks were extracted for individual tissues (using the results from the first model) and across tissues (using results from the second model) using the 'topTable' function, applying a Benjamini-Hochberg [41] FDR correction to define peaks significantly changing accessibility (differentially-accessible, DA) (adj. P-val < 0.05). Subsequently, the peaks defined as DA across tissues with time were compared to those defined as DA within tissues using R, with the resulting intersections visualized using ggplot2 version 2.3.3 and gridExtra version 2.3 as shown in Figure 1C. Per-peak DA statistic results for the cross-tissue fetal/adult comparison are provided in Supplementary Table 1, Sheet 2.

Visualizing genomic distribution of epigenetic change

To visualize the distribution of regions exhibiting altered accessibility across the genome (i.e., the DA

peaks defined above), we defined genome-wide windows using the bedtools 'makewindows' function, then intersected our peak sets via bedtools intersect. The resulting tracks were loaded into R using the rtracklayer [42] package version 1.50. To visualize the density of altered peaks generally, for each chromosome the number of regions (adult- and fetal-biased) falling within windows were summed per-window, and subsequently smoothened using the 'smooth.spline' function in R. We subsequently defined a red/blue colour scale based on these smoothened counts. In addition this general density, we also calculated the difference in the occurrence of adult-/fetal-biased peaks/regions within windows, smoothening these values within a given chromosome. We used the karyoploteR [43] package version 1.16 to plot karyotypes for all chromosomes, plotting the density of DA peak occurrence as a red/blue density bar, while the differences in adult-/fetal-biased peak occurrence were visualized as a curve (with diagonal red line indicating no difference in smoothened values). These plots for the first ten autosomes are shown in Figure 1B, with the full set of autosomes shown in Supplementary Figure 2.

Defining age-altered regions

In order to compare DNase-I accessibility across adult samples, the set of adult samples used in the above analysis was subsequently split into those from individuals younger than 50 ('young-adult') and those older ('old-adult'), this age representing a roughly equal split of sample numbers. Not all tissues used in the initial fetal/adult comparison were represented in these age-stratified sets – thus we restricted the tissue comparisons to brain, heart, lung, muscle and stomach tissues. The read coverage matrix defined above was restricted to just these adult samples. Given our interest in considering accessibility change with age in the context of earlier fetal/adult epigenetic change, we further subset the coverage matrix to consider age-altered accessibility in peaks defined as DA between fetal/adult samples (adj. P-val < 0.05). The resulting matrix was again loaded into R using limma, with the subsequent analyses performed similarly to that described above – considering two different models (within-tissue and across-tissue aging differences) to compare young/old samples. We finally compared within- and across-tissue DA peak definitions using R, though due to the reduced sample sizes for performing the within-tissue comparisons there was limited overlap of significant results despite agreement in direction-of-effect (data not shown). Per-peak DA statistic results for the cross-tissue young/old-adult comparison are provided in Supplementary Table 1, Sheet 3.

Generating accessibility heatmaps

To visualize accessibility across different fetal/adult tissues (as see in Figure 1A), we took the TMM-normalized counts matrix defined above and converted counts to counts-per-million (CPM) using the 'cpm' function from edgeR with the following parameters: 'log = T, prior.count = 3'. This CPM matrix was then subset to those peaks which were significantly DA (adj p. < 0.05). For visualization, we then sorted all peaks by their limma-calculated t-statistic, taking the top 1000 peaks showing the strongest increase/decrease in accessibility (between fetal/adult). Normalized CPM values were averaged across individual replicates for a given tissue, with the resulting matrix finally z-score-normalized (per-peak), and plotted using the ComplexHeatmap [44] package version 2.6.2. A similar method was performed using peak sets defined in the above age-altered region analysis, as shown in Supplementary Figure 3. Additionally, we performed the above analyses for individual replicates of a given tissue (e.g., heart samples), as shown in Supplementary Figure 1.

Comparing development and age-associated changes

Peak sets defined as differentially-accessible in either the fetal/adult, or young-adult/old-adult comparisons were read into R and compared for overlaps visually using the VennDiagram [45] package version 1.6.20, as seen in Figure 1D. The directionality of peak overlaps, i.e., fetal-/adult-biased vs. young/old-biased, were compared using a chi-sq test in base R, the results of which are shown in Supplementary Table 1, Sheet 3.

Assigning epigenetic states to region sets

To define the epigenetic context within which our development- and age-altered regions fall, we utilized genome-wide assignments of epigenetic state as defined by the Roadmap consortium [3]. This employs a Hidden Markov Model to analyze epigenetic data, including chromatin modification (ChIP-seq) and accessibility (DNase-seq) data, for a given sample and assign one of several possible epigenetic states for individual 200bp segments genome-wide. The Roadmap dataset contains several such genome-wide state definitions for different tissue and cell-line samples (e.g., skin, brain, etc.). We downloaded state definitions for the 25 state model, which incorporates imputed data for 12 marks, for 127 reference genomes, subsetting to those obtained from adult tissue samples. For each individual 200bp segment we then considered the assigned epigenetic state of this segment across all samples – given our pan-tissue approach to chromatin accessibility changes, we defined an 'adult-majority' state assignment based on the assigned state recurrent across the majority of samples.

For simplicity, we collapsed down similar definitions (e.g., 'Active Enhancer 1' and 'Active Enhancer 2' being considered 'Enhancer') (see Supplementary Figure 4 for final reduced set of states). Our sets of development- and age-altered regions were subsequently intersected with these genome-wide states using bedtools intersect, counting the number of segments intersected that belonged to different categories. This was done considering the unique numbers of segments (i.e., segments intersected by more than one region were only counted once) – allowing for repeat segment counting did not substantially alter enrichment results (data not shown). Finally, for each epigenetic state we compared the number of segments intersected by a given region set (e.g., old-biased regions) to the total number of segments assigned this state genome-wide using the phyper function from base R. P-values from these hypergeometric tests were adjusted for the number of states tested using the Benjamin-Hochberg method – enrichment/depletion results were similar when considering all 25 epigenetic states (data not shown). Enrichments/depletions for each region set were plotted as logFC values using ggplot2 (see Supplementary Figure 4).

LOLA enrichment analysis

The LOLA software [5] version 1.12 was used to test for significant enrichments of our region sets with publicly-available sets of genomic annotations and epigenetic datasets. For these sets of developmentally-altered regions, we used the set of DNase-I regions used in the initial differential-accessibility analysis (i.e., reproducible peaks pooled from adult and fetal tissues) as the background region set (to account for the possibility of inherent biases of open-chromatin regions towards certain datasets/annotations). To visualize these enrichment results, significant enrichments (defined as calculated q-value < 0.05) were first sorted by odds-ratio values, then filtered to remove similar entries (e.g., replicate datasets for a given histone mark in a given cell-type). Furthermore, given our interest in epigenetic and genomic annotation terms, we further filtered significant results to retain histone-mark datasets and annotations. Of this set, the top 20 terms (by odds-ratio) were plotted using ggplot2. For LOLA enrichments using young- and old-biased region sets, the set of regions used in the initial young/old comparison (i.e., peaks differentially-accessible across the fetal/adult comparison) was used as the background region set.

Comparing developmental epigenetic changes with bivalent developmental promoters

A set of bivalent promoter domains defined by Yan et al. 2016 [1] using ChIP-seq datasets generated from fetal brain, heart and liver samples was obtained and pooled (Supplementary Table 2 of Yan et al.). To establish a genome-wide background for promoters, all hg19 Refseq gene TSS were obtained from the UCSC genome browser [46] and padded 2kb up/downstream, following the definition of promoter regions used in Yan et al. The adult-biased and fetal-biased region sets were subsequently intersected with these promoter regions using bedtools intersect. The number of bivalent promoters intersected by development-altered regions were compared to the total number of promoters intersected using the 'phyper' function of base R to test for enrichment/depletion. As an additional validation, we randomly sampled promoter regions genome-wide to match the number of promoter regions intersected by adult/fetal-biased sets, generating a background of 1000 sets of randomized promoters for each. The number of bivalent domains intersecting these randomized sets was compared to the number of bivalent domains intersected by adult/fetal-biased regions using the 'pnorm' function in base R, confirming the depleted intersections of adult-biased regions and enriched intersections of fetal-biased regions (data not shown).

Processing ChIP-seq datasets

For our analyses comparing patterns of chromatin accessibility with histone modifications, histone mark ChIP-seq datasets were obtained from ENCODE for H3K27ac, H3K27me3, and H3K9me3 marks. These datasets were obtained from fetal and adult tissue samples for tissues overlapping those used in the DNase accessibility analyses above – see Supplementary Table 1 for accession codes and metadata. ChIP-seq peaks called by the ENCODE pipeline were obtained along with mapped (hg19) bam files. Peak calls from biological replicates for individual tissues were consolidated by requiring that peaks be replicated in 2/3 of samples to be considered replicable for downstream analyses. Overlapping peaks were merged and fixed to constant size of 400bp (for H3K27ac) and 300bp (for H3K9me3 and H3K27me3) (size based on average peak call size in individual replicates) using bedtools. Replicable peaks were then pooled across tissues, and subsequently pooled across fetal/adult samples, overlapping peaks again merged and fixed to a constant size.

In order to address the expected concordance between called DNase-I hypersensitivity sites and the presence of nearby histone ChIP-seq peaks, replicable DNase-I hypersensitivity sites defined for fetal and adult tissues were taken and compared with replicable ChIP-seq peaks looking for adjacency. This was done using the bedtools 'slop' function, looking for the presence of ChIP-seq peaks within a 1kb window (centred on each

ChIP-seq peak) of a given DNase peak. Nearby adjacency was checked for matched tissues – e.g., H3K27ac peaks defined in adult muscle tissue were compared with DNase peaks defined in adult muscle tissue, with the percent of called DNase peaks having nearby ChIP-seq peaks calculated.

We then applied a pipeline similar to that described above in the treatment of DNase datasets.

ChIP-seq read-coverage was quantified within the final peak set using the 'bedcov' function of samtools (version 1.5) for each mapped .bam file initially obtained, resulting in a final matrix of read coverages for all peaks across all tissue samples.

Read coverages were imported into R via the limma package; coverages were subsequently normalized using the TMM method using the 'calcNormFactors' function from edgeR. Given the reduced number of ChIP-seq samples available for any given fetal/adult tissue comparison, only pan-tissue defined peaks were used in subsequent comparisons with altered-accessibility regions (results for individual tissue comparison models not shown). We performed a standard limma-based analysis using the functions 'voomWithQualityWeights' (setting normalized = 'none', all others left to defaults), 'lmFit', 'makeContrasts', 'contrasts.fit' and finally 'eBayes'. The final sets of statistics comparing differential-accessibility across all peaks were extracted from the pan-tissue model using the 'topTable' function, applying a Benjamini-Hochberg FDR correction to define peaks significantly changing accessibility (differentially-accessible, DA) (adj. P-val < 0.05).

Methylation-site analysis

The set of methylation sites used in defining the methylation-aging clock from Horvath 2013 [47] were obtained (Additional File 3). These sites were separated into those either increasing or decreasing methylation status with age, with the resulting sets of genomic coordinates lifted-over from hg18 to hg19 using the 'liftOver' utility from UCSC [48]. These sites were then intersected with our sets of development- and age-altered regions using regioneR [49] (version 1.8.1) using the 'permTest' function, generating 1000 randomized region sets as a background using the 'circularRandomizeRegions' option and the 'count.once' flag, with all other options set to defaults. Significance was assessed at $p < 0.05$ (Supplementary Table 1). For hypergeometric testing at the gene-locus level, gene annotations for hyper/hypo-methylated sites (as defined in the Horvath dataset) were intersected with the sets of genes associated with our different region sets (defined as described below under 'Defining Region-Associated Genes'), using the 'phyper' function in base R to compare the numbers of overlaps relative to all genes captured in the promoter-capture datasets used (see below). Directional bias (e.g., old-age-associated genes and hypo-methylated regions) was tested using the 'chisq.test' function in base R.

Promoter accessibility change processing

All hg19 Refseq gene TSS were obtained from the UCSC genome browser [50] and padded 1kb up/downstream to define promoter regions. For each promoter region, DNase read coverage was calculated for all fetal and adult tissue samples using the 'bedcov' function of samtools (version 1.5) for each mapped .bam file initially obtained, resulting in a final matrix of read coverages for all peaks across all tissue samples. A limma-voom analysis to define promoters whose accessibility were significantly different across tissues in the fetal/adult comparison was performed, similar to that described above in our initial DNase-I region analysis. Significance was defined as adjusted p-value < 0.05. The same analysis was performed using age-stratified adult samples in order to define promoter regions changing accessibility across tissues (i.e., age-altered promoter regions). To visualize promoter accessibility across fetal/adult and young/old-age tissues (as seen in Supplementary Figure 6), the promoter read-coverage matrices was treated similar to that described above. Given the large number of promoters defined as differentially-accessible, we also defined a more stringent definition of changing promoter accessibility. We intersected promoter regions with our region sets using bedtools – that is, a promoter intersected by a fetal-biased region was considered a fetal-biased promoter, and similarly for age-altered region intersections.

Promoter contact processing

Promoter-capture data was obtained from Jung et al., 2019 [12], particularly the file 'GSE86189_ all_interaction.po.txt.gz' which contains processed information on regions contacting the promoters assayed in this study. This dataset was generated from promoter-capture assays across a number of different tissues and cell-types; given our pan-tissue approach, we considered all data (with the exception of OV2, as we excluded sex-specific tissues from all previous obtained datasets). To generate a set of genomic regions which show evidence of contacting gene promoters, we filtered interacting regions to those which contacted their respective promoters in at least two different tissues/cell-types. This moderate filter was used to exclude those regions for which interactions appear to be exclusive to one dataset, while allowing for regions that do not show such exclusivity. We then intersected

these interacting regions with our sets of altered regions in order to suggest the possible regulatory roles that our sets may have (in terms of regulating possible target genes).

Preferential contacts:

We first tested to see whether adult-biased or fetal-biased regions differed in their tendency to contact gene promoters. Interacting regions were labeled as adult-/fetal-biased based on these intersections, and the numbers of said regions interacting with promoters was tested using hurdle modelling as implemented using the 'hurdle' function from the pscl [51, 52] package in R (version 1.5.2). A binomial model was applied for the initial hurdle/zero-counts step, with the subsequent counts modeling done using a negative binomial regression model. Tukey post-hoc testing was performed using the emmeans package version 1.5.5 in R. A similar analysis was performed using young- and old-biased regions.

To test whether adult- or fetal-biased regions preferentially intersected with promoter-capture regions contacting promoters either gaining or losing accessibility (differential accessibility as defined above, adjusted p-value < 0.05), we used the 'chisq.test' function in base R for both the adult/fetal comparison as well as young/old-age. As a more stringent test, we performed a similar chi-sq test for promoters gaining/losing accessibility as defined by intersections with development- or age-altered regions.

Defining region-associated genes

To associate genes with our region sets to suggest regulatory patterns (e.g., adult-biased regions contacting a promoter with increased accessibility across adult tissues relative to fetal), we took the set of promoters for which differential-accessibility was significant in the fetal/adult (or young/old-age) comparison (adjusted p-value < 0.05) and considered the regions putatively contacting these promoters, as defined above. Given that a given promoter may be contacted by regions both gaining and losing accessibility (e.g., adult- and fetal-biased regions) (there being few genes contacted by exclusively one set of regions – data not shown), a chi-sq test was performed per-promoter to test for significant bias in the number of putatively-contacting regions (i.e., a fetal-biased promoter with a greater proportion of putative fetal-biased region contacts), controlling for the global proportion of putative contacts (given that we observed biases in different region sets for having more putative contacts given the above zero-hurdle modelling analyses). These multiple tests were corrected using a Benjamini-Hochberg correction, with genes showing a significant bias in putative contacts sharing direction with promoter accessibility change retained for subsequent gene-set enrichment analyses (see below, Supplementary Table 2).

GREAT: GREAT [53] takes an input set of genomic regions along with a defined ontology of gene annotations; firstly, it defines regulatory domains for all genes genome-wide, then measures the fraction of the genome covered by the regulatory domains of genes associated with a particular annotation (e.g., 'cartilage development'). These fractions are used as the expectation in a binomial test counting the number of input genomic regions falling within a given set of regulatory domains, which results in the reported significance of association between an input region set and a particular gene ontology term. GREAT also performs a more traditional gene-based hypergeometric test to test for significance of region set-ontology association. The program returns a set of enriched ontologies sorted by the joint rankings of FDR-corrected binomial and hypergeometric tests, as reported here in our Supplementary Tables. For each given set of ontologies (e.g., GO Biological Processes) we took the set of ranked terms and filtered for those having either an FDR-corrected binomial or hypergeometric p-value of < 0.05; this was done as, given our large peak sets, the hypergeometric test can become saturated (hence, the option to show enrichments significant by the region-based binomial with the GREAT online service). The top thirty filtered terms were then subset and are provided in Supplementary Table 1.

Gene-set enrichment analyses

Genes associated with our different region sets (as described above) were tested for enrichment in different GO Biological Process terms using the 'enrichGO' function from the clusterProfiler [54] package version 3.16.1. The background gene set was defined as all genes for which promoter-capture data was available for use in our above region-gene association processing. Semantically-similar enriched GO terms were subsequently collapsed using the 'simplify' function from clusterProfiler, using default settings. The top enriched GO terms (sorted by adjusted p-value) for each region-associated gene set are reported in Supplementary Table 2, limiting to the top twenty significant (adjusted p-value < 0.05) terms. Similar results are shown for gene sets defined using expression datasets (Supplementary Table 2).

ENCODE fetal/adult RNA-seq processing

Processed per-gene quantification files, as generated by the ENCODE pipeline, were obtained from the ENCODE

web portal [8] (see Supplementary Table 2 for file accessions). Given the limited availability of adult tissue samples with which to perform a differential-expression analysis, we instead defined a less-stringent method to look for broad changes in expression of genes across tissues, as follows. For each individual tissue, replicates for adult and fetal samples were collapsed by calculating the geometric mean of expression values for each gene. The difference in average expression for each gene was then calculated, with all expressed genes subsequently ranked by these differences. The gene-set ranks for each individual tissue comparison were then aggregated using the 'aggregateRanks' function from the RobustRankAggreg library version 1.1 [55]. Briefly, this method considers the ranking of genes across multiple conditions, detecting genes that are ranked consistently higher than expected given a null hypothesis of uncorrelated ranked sets by assigning a per-gene significance score. We applied this method to genes ranked based on differences calculated as (adult – fetal) as well as (fetal – adult), defining our final sets of 'broadly adult-biased' and 'broadly fetal-biased' genes using an RRA significance cutoff of < 0.05. Overlaps of these gene sets with those defined above based on our region sets was done in R, testing for significant overlap with the 'phyper' function, as well as biases in the direction of these overlaps (i.e., adult-biased by region-association, adult-biased by RRA RNA-seq) using the 'chisq.test' function.

GTEx young/old-adult RNA-seq processing

The following processed RNA-seq quantification files were obtained from the GTEx web portal [15]: GTEx_Analysis_2017-06-05_v8_RNASeQCv1.1.9_gene_reads.gct, GTEx_Analysis_v8_Annotations_SubjectPhenotypesDS.txt, GTEx_Analysis_v8_Annotations_SampleAttributesDS.txt. The scripting written for processing this initial metadata was modeled after similar code used in a study of age-associated expression changes that also made use of the GTEx dataset [56]. Samples were subset to just those used in the young-age/old-age accessibility comparison; brain (Brain - Cerebellum), heart (Heart – Left Ventricle), lung (Lung), muscle (Muscle - Skeletal) and stomach (Stomach). Similar to Benayoun et al., the set of human protein-coding genes was obtained from UCSC [50] (Homo_sapiens.GRCh38.pep.all.fa) and intersected with the subset GTEx expression matrix. Similarly, we subset the GTEx matrix to include only male individuals, though testing yielded similar sets of differentially-expressed genes when considering both sexes (data not shown), and filtered for samples having genotype data as well as RIN scores >= 5. We used the same definitions for 'young-age' (< 50) and 'old-age' (> 50) as in the above accessibility analyses.

We utilized similar processing steps as those outlined above in our young/old-age accessibility analyses. The subset expression matrix was imported into R version 4.0.2 via the limma package version 3.46, applying a quality filter by requiring that genes have an expression value of at least 1 counts-per-million in at least three different samples. The filtered matrix was then normalized using the TMM method via the 'calcNormFactors' function from edgeR version 3.32.1. Two different models for comparing differential-accessibility across adult/fetal samples were used. Firstly, we considered within-tissue differences in accessibility with time (i.e., the interaction between tissue*time). Secondly, we considered across-tissue differences in accessibility with time to by accounting for all tissues simultaneously (i.e., using a model of tissue + time). For both models, we performed a standard limma-based analysis using the functions 'voomWithQualityWeights' (setting normalized = 'none', all others left to defaults), 'lmFit', 'makeContrasts', 'contrasts.fit' and finally 'eBayes'. The final sets of differential-expression statistics extracted for individual tissues (using the results from the first model) and across tissues (using results from the second model) using the 'topTable' function, applying a Benjamini-Hochberg FDR correction to define genes significantly changing expression (differentially-expressed, DE) (adj. P-val < 0.05). Subsequently, the DE genes defined across tissues with time were compared to those defined as DE within-tissues using R, with the majority (> 60%) of pan-tissue-defined DE genes also considered DE in at least two different tissues (data not shown).

Overlaps of pan-tissue-defined DE genes with those defined above based on our young-/old-biased region sets was done in R, testing for significant overlap with the 'phyper' function, as well as biases in the direction of these overlaps (i.e., old-biased by region-association, old-biased by GTEx RNA-seq) using the 'chisq.test' function.

Human-divergent sequence analyses

We took an aggregated set of sequences showing increased divergence along the human lineage [18–23] (see Supplementary Table 3, Sheet 2) and intersected with our regions sets (e.g., fetal-biased regions), along with ATAC-seq data obtained from a separate adult post-mortem brain tissue datasets [57], as well as a previously-published B-lymphocyte dataset [58], to act as controls. GM12878 ATAC-seq data was obtained from GEO datasets (GSE47753) as raw .fastq files (for 50K samples); reads were subsequently mapped to hg19 using the ATAC-seq processing pipeline described in Richard et al [59], with IDR replication performed for n = 4 replicates. Adult brain open-chromatin regions were

obtained from the Brain Open Chromatin Atlas (BOCA) [57], downloading the file 'https://bendlj01.u.hpc.mssm.edu/multireg/resources/boca_peaks.zip'. Called peaks were pooled across different cell types using the 'bedtools merge' function. To account for differences in set size when performing intersections, the number of intersections for any given region set were calculated as intersections/bp of sequence in said set. A background distribution was made by generating 1000 random region sets consisting of 100,000 regions (based on the general set size of our altered-accessibility sets, again accounting for total bp of sequence in each randomized set) with a constant length of 150bp via the bedtools 'random' function. These background sets were subsequently intersected with our set of human-divergent sequences to establish a background distribution of randomized intersection counts/bp. The distribution of intersection/bp values for this background set was assessed using the 'qqnorm' (R base, version 4.0.3) and 'qqPlot' (car [60] version 3.0.8) functions – no obvious deviations from a normal distribution were observed. Additionally as a more stringent significance test, we utilized the fitdistrplus [61] package (version 1.1.1) to determine a possible alternative distribution to fit the data. The 'descdist' function was initially used to assess curve behavior; goodness-of-fit statistics (from the 'gofstat' function) for gamma, beta, exponential, and log-normal distributions were subsequently compared, with the beta-distribution subsequently selected (this choice also being appropriate given the fractional nature of the datapoints [62]. Beta distribution parameters ('shape1' and 'shape2' in the R implementation of 'pbeta') were fit using a bootstrap method ('bootdist' from 'fitdistrplus'), with the median parameter estimates from 1000 samples used to define the distribution for significance testing of target set intersections/bp values with 'pbeta' (upper-tail p-values). Results were subsequently adjusted using BH correction, along with those obtained using the normal CDF distribution ('pnorm' in base R). Regions intersecting human-divergent sequences were associated with the closest annotated TSS with the HOMER (version 4.11) [63] 'annotatePeaks.pl' script. Subsequently, these regions were merged with the promoter-capture datasets described above, indicating those regions for which contact data is suggestive of possible interactions with the nearest gene promoter (Supplementary Table 3).

Cross-species sequence conservation within region sets

Per-bp phyloP20ways conservation scores [64] were obtained from the UCSC table browser [50] for the hg19 genome. For a given region, scores were averaged over the length of all bp using the 'bigWigAverageOverBed' utility from UCSC [48]. Scores across all regions in different sets were compared using the 'pairwise.wilcox.test' function in base R, applying a BH post-hoc correction (see Supplementary Table 3). Similar comparison results were observed when using a broader 100-ways alignment score (data not shown). For visualizing distributions of scores across sets (as shown in Figure 2A), the region-averaged phyloP scores for different sets were plotted using the 'density' function in base R with default settings.

The sets of altered regions were also compared to those DNase regions considered in our accessibility analyses which did not significantly change in the fetal/adult comparison to act as a control dataset. Region-averaged values for target and control sets were compared using the 't.test' function in base R for a one-sided comparisons. This was done for developmentally-altered region sets, as well as age-altered region sets (the control for the latter being those regions in the age-accessibility analysis which did not significantly change between young/old-age tissue samples) (see Supplementary Table 3, Sheet 1).

Species diversity patterns within region sets

Zero-hurdle modelling

Variation data from the 1000 Genomes Project phase 3 (1KGP) [65] (n = 2504 individuals) in .vcf.gz format was obtained and intersected with our region sets using tabix [66] (version 1.9) to obtain variants occurring within these altered-accessibility regions. Chimpanzee (n = 25) and gorilla (n = 31) sequence data was similarly obtained via the Great Ape Genome Diversity Project (GADP) [67]. Peak sets were lifted-over from hg19 to hg18 for use with the GADP datasets with the UCSC 'liftover' utility and relevant liftover chain file. Resulting subset VCF files were converted to tab format with the following Unix command, using bcftools [68] (version 1.8):

bcftools query -f '%CHROM\t%POS\t%ID\t%REF\t%ALT[\t%SAMPLE=%TGT]\n' -o out.vcf in.vcf.

Variant data for all region sets were down-sampled to n=25 (with replacement, 5 resamples for gorilla and 200 re-samples for the human set) in order to match sample size for all comparisons based on the least-sampled species (chimp), using a custom R script.

Common variants were defined using a minor allele frequency (MAF) threshold of >= 0.05 for all datasets, filtering tab-formatted files using a custom Python script. Counts data was defined as the number of variants intersecting a given region and were averaged over resampled variant sets (see below). Counts data across apes were then compared within a given region set (e.g., young-age regions) to compare intra-species diversity within sequences. Hurdle modeling was used to test for

significant differences in both total number of sequences containing variants (hurdle) as well as degree of variation between species (counts); implemented using the 'hurdle' function from the pscl [51, 52] package in R (version 1.5.5). A binomial model was applied for the initial hurdle/zero-counts step, with the subsequent counts modelling done using a negative binomial regression model. Tukey post-hoc testing was performed using the emmeans package in R (version 1.4.7) for both hurdle/zero-counts and counts models, with significance assessed at adjusted p-value < 0.05 (Supplementary Table 3). Additionally, region sets were compared to one another (e.g., fetal-biased vs. adult-biased regions) within a given species using the above methods.

In order to look at sequence constraint of our region sets within humans, a background distribution was made by generating 1000 random region sets consisting of 100,000 regions (based on the general set size of our altered-accessibility sets) with a constant length of 150bp via the bedtools 'random' function. These sets were subsequently pooled, sorted, and merged using bedtools, with the resulting bed file used to extract variants from the 1KG3 set with tabix (version 1.9). The pooled set of altered-accessibility regions was also used to extract variants from the 1KG3 set. We also considered intersection sets in this analysis (e.g., young-biased / adult-biased regions, etc.).

Additionally, several genomic features were extracted from the HOMER (version 4.0.4) set of genomic annotations provided with the program, including the following sets: exon, intronic, promoter-TSS, and TTS. Regions from RepeatMasker were also obtained from the UCSC Table Browser. These additional sets were used to extract variants from the 1KG3 set. The resulting files were filtered for duplicate variants and subsequently MAF >= 0.05 with bcftools (version 1.8). Variants falling within particular regions in the random background, target (i.e., altered-accessibility regions), and genomic annotation sets were then extracted using tabix. Variants extracted for each set were counted using vcftools (version 0.1.15) '--counts2 --stdout' arguments. Variant counts were then adjusted to account for the number of bp within a given set. The background distribution of these values was investigated using the 'qqnorm' (R base) and 'qqPlot' (car package) functions to look for visible deviations from normality, for which no obvious deviations were observed. Values were standardized and statistical significance was assessed using a CDF of the standard normal distribution as implemented in the 'pnorm' function in R (version 4.0.3). P-values for significant deviations from the background distribution were corrected for the number of sets (n = 13) tested using a BH correction. Significance was defined as adjusted p < 0.05 (Supplementary Table 3).

Chimpanzee genomic depletion analysis

A similar sequence constraint analysis was also performed for chimpanzees. Altered-accessibility region sets were pooled and lifted-over to hg18 using the 'liftOver' utility; a set of 1,000 randomly-generated region sets, consisting of 100,000 regions (based on the general set size of our altered-accessibility sets) with a constant length of 150bp via the bedtools 'random' function. Randomized sequence sets were subsequently pooled, sorted, and merged using bedtools, with the resulting bed file used to extract variants from the GADP set with tabix. Several genomic features were extracted from chimpanzee HOMER genomic annotations, including the following sets: intronic, promoter-TSS, TTS, and exon. Additionally, RepeatMasker elements called for the panTro4 genome were obtained from the UCSC Table Browser. These additional sets were lifted-over to hg18 (flags as indicated above) and used to extract variants from the GADP. The resulting files were filtered for duplicate variants and subsequently MAF >= 0.05 with bcftools (version 1.8). Variants falling within particular elements in the random background, target, and genomic annotation sets were then extracted using tabix. Variants per-set were counted using vcftools (version 0.1.15) '--counts2 --stdout' arguments. Variant counts were then adjusted to account for the number of bp within a given set. The background distribution of these values was investigated using the 'qqnorm' (R base) and 'qqPlot' (car package) functions to look for visible deviations from normality, for which no obvious deviations were observed. For comparison with the above human analysis, background values were standardized and statistical significance was assessed using a CDF of the standard normal distribution with the 'pnorm' function in base R. P-values for significant deviations from the background distribution were corrected for the number of sets (n = 13) tested using a BH correction. Significance was defined as adjusted p < 0.05 (Supplementary Table 3).

Obtaining and processing GWAS summary statistics data

To define a set of aging-associated diseases for use in our analyses, we first used broadly-defined categories as described in Chang et al., 2019 [69]. This study described 92 age-related diseases grouped into broader disease categories based on analyses of large-scale demographic datasets. We took these diseases and used them as the basis for manually searching the set of ICD10 disease codes, data for which was obtained from https://www.cdc.gov/nchs/icd/icd10cm.htm. We pulled all ICD codes which matched keywords from this set of defined age-related diseases and aggregated them across

different ICD categories (e.g., diseases of the circulatory system, nervous system, etc.).

Pre-processed data files from the UK Biobanks study [70] were obtained from the Neale lab (https://nealelab.github.io/UKBB_ldsc/downloads.html) (via the link https://docs.google.com/spreadsheets/d/1EmwlCYYqkoVKqAS71nNDKoN18PyKwysYUppKTSMvKiM/edit?usp=sharing), for all summary-statistics results in this UKB dataset for which ICD10 codes matched those aggregated above for aging-associated diseases. We further subset these traits to those for which liability-scaled h^2 estimates (based on LDSC analyses previously performed on these data [71], taken from the 'UKBiobanks_2019_heritabilities_per_trait.tsv.gz' file) were positive. This resulted in a final set of 129 different summary-statistics datasets for further processing (see Supplementary Table 4 for file accessions and trait descriptions). For these summary statistics, the per-SNP hg19 coordinates were obtained from https://www.dropbox.com/s/puxks683vb0omeg/variants.tsv.bgz.

Adjacent accessibility region associations – per-disease enrichment testing

For a given disease, we took the summary-level statistics and defined a set of variants having an association p-value less than a given significance threshold (using both 1e-6 and a more stringent 1e-8 cutoff, the latter yielding similar results - data not shown), generating a .bed output of SNPs (hg19 coordinates). Subsequently, for a given altered-accessibility region set (e.g., adult-biased regions), we considered the presence of SNPs nearby these regions – this was done to capture the possible effects of local linkage-disequilibrium, wherein a strongly-associated SNP may not fall immediately within a region, but a nearby proxy SNP (which may be the causal variant for the association signal) does intersect. This was done using the 'window' function in bedtools to consider significance-thresholded SNPs falling within 1000bp of a given region. As a robusticity check, we also performed the following per-disease enrichment tests using only those significance-thresholded SNPs falling immediately within regions, observing similar enrichments for DNase regions relative to genomic backgrounds, as well as altered-accessibility sets relative to all DNase regions (data not shown).

To first test whether the global set of DNase regions used in our accessibility analyses (i.e., all regions defined across all adult and fetal tissues) were enriched for nearby significance-thresholded SNPs, we defined a genomic background set by randomly subsampling 972,073 regions of 150bp size (matching the set-size of the global DNase set) from the hg19 genome using the bedtools 'random' function, generating 1000 sets of randomized backgrounds. These randomized sets were then subsequently used to count for nearby significance-thresholded SNPs (for a given disease/trait) using the bedtools 'window' function. These randomized background counts were assessed using the 'qqnorm' (R base) and 'qqPlot' (car package) functions to look for visible deviations from normality, for which no obvious deviations were observed. Values were standardized and statistical significance was assessed using a CDF of the standard normal distribution as implemented in the 'pnorm' function in R (version 4.0.3). P-values for significant deviations from the background distribution were corrected for the number of traits tested (n = 129) tested using a BH correction. Significance was defined as adjusted $p < 0.05$ (Supplementary Table 4).

Similar testing was done for our different accessibility-altered region sets, whereby customized genome-wide background sets were generated, randomized set counts were calculated, and target/background enrichments were performed. After p-value adjusting, we observed enrichment for all region sets across the majority diseases, which follows with the general enrichment for nearby significance-thresholded SNPs of all DNase regions (significant enrichments seen for 119 of 129 diseases – Supplementary Table 4). Thus, to condition on this general DNase-GWAS enrichment we implemented a hypergeometric testing approach. For each disease/trait showing significant enrichment/depletion using all DNase regions, we counted the number of unique regions (in the set, e.g., adult-biased regions) for which nearby significance-thresholded SNPs were observed, comparing this to the number of general DNase regions for which nearby significance-thresholded SNPs were observed (via the 'phyper' function in base R). For each region-set considered, the resulting set of p-values was adjusted for the number of diseases tested (n = 127) (Supplementary Table 4). In order to perform hypergeometric tests comparing the GWAS associations of developmental-aging intersection sets (e.g., adult-biased, young-biased regions), we defined the background set for testing as the respective set of developmentally-altered regions (i.e., we compare the occurrence of nearby significance-thresholded SNPs for adult-biased, young-biased regions to their occurrence nearby the adult-biased region set as a whole).

To visualize these hypergeometric test results (Figure 3A), adjusted p-values for hyper-geometric tests done using different region sets (e.g., adult-biased regions) were plotted as a barplot using ggplot2 version 3.3.3. For visualization purposes, significant enrichment results were plotted as positive values, while significant depletion results were plotted as negative values.

Additional developmental trait GWAS processing

We manually searched GWAS summary-statistic datasets for traits associated with fetal/adult development, pulling largely from data assembled by the EGG consortium (http://egg-consortium.org/index.html), as well as using a combination of GWAS Central [72], GWAS Catalog [73] and GWAS ATLAS [74]. Both general developmental traits (e.g., birth weight), as well as traits relating to particular tissues relevant to the tissues used in our accessibility analyses (e.g., stomach, brain) were searched for, with data availability (in terms of sufficiently-powered studies) largely limited to the former. The following datasets were obtained:

Birth weight

- Birthweight [27] ftp://ftp.ebi.ac.uk/pub/databases/gwas/summary_statistics/GCST005001-GCST006000/GCST005146
- Fetal-effect birthweight [75] (http://egg-consortium.org/birth-weight-2019.html)
- Maternal-effect birthweight [75] (http://egg-consortium.org/birth-weight-2019.html)
- Childhood obesity [76] (http://egg-consortium.org/childhood-obesity-2019.html)
- Pubertal growth (PGF + PGM combined) [77] http://egg-consortium.org/pubertal-growth.html
- Gestational duration (fetal genome) [78] http://egg-consortium.org/gestational-duration-2019.html
- Birth length [79] http://egg-consortium.org/birth-length.html
- Gastrointestinal congenital defects [80] http://biobanks.dk/GWAS/MEGA_CIDR_IHPS_summaryStats.txt.gz
- Childhood epilepsy [81] http://www.epigad.org/gwas_ilae2018_16loci/JME_BOLT-LMM_final.gz
- Height [28] https://portals.broadinstitute.org/collaboration/giant/images/6/63/Meta-analysis_Wood_et_al%2BUKBiobank_2018.txt.gz

Similar to our above treatment of UK Biobanks summary statistics, for each study we filtered for variants below a significance threshold of 1e-6. We then counted the occurrence of these sets of variants falling nearby our region-altered sets (using bedtools window as above), and compared this occurrence to that observed when considering all DNase regions using a hypergeometric test. For each region set considered we adjusted the resulting hypergeometric p-values for the number of GWAS datasets tested (n = 10). As before, when considering the age-altered accessibility region sets, the background set was defined as those regions changing accessibility in our developmental accessibility analyses.

Summary statistics for additional developmental traits, such as congenital heart defects, celiac disease, etc., were obtained, however, these studies had few or no significant SNPs at the 1e-6 significance threshold used (data not shown).

Additional longevity GWAS dataset processing:

Longevity GWAS summary statistics were obtained from Timmers et al. 2019 [29] and Pilling et al. 2017 [30], particularly:

Parental lifespan (Timmers et. al) (GWAS Catalog ID: GCST009890)
Parental lifespan (mother's attained age, Pilling et al.) (GWAS Catalog ID: GCST006696)
Parental lifespan (father's attained age, Pilling et al.) (GWAS Catalog ID: GCST006701)
Parental lifespan (combined parental age, Pilling et al.) (GWAS Catalog ID: GCST006697)

Similar to our above treatment of UK Biobanks summary statistics, for each set of summary statistics we filtered for variants below a significance threshold of 1e-6. We then counted the occurrence of these sets of variants falling nearby our region-altered sets (using bedtools window as above), and compared this occurrence to that observed when considering all DNase regions using a hypergeometric test. For each region set considered we adjusted the resulting hypergeometric p-values for the number of GWAS datasets tested (n = 4). As before, when considering the age-altered accessibility region sets, the background set was defined as those regions changing accessibility in our developmental accessibility analyses.

Effect-size distribution of variants

For a given disease, the set of significance-thresholded SNPs falling nearby a given set of accessibility-altered regions were extracted from the summary-statistic data along with their reported effect-size (estimated beta value). In order to compare effect-size distributions of SNPs nearby different region sets (e.g., fetal-biased vs. adult-biased regions), the absolute effect size values for SNPs falling nearby the two sets were compared using a two-tailed non-parametric Wilcoxon rank-sum test via the 'wilcox.test' function in base R. The resulting p-values were corrected for the number of diseases compared (n = 127) using a BH correction (see Supplementary Table 4). This testing was carried out first using significance-thresholded SNPs (association p-value < 1e-6), and subsequently tested using all nearby SNPs (not applying a significance threshold).

Per-SNP definitions

We defined a cross-trait metric of disease association which considers the assigned association p-value between a given SNP and multiple different aging-associated diseases. The UK Biobanks summary statistics datasets provide association statistics across the same set of SNPs, such that directly comparing the association values for a single variant across multiple datasets is possible. We first defined the global set of shared variants reported in the majority of GWAS files (for a final set of 13,789,793 SNPs), filtering out those summary statistics data which did not have information for this shared set. For a given summary statistic file, the association p-values assigned to these shared variants were extracted and subsequently standardized using the 'stats.zscore' function from the 'scipy' package [82] version 1.15.4 in Python 3. This was done across all diseases, with the final set of per-SNP z-scores converted to a matrix. This matrix was subsequently summed per-row using 'awk' to produce a per-SNP summarized z-score metric reflecting cross-disease risk associations, such that SNPs having stronger associations across multiple diseases (standardized within each disease) will have larger summed Z-scores.

Region integration with per-SNP metric

Similar to the above per-disease hyper-geometric testing, we considered the cross-disease association metric of SNPs falling nearby accessiblity-altered region sets using the bedtools 'window' function with a window of 1000bp. As above, we similarly performed a robusticity check to confirm that these results were consistent with those generated when considering only variants falling immediately within regions (data not shown). To compare the behavior of SNPs associated with our developmentally-altered region sets, we aggregated these per-SNP metrics across adult-biased (n = 3,688,911) and fetal-biased (n = 1,977,122) region sets and compared them using the 'aov' function in base R. As additional controls for this analysis, we also considered the per-SNP metrics of variants falling nearby DNase regions not significantly changing accessibility (acting as a DNase control, n = 2,554,671), and finally compared all these region-associated variants to those variants not associated with any nearby DNase regions (acting as a genome-wide, non-regulatory-element control, n = 6,742,487). Tukey post-hoc analysis was performed with the 'TukeyHSD' function in base R (see Supplementary Table 4). To visualize these results (Figure 3B), we used the 'plotmeans' function from gplots version 3.1.1.

To compare our aging-altered region sets to developmentally-altered regions, as well as the behaviors of intersection sets (e.g., adult-biased, young-biased regions), we similarly aggregated per-SNP metrics across all sets and compared them as above. For the comparisons of intersect sets, we used fetal-biased and adult-biased regions which were not intersected with aging-altered regions, rather than the full region sets, while the DNase control regions, as well as genome-wide control set, remained unchanged. For graphical purposes, the comparison was simplified to show age-altered and developmentally-altered region sets separately (Figure 3B).

Comparing cross-set SNP metric with PhastCons

PhastCons [83] 20ways-defined conserved regions were downloaded from the UCSC table browser in hg38 coordinates, and subsequently lifted-over to hg19 with the 'liftOver' tool. We partitioned SNPs genome-wide as those falling within or outside these PhastCons elements, then compared the cross-trait SNP metrics of these two partitions using a two-sided Wilcoxon test using the 'wilcox.test' function in base R. SNPs nearby accessibility-altered region sets were also partitioned based on PhastCons elements to confirm the cross-set metric behavior of subset variants. We also ran these PhastCons comparisons for SNPs subset by different region set, consistently observed an increased cross-set metric for variants falling nearby phastCons elements (Supplementary Table 4).

Integrating additional per-SNP information

phyloP20ways per-nucleotide data was intersected with the global set of variants for which the per-SNP cross-set association metric was calculated to assign a single phyloP20ways score to each variant. Argweaver [84] estimated allele ages, based on the European subset of the 1000 Genomes project [65], were obtained from http://compgen.cshl.edu/ARGweaver/CG_results/download/bigWigs/?C=S;O=A, and assigned to individual variants using the 'bigWigAverageOverBed' utility from UCSC. Variants for which estimated allele ages were not available were excluded from subsequent analyses. Pre-computed LINSIGHT [85] scores were obtained for the hg19 genome from https://github.com/CshlSiepelLab/LINSIGHT. These were similarly assigned to individual variants using the 'bigWigAverageOverBed' utility.

ClinVar variant testing

ClinVar variants were obtained from the UCSC table browser in hg19 coordinates. We intersected this SNP set with the global set of variants (filtered based on integration of additional per-SNP information) for which the per-SNP cross-set association was calculated.

Given the larger number of SNPs not part of the ClinVar set, we subsampled these SNPs to match the number of ClinVar variants used (n = 76778 SNPs), generating 1000 sets of randomized background variants. For each subset the average cross-trait association metric, phyloP20ways, estimated allele age and LINSIGHT score for all variants was calculated. These averages were used as a background set to compare against the average values in the ClinVar set; for each feature the distribution of randomized values was assessed using the 'qqnorm' (R base) and 'qqPlot' (car package) functions to look for visible deviations from normality, for which no obvious deviations were observed for different features. Values were standardized and statistical significance was assessed using a CDF of the standard normal distribution as implemented in the 'pnorm' function in R (version 4.0.3) (see Supplementary Table 4). As an additional robusticity check, the first and third quartiles for all of these values were also used to calculate significant deviations from randomized background values.

Cross-disease gene ranking

All hg19 Refseq gene TSS were obtained from the UCSC genome browser, and filtered for genes with assigned peptide sequences (obtained from the Table Browser as a 'known canonical' gene table) (i.e., protein-coding genes). This gene set was then padded 100kb up/downstream to define 200kb per-gene windows. For a given disease, we considered all variants falling within all gene windows, selecting the strongest-associated variant falling within each and assigning this association p-value to that particular gene. All genes were then ranked according to their assigned association p-values within a given disease.

To test for significant-enrichment of ranks for a particular set of genes (i.e., a set of genes have nearby assigned SNPs that rank them consistently higher across a number of diseases), all protein-coding genes were first considered: counting how often a given gene appeared in the top 75th percentile of ranked protein-coding genes across different diseases (ranging from 1 to 127). The distribution of these counts for the target set of genes was compared to that of the global distribution of protein-coding genes (exclusive of the target set) using a one-sided (alternative = "greater") Student's t-test in base R.

As a positive control for this analysis, genes associated with the GO term 'homeostatic process' (GO:0042592) were used as a target set for testing. As a negative control, genes associated with the GO term 'developmental process involved in reproduction' (GO:0003006) were used as a target set for testing.

Defining 'core' aging genes

These sets of gene rankings were then aggregated using the 'aggregateRanks' function from the RobustRankAggreg [55] library version 1.1. Given that we considered all protein-coding gene loci, we applied a conservative filter to the resulting RRA significance values via the use of a Bonferroni correction – retaining all genes with a corrected value < 0.05. Gene-set enrichment analysis was then performed with the 'enrichGO' function from the clusterProfiler [54] library version 3.16.1, with the background defined as all protein-coding genes used in the gene-ranking analysis. Significant gene-set enrichments were defined as adjusted p-value < 0.05.

In addition to applying this cutoff-based approach to defining highly-ranked gene sets, we also implemented an approach that did not rely on defining a strict cutoff with the RRA method. For a given gene, we took all of the ranks across the different diseases and calculated the geometric mean of ranks. All genes were then sorted based on this final mean-of-ranks, with this ranking used with 'gseGO' function from the clusterProfiler library version 3.16.1 to perform an FGSEA analysis with the following flags: OrgDb = org.Hs.eg.db, ont = "BP", minGSSize = 15, maxGSSize = 500. Significant gene-set enrichments were defined as adjusted p-value < 0.05.

Given our gene-window based method, it is possible that a single strongly-associated variant may be assigned to two or more closely-adjacent genes. We performed a separate ranking analysis collapsing overlapping gene windows, though found that this led to a reduction in the strength of gene-set enrichments of the RRA ranking results (data not shown).

In order to integrate the effects of local accessibility change into these gene-set rankings, the above ranking procedure was done considering only those variants nearby altered-accessibility regions (e.g., young-biased regions) when assigning per-gene association p-values for ranking (Supplementary Table 4).

Characterizing gene-ranking histone-deacetylase enrichments

To visualize the increased average geometric-mean rank of genes associated with histone deacetylation, the set of 'leading edge' genes associated with the GO term 'histone deacetylase' (HDAC) (GO:0016575) from the FGSEA gene-wise ranking analysis (gene set in Supplementary Table 4) was taken and compared with the geometric-mean rank of all other protein-coding genes used in this analysis. This was done for gene-wise

rankings defined when considering all variants falling within a given gene window (Figure 4A, left), as well as rankings defined when considering those variants with nearby young-biased regions falling within a given gene window (Figure 4B, right).

To compare the differences in GWAS signal associations of these HDAC genes when stratifying variants by nearby altered-accessibility regions, we made use of the per-SNP cross-trait association metric defined above.

The sets of gene windows defined for all protein-coding genes were again taken and variants falling within each gene window were collected. Similar to above, variants were binned based on the presence of nearby altered-accessibility regions (e.g., young-biased regions) – rather than considering the strongest variant signal for a given disease and aggregating ranks across, instead the per-SNP cross-trait association metric for variants was used to assign the strongest signal to a given gene window. This was done considering all variants within a window, as well as binned variants, such that a single gene window has multiple assigned values (one per region set used, as well as a region-independent value). These values were assigned for: all variants, variants with no nearby DNase regions ('Background'), variants with nearby DNase regions not significantly changing accessibility ("DNase Unchanged"), variants with nearby fetal-biased regions ("Fetal-biased"), variants with nearby adult-biased regions ("Adult-biased"), variants with nearby young-biased regions ("Young-Age"), and variants with nearby old-biased regions ("Old-Age").

The gene-window values for the HDAC gene set were used as target values. The remaining values of all protein-coding genes (exclusive of this target set) was randomly sampled, generating 1000 sets of genes matching the size of the HDAC target set. The seven different types of assigned values (enumerated above) for each gene window were calculated for both target and test sets. For comparing the target and randomized background sets, the average assigned value for each gene set (target and random) was calculated.

For each type of assigned value, the randomized background set values were assessed using the 'qqnorm' (R base) and 'qqPlot' (car package) functions to look for visible deviations from normality, for which no obvious deviations were observed. Values were standardized and statistical significance was assessed using a CDF of the standard normal distribution as implemented in the 'pnorm' function in R (version 4.0.3). To determine whether stronger GWAS variants falling within HDAC gene windows tend to be stratified by nearby altered-accessibility regions (particularly, young-biased regions as suggested by Figure 4A), the enrichment/depletion values for each different type of gene-wise values (relative to their own respective backgrounds) were compared to the enrichment/depletion values calculated when considering all variants (the region-independent value). This was calculated as: -log10((region-specific CDF test p-value) / (region-independent CDF test p-value)), with positive values indicating a stronger deviation from the background distribution when using region-stratified variants when compared to all variants within a given gene window. These values were visualized using ggplot2, as seen in Figure 4B and Supplementary Table 4.

Visualizing promoter-contact datasets

To visualize the interactions between young-biased regions harbouring nearby genetic variants and the *SIRT6* promoter (Figure 4C) we extracted significant promoter-capture interactions (p-value < 0.01) from the *SIRT6* anchor across a subset of cell types representative of our tissue sets (AD2, AO, GA, Hcmerge, IMR90, PO3 and SX, referring to adrenal gland, aorta, gastric tissue, brain, fibroblast (lung), muscle and spleen labels, respectively). These interaction data were visualized using the GenomicInteractions [86] library version 1.24.0.

Supplementary References

1. Yan L, Guo H, Hu B, Li R, Yong J, Zhao Y, Zhi X, Fan X, Guo F, Wang X, Wang W, Wei Y, Wang Y, et al. Epigenomic Landscape of Human Fetal Brain, Heart, and Liver. J Biol Chem. 2016; 291:4386–98. https://doi.org/10.1074/jbc.M115.672931 PMID:26719341

2. Zhu J, Adli M, Zou JY, Verstappen G, Coyne M, Zhang X, Durham T, Miri M, Deshpande V, De Jager PL, Bennett DA, Houmard JA, Muoio DM, et al. Genome-wide chromatin state transitions associated with developmental and environmental cues. Cell. 2013; 152:642–54. https://doi.org/10.1016/j.cell.2012.12.033 PMID:23333102

3. Roadmap Epigenomics Consortium, Kundaje A, Meuleman W, Ernst J, Bilenky M, Yen A, Heravi-Moussavi A, Kheradpour P, Zhang Z, Wang J, Ziller MJ, Amin V, Whitaker JW, Schultz MD, et al. Integrative analysis of 111 reference human epigenomes. Nature. 2015; 518:317–30. https://doi.org/10.1038/nature14248 PMID:25693563

4. Booth LN, Brunet A. The Aging Epigenome. Mol Cell. 2016; 62:728–44. https://doi.org/10.1016/j.molcel.2016.05.013 PMID:27259204

5. Sheffield NC, Bock C. LOLA: enrichment analysis for genomic region sets and regulatory elements in R and Bioconductor. Bioinformatics. 2016; 32:587–89. https://doi.org/10.1093/bioinformatics/btv612 PMID:26508757

6. Voigt P, Tee WW, Reinberg D. A double take on bivalent promoters. Genes Dev. 2013; 27:1318–38. https://doi.org/10.1101/gad.219626.113 PMID:23788621

7. Yue F, Cheng Y, Breschi A, Vierstra J, Wu W, Ryba T, Sandstrom R, Ma Z, Davis C, Pope BD, Shen Y, Pervouchine DD, Djebali S, et al. A comparative encyclopedia of DNA elements in the mouse genome. Nature. 2014; 515:355–64. https://doi.org/10.1038/nature13992 PMID:25409824

8. Davis CA, Hitz BC, Sloan CA, Chan ET, Davidson JM, Gabdank I, Hilton JA, Jain K, Baymuradov UK, Narayanan AK, Onate KC, Graham K, Miyasato SR, et al. The Encyclopedia of DNA elements (ENCODE): data portal update. Nucleic Acids Res. 2018; 46:D794–801. https://doi.org/10.1093/nar/gkx1081 PMID:29126249

9. Horvath S, Raj K. DNA methylation-based biomarkers and the epigenetic clock theory of ageing. Nat Rev Genet. 2018; 19:371–84. https://doi.org/10.1038/s41576-018-0004-3 PMID:29643443

10. Horvath S, Mah V, Lu AT, Woo JS, Choi OW, Jasinska AJ, Riancho JA, Tung S, Coles NS, Braun J, Vinters HV, Coles LS. The cerebellum ages slowly according to the epigenetic clock. Aging (Albany NY). 2015; 7:294–306. https://doi.org/10.18632/aging.100742 PMID:26000617

11. Hannum G, Guinney J, Zhao L, Zhang L, Hughes G, Sadda S, Klotzle B, Bibikova M, Fan JB, Gao Y, Deconde R, Chen M, Rajapakse I, et al. Genome-wide methylation profiles reveal quantitative views of human aging rates. Mol Cell. 2013; 49:359–67. https://doi.org/10.1016/j.molcel.2012.10.016 PMID:23177740

12. Jung I, Schmitt A, Diao Y, Lee AJ, Liu T, Yang D, Tan C, Eom J, Chan M, Chee S, Chiang Z, Kim C, Masliah E, et al. A compendium of promoter-centered long-range chromatin interactions in the human genome. Nat Genet. 2019; 51:1442–49. https://doi.org/10.1038/s41588-019-0494-8 PMID:31501517

13. Georgountzou A, Papadopoulos NG. Postnatal Innate Immune Development: From Birth to Adulthood. Front Immunol. 2017; 8:957. https://doi.org/10.3389/fimmu.2017.00957 PMID:28848557

14. Franceschi C, Garagnani P, Vitale G, Capri M, Salvioli S. Inflammaging and 'Garb-aging'. Trends Endocrinol Metab. 2017; 28:199–212. https://doi.org/10.1016/j.tem.2016.09.005 PMID:27789101

15. GTEx Consortium. The Genotype-Tissue Expression (GTEx) project. Nat Genet. 2013; 45:580–85. https://doi.org/10.1038/ng.2653 PMID:23715323

16. Blagosklonny MV, Hall MN. Growth and aging: a common molecular mechanism. Aging (Albany NY). 2009; 1:357–62. https://doi.org/10.18632/aging.100040 PMID:20157523

17. de Magalhães JP. Programmatic features of aging originating in development: aging mechanisms beyond molecular damage? FASEB J. 2012; 26:4821–26. https://doi.org/10.1096/fj.12-210872 PMID:22964300

18. Bird CP, Stranger BE, Liu M, Thomas DJ, Ingle CE, Beazley C, Miller W, Hurles ME, Dermitzakis ET. Fast-evolving noncoding sequences in the human genome. Genome Biol. 2007; 8:R118. https://doi.org/10.1186/gb-2007-8-6-r118 PMID:17578567

19. Bush EC, Lahn BT. A genome-wide screen for noncoding elements important in primate evolution. BMC Evol Biol. 2008; 8:17. https://doi.org/10.1186/1471-2148-8-17 PMID:18215302

20. Gittelman RM, Hun E, Ay F, Madeoy J, Pennacchio L, Noble WS, Hawkins RD, Akey JM. Comprehensive identification and analysis of human accelerated regulatory DNA. Genome Res. 2015; 25:1245–55. https://doi.org/10.1101/gr.192591.115 PMID:26104583

21. Pollard KS, Salama SR, King B, Kern AD, Dreszer T, Katzman S, Siepel A, Pedersen JS, Bejerano G, Baertsch R, Rosenbloom KR, Kent J, Haussler D. Forces shaping the fastest evolving regions in the human genome. PLoS Genet. 2006; 2:e168. https://doi.org/10.1371/journal.pgen.0020168 PMID:17040131

22. Prabhakar S, Noonan JP, Pääbo S, Rubin EM. Accelerated evolution of conserved noncoding sequences in humans. Science. 2006; 314:786. https://doi.org/10.1126/science.1130738 PMID:17082449

23. Kostka D, Holloway AK, Pollard KS. Developmental Loci Harbor Clusters of Accelerated Regions That Evolved Independently in Ape Lineages. Mol Biol Evol. 2018; 35:2034–45. https://doi.org/10.1093/molbev/msy109 PMID:29897475

24. Ornitz DM, Itoh N. The Fibroblast Growth Factor signaling pathway. Wiley Interdiscip Rev Dev Biol. 2015; 4:215–66. https://doi.org/10.1002/wdev.176 PMID:25772309

25. Sebastiani P, Solovieff N, Dewan AT, Walsh KM, Puca A, Hartley SW, Melista E, Andersen S, Dworkis DA, Wilk JB, Myers RH, Steinberg MH, Montano M, et al. Genetic signatures of exceptional longevity in humans. PLoS One. 2012; 7:e29848. https://doi.org/10.1371/journal.pone.0029848 PMID:22279548

26. de Magalhães JP, Budovsky A, Lehmann G, Costa J, Li Y, Fraifeld V, Church GM. The Human Ageing Genomic Resources: online databases and tools for biogerontologists. Aging Cell. 2009; 8:65–72. https://doi.org/10.1111/j.1474-9726.2008.00442.x PMID:18986374

27. Horikoshi M, Beaumont RN, Day FR, Warrington NM, Kooijman MN, Fernandez-Tajes J, Feenstra B, van Zuydam NR, Gaulton KJ, Grarup N, Bradfield JP, Strachan DP, Li-Gao R, et al. Genome-wide associations for birth weight and correlations with adult disease. Nature. 2016; 538:248–52. https://doi.org/10.1038/nature19806 PMID:27680694

28. Yengo L, Sidorenko J, Kemper KE, Zheng Z, Wood AR, Weedon MN, Frayling TM, Hirschhorn J, Yang J, Visscher PM, and GIANT Consortium. Meta-analysis of genome-wide association studies for height and body mass index in ~700000 individuals of European ancestry. Hum Mol Genet. 2018; 27:3641–49. https://doi.org/10.1093/hmg/ddy271 PMID:30124842

29. Timmers PR, Mounier N, Lall K, Fischer K, Ning Z, Feng X, Bretherick AD, Clark DW, Shen X, Esko T, Kutalik Z, Wilson JF, Joshi PK, and eQTLGen Consortium. Genomics of 1 million parent lifespans implicates novel pathways and common diseases and distinguishes survival chances. Elife. 2019; 8:e39856. https://doi.org/10.7554/eLife.39856 PMID:30642433

30. Pilling LC, Kuo CL, Sicinski K, Tamosauskaite J, Kuchel GA, Harries LW, Herd P, Wallace R, Ferrucci L, Melzer D. Human longevity: 25 genetic loci associated in 389,166 UK biobank participants. Aging (Albany NY). 2017; 9:2504–20. https://doi.org/10.18632/aging.101334 PMID:29227965

31. Klemm SL, Shipony Z, Greenleaf WJ. Chromatin accessibility and the regulatory epigenome. Nat Rev Genet. 2019; 20:207–20. https://doi.org/10.1038/s41576-018-0089-8 PMID:30675018

32. Boyle EA, Li YI, Pritchard JK. An Expanded View of Complex Traits: From Polygenic to Omnigenic. Cell. 2017; 169:1177–86. https://doi.org/10.1016/j.cell.2017.05.038 PMID:28622505

33 Dunham I, Kundaje A, Aldred SF, Collins PJ, Davis CA, Doyle F, Epstein CB, Frietze S, Harrow J, Kaul R, Khatun J, Lajoie BR, Landt SG, et al. ENCODE Project Consortium. An integrated encyclopedia of DNA elements in the human genome. Nature. 2012; 489:57–74. https://doi.org/10.1038/nature11247 PMID:22955616

34. Li Q, Brown JB, Huang H, Bickel PJ. Measuring reproducibility of high-throughput experiments. Ann. Appl. Stat. 5. 2011; 1752–79. https://doi.org/10.1214/11-AOAS466

35. Yang Y, Fear J, Hu J, Haecker I, Zhou L, Renne R, Bloom D, McIntyre LM. Leveraging biological replicates to improve analysis in ChIP-seq experiments. Comput Struct Biotechnol J. 2014; 9:e201401002. https://doi.org/10.5936/csbj.201401002 PMID:24688750

36. Quinlan AR, Hall IM. BEDTools: a flexible suite of utilities for comparing genomic features. Bioinformatics. 2010; 26:841–42. https://doi.org/10.1093/bioinformatics/btq033 PMID:20110278

37. Li H, Handsaker B, Wysoker A, Fennell T, Ruan J, Homer N, Marth G, Abecasis G, Durbin R, and 1000 Genome Project Data Processing Subgroup. The Sequence Alignment/Map format and SAMtools. Bioinformatics. 2009; 25:2078–79. https://doi.org/10.1093/bioinformatics/btp352 PMID:19505943

38. R Development Core Team, R: A Language and Environment for Statistical Computing. 2008. http://www.r-project.org

39. Ritchie ME, Phipson B, Wu D, Hu Y, Law CW, Shi W, Smyth GK. limma powers differential expression analyses for RNA-sequencing and microarray studies. Nucleic Acids Res. 2015; 43:e47. https://doi.org/10.1093/nar/gkv007 PMID:25605792

40. Robinson MD, McCarthy DJ, Smyth GK. edgeR: a Bioconductor package for differential expression analysis of digital gene expression data. Bioinformatics. 2010; 26:139–40. https://doi.org/10.1093/bioinformatics/btp616 PMID:19910308

41. Benjamini Y, Hochberg Y, Controlling the false discovery rate: a practical and powerful approach to multiple testing. J. R. Stat. Soc. Ser. B,. 1995; 289–300.

https://doi.org/10.1111/j.2517-6161.1995.tb02031.x

42. Lawrence M, Gentleman R, Carey V. rtracklayer: an R package for interfacing with genome browsers. Bioinformatics. 2009; 25:1841–42. https://doi.org/10.1093/bioinformatics/btp328 PMID:19468054

43. Gel B, Serra E. karyoploteR: an R/Bioconductor package to plot customizable genomes displaying arbitrary data. Bioinformatics. 2017; 33:3088–90. https://doi.org/10.1093/bioinformatics/btx346 PMID:28575171

44. Gu Z, Eils R, Schlesner M. Complex heatmaps reveal patterns and correlations in multidimensional genomic data. Bioinformatics. 2016; 32:2847–49. https://doi.org/10.1093/bioinformatics/btw313 PMID:27207943

45. Chen H, Boutros PC. VennDiagram: a package for the generation of highly-customizable Venn and Euler diagrams in R. BMC Bioinformatics. 2011; 12:35. https://doi.org/10.1186/1471-2105-12-35 PMID:21269502

46. Kent WJ, Sugnet CW, Furey TS, Roskin KM, Pringle TH, Zahler AM, Haussler D. The human genome browser at UCSC. Genome Res. 2002; 12:996–1006. https://doi.org/10.1101/gr.229102 PMID:12045153

47. Horvath S. DNA methylation age of human tissues and cell types. Genome Biol. 2013; 14:R115. https://doi.org/10.1186/gb-2013-14-10-r115 PMID:24138928

48. Karolchik D, Barber GP, Casper J, Clawson H, Cline MS, Diekhans M, Dreszer TR, Fujita PA, Guruvadoo L, Haeussler M, Harte RA, Heitner S, Hinrichs AS, et al. The UCSC Genome Browser database: 2014 update. Nucleic Acids Res. 2014; 42:D764–70. https://doi.org/10.1093/nar/gkt1168 PMID:24270787

49. Gel B, Díez-Villanueva A, Serra E, Buschbeck M, Peinado MA, Malinverni R. regioneR: an R/Bioconductor package for the association analysis of genomic regions based on permutation tests. Bioinformatics. 2016; 32:289–91. https://doi.org/10.1093/bioinformatics/btv562 PMID:26424858

50. Karolchik D, Hinrichs AS, Furey TS, Roskin KM, Sugnet CW, Haussler D, Kent WJ. The UCSC Table Browser data retrieval tool. Nucleic Acids Res. 2004; 32:D493–96. https://doi.org/10.1093/nar/gkh103 PMID:14681465

51. Jackman S. Classes and Methods for {R} Developed in the Political Science Computational Laboratory. 2017. https://github.com/atahk/pscl/

52. Zeileis A, Kleiber C, Jackman S, Regression Models for Count Data in {R}. J. Stat. Softw. 2008. http://www.jstatsoft.org/v27/i08/

53. McLean CY, Bristor D, Hiller M, Clarke SL, Schaar BT, Lowe CB, Wenger AM, Bejerano G. GREAT improves functional interpretation of cis-regulatory regions. Nat Biotechnol. 2010; 28:495–501. https://doi.org/10.1038/nbt.1630 PMID:20436461

54. Yu G, Wang LG, Han Y, He QY. clusterProfiler: an R package for comparing biological themes among gene clusters. OMICS. 2012; 16:284–87. https://doi.org/10.1089/omi.2011.0118 PMID:22455463

55. Kolde R, Laur S, Adler P, Vilo J. Robust rank aggregation for gene list integration and meta-analysis. Bioinformatics. 2012; 28:573–80. https://doi.org/10.1093/bioinformatics/btr709 PMID:22247279

56. Benayoun BA, Pollina EA, Singh PP, Mahmoudi S, Harel I, Casey KM, Dulken BW, Kundaje A, Brunet A. Remodeling of epigenome and transcriptome landscapes with aging in mice reveals widespread induction of inflammatory responses. Genome Res. 2019; 29:697–709. https://doi.org/10.1101/gr.240093.118 PMID:30858345

57. Fullard JF, Hauberg ME, Bendl J, Egervari G, Cirnaru MD, Reach SM, Motl J, Ehrlich ME, Hurd YL, Roussos P. An atlas of chromatin accessibility in the adult human brain. Genome Res. 2018; 28:1243–52. https://doi.org/10.1101/gr.232488.117 PMID:29945882

58. Buenrostro JD, Giresi PG, Zaba LC, Chang HY, Greenleaf WJ. Transposition of native chromatin for fast and sensitive epigenomic profiling of open chromatin, DNA-binding proteins and nucleosome position. Nat Methods. 2013; 10:1213–18. https://doi.org/10.1038/nmeth.2688 PMID:24097267

59. Richard D, Liu Z, Cao J, Kiapour AM, Willen J, Yarlagadda S, Jagoda E, Kolachalama VB, Sieker JT, Chang GH, Muthuirulan P, Young M, Masson A, et al. Evolutionary Selection and Constraint on Human Knee Chondrocyte Regulation Impacts Osteoarthritis Risk. Cell. 2020; 181:362–81.e28. https://doi.org/10.1016/j.cell.2020.02.057 PMID:32220312

60. Fox J, Weisberg S. An R Companion to Applied Regression, Third Edition. 2019. https://socialsciences.mcmaster.ca/jfox/Books/Companion/

61. Delignette-Muller ML, Dutang C, fitdistrplus : An R

Package for Fitting Distributions. J. Stat. Softw. 2015; 64:1–34. https://doi.org/10.18637/jss.v064.i04

62. Mun J, Advanced analytical models : over 800 models and 300 applications from the Basel II Accord to Wall Street and beyond Wiley 2008. https://dl.acm.org/citation.cfm?id=1386324

63. Heinz S, Benner C, Spann N, Bertolino E, Lin YC, Laslo P, Cheng JX, Murre C, Singh H, Glass CK. Simple combinations of lineage-determining transcription factors prime cis-regulatory elements required for macrophage and B cell identities. Mol Cell. 2010; 38:576–89. https://doi.org/10.1016/j.molcel.2010.05.004 PMID:20513432

64. Pollard KS, Hubisz MJ, Rosenbloom KR, Siepel A. Detection of nonneutral substitution rates on mammalian phylogenies. Genome Res. 2010; 20:110–21. https://doi.org/10.1101/gr.097857.109 PMID:19858363

65. Gibbs RA, Boerwinkle E, Doddapaneni H, Han Y, Korchina V, Kovar C, Lee S, Muzny D, Reid JG, Zhu Y, Wang J, Chang Y, Feng Q, et al. A global reference for human genetic variation. Nature. 2015; 526:68–74. https://doi.org/10.1038/nature15393 PMID: 26432245

66. Li H. Tabix: fast retrieval of sequence features from generic TAB-delimited files. Bioinformatics. 2011; 27:718–19. https://doi.org/10.1093/bioinformatics/btq671 PMID:21208982

67. Prado-Martinez J, Sudmant PH, Kidd JM, Li H, Kelley JL, Lorente-Galdos B, Veeramah KR, Woerner AE, O'Connor TD, Santpere G, Cagan A, Theunert C, Casals F, et al. Great ape genetic diversity and population history. Nature. 2013; 499:471–75. https://doi.org/10.1038/nature12228 PMID:23823723

68. Li H. A statistical framework for SNP calling, mutation discovery, association mapping and population genetical parameter estimation from sequencing data. Bioinformatics. 2011; 27:2987–93. https://doi.org/10.1093/bioinformatics/btr509 PMID:21903627

69. Chang AY, Skirbekk VF, Tyrovolas S, Kassebaum NJ, Dieleman JL. Measuring population ageing: an analysis of the Global Burden of Disease Study 2017. Lancet Public Health. 2019; 4:e159–67. https://doi.org/10.1016/S2468-2667(19)30019-2 PMID:30851869

70. Sudlow C, Gallacher J, Allen N, Beral V, Burton P, Danesh J, Downey P, Elliott P, Green J, Landray M, Liu B, Matthews P, Ong G, et al. UK biobank: an open access resource for identifying the causes of a wide range of complex diseases of middle and old age. PLoS Med. 2015; 12:e1001779. https://doi.org/10.1371/journal.pmed.1001779 PMID:25826379

71. Bulik-Sullivan B, Finucane HK, Anttila V, Gusev A, Day FR, Loh PR, Duncan L, Perry JR, Patterson N, Robinson EB, Daly MJ, Price AL, Neale BM, ReproGen Consortium, Psychiatric Genomics Consortium, and Genetic Consortium for Anorexia Nervosa of the Wellcome Trust Case Control Consortium 3. An atlas of genetic correlations across human diseases and traits. Nat Genet. 2015; 47:1236–41. https://doi.org/10.1038/ng.3406 PMID:26414676

72. Beck T, Shorter T, Brookes AJ. GWAS Central: a comprehensive resource for the discovery and comparison of genotype and phenotype data from genome-wide association studies. Nucleic Acids Res. 2020; 48:D933–40. https://doi.org/10.1093/nar/gkz895 PMID:31612961

73. Buniello A, MacArthur JA, Cerezo M, Harris LW, Hayhurst J, Malangone C, McMahon A, Morales J, Mountjoy E, Sollis E, Suveges D, Vrousgou O, Whetzel PL, et al. The NHGRI-EBI GWAS Catalog of published genome-wide association studies, targeted arrays and summary statistics 2019. Nucleic Acids Res. 2019; 47:D1005–12. https://doi.org/10.1093/nar/gky1120 PMID:30445434

74. Watanabe K, Stringer S, Frei O, Umićević Mirkov M, de Leeuw C, Polderman TJ, van der Sluis S, Andreassen OA, Neale BM, Posthuma D. A global overview of pleiotropy and genetic architecture in complex traits. Nat Genet. 2019; 51:1339–48. https://doi.org/10.1038/s41588-019-0481-0 PMID:31427789

75. Warrington NM, Beaumont RN, Horikoshi M, Day FR, Helgeland Ø, Laurin C, Bacelis J, Peng S, Hao K, Feenstra B, Wood AR, Mahajan A, Tyrrell J, et al. Maternal and fetal genetic effects on birth weight and their relevance to cardio-metabolic risk factors. Nat Genet. 2019; 51:804–14. https://doi.org/10.1038/s41588-019-0403-1 PMID:31043758

76. Bradfield JP, Vogelezang S, Felix JF, Chesi A, Helgeland Ø, Horikoshi M, Karhunen V, Lowry E, Cousminer DL, Ahluwalia TS, Thiering E, Boh ET, Zafarmand MH, et al. A trans-ancestral meta-analysis of genome-wide association studies reveals loci associated with childhood obesity. Hum Mol Genet. 2019; 28:3327–38. https://doi.org/10.1093/hmg/ddz161 PMID:31504550

77. Cousminer DL, Berry DJ, Timpson NJ, Ang W, Thiering E, Byrne EM, Taal HR, Huikari V, Bradfield JP, Kerkhof M, Groen-Blokhuis MM, Kreiner-Møller E, Marinelli M, et al. Genome-wide association and longitudinal analyses reveal genetic loci linking pubertal height growth, pubertal timing and childhood adiposity. Hum Mol Genet. 2013; 22:2735–47. https://doi.org/10.1093/hmg/ddt104 PMID:23449627

78. Liu X, Helenius D, Skotte L, Beaumont RN, Wielscher M, Geller F, Juodakis J, Mahajan A, Bradfield JP, Lin FTJ, Vogelezang S, Bustamante M, Ahluwalia TS, et al. Variants in the fetal genome near pro-inflammatory cytokine genes on 2q13 associate with gestational duration. Nat Commun. 2019; 10:3927. https://doi.org/10.1038/s41467-019-11881-8 PMID:31477735

79. van der Valk RJ, Kreiner-Møller E, Kooijman MN, Guxens M, Stergiakouli E, Sääf A, Bradfield JP, Geller F, Hayes MG, Cousminer DL, Körner A, Thiering E, Curtin JA, et al. A novel common variant in DCST2 is associated with length in early life and height in adulthood. Hum Mol Genet. 2015; 24:1155–68. https://doi.org/10.1093/hmg/ddu510 PMID:25281659

80. Fadista J, Skotte L, Geller F, Bybjerg-Grauholm J, Gørtz S, Romitti PA, Caggana M, Kay DM, Matsson H, Boyd HA, Hougaard DM, Nordenskjöld A, Mills JL, et al. Genome-wide meta-analysis identifies BARX1 and EML4-MTA3 as new loci associated with infantile hypertrophic pyloric stenosis. Hum Mol Genet. 2019; 28:332–40. https://doi.org/10.1093/hmg/ddy347 PMID:30281099

81. International League Against Epilepsy Consortium on Complex Epilepsies. Genome-wide mega-analysis identifies 16 loci and highlights diverse biological mechanisms in the common epilepsies. Nat Commun. 2018; 9:5269. https://doi.org/10.1038/s41467-018-07524-z PMID:30531953

82. Virtanen P, Gommers R, Oliphant TE, Haberland M, Reddy T, Cournapeau D, Burovski E, Peterson P, Weckesser W, Bright J, van der Walt SJ, Brett M, Wilson J, et al. SciPy 1.0: fundamental algorithms for scientific computing in Python. Nat Methods. 2020; 17:261–72. https://doi.org/10.1038/s41592-019-0686-2 PMID:32015543

83. Siepel A, Bejerano G, Pedersen JS, Hinrichs AS, Hou M, Rosenbloom K, Clawson H, Spieth J, Hillier LW, Richards S, Weinstock GM, Wilson RK, Gibbs RA, et al. Evolutionarily conserved elements in vertebrate, insect, worm, and yeast genomes. Genome Res. 2005; 15:1034–50. https://doi.org/10.1101/gr.3715005 PMID:16024819

84. Rasmussen MD, Hubisz MJ, Gronau I, Siepel A. Genome-wide inference of ancestral recombination graphs. PLoS Genet. 2014; 10:e1004342. https://doi.org/10.1371/journal.pgen.1004342 PMID:24831947

85. Huang YF, Gulko B, Siepel A. Fast, scalable prediction of deleterious noncoding variants from functional and population genomic data. Nat Genet. 2017; 49:618–24. https://doi.org/10.1038/ng.3810 PMID:28288115

86. Harmston N, Ing-Simmons E, Perry M, Barešić A, Lenhard B. GenomicInteractions: An R/Bioconductor package for manipulating and investigating chromatin interaction data. BMC Genomics. 2015; 16:963. https://doi.org/10.1186/s12864-015-2140-x PMID:26576536

Supplementary Figures

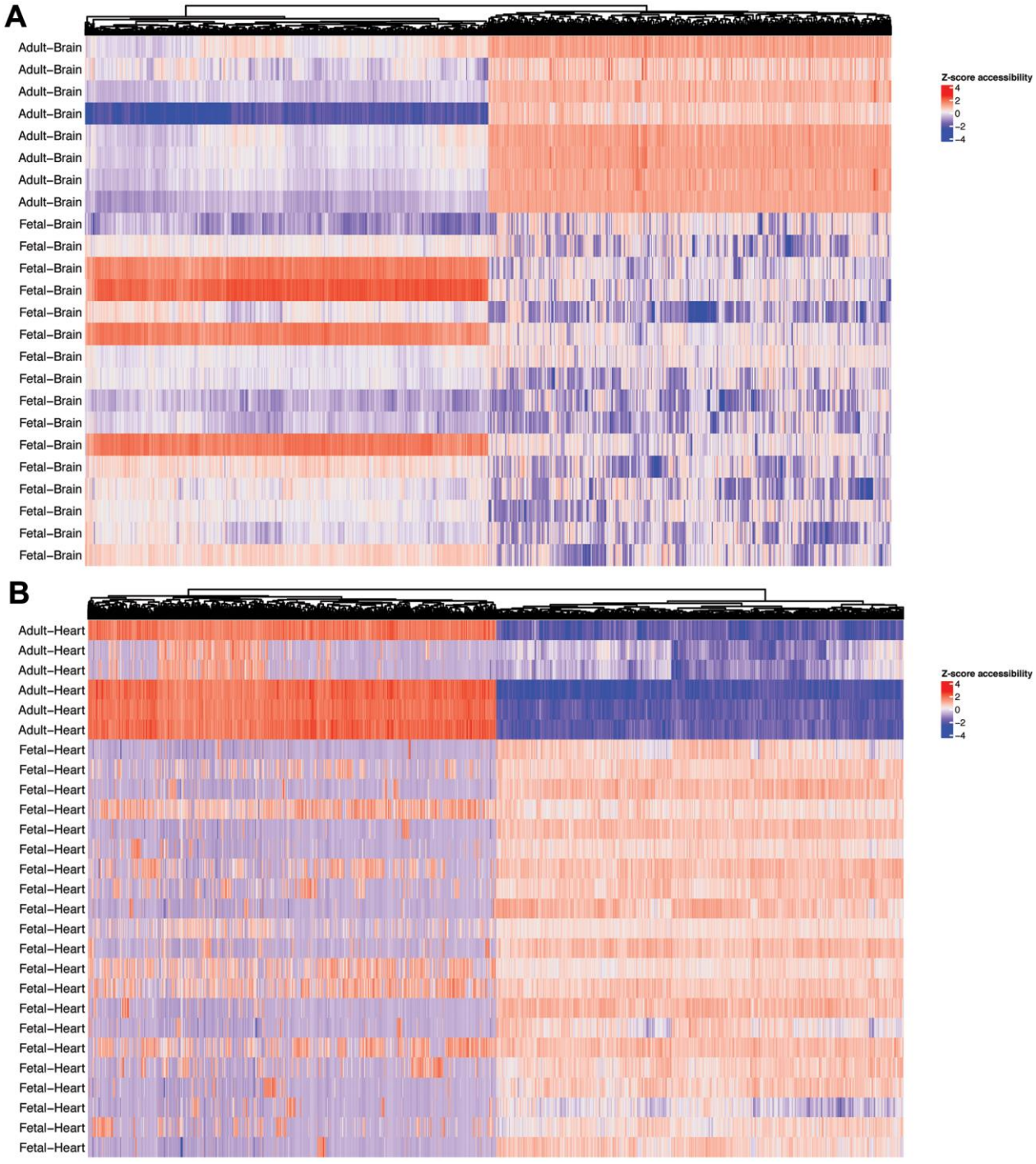

Supplementary Figure 1. Per-tissue heatmaps for brain and heart tissue. (**A**) Z-score accessibility values for regions defined as differentially-accessible comparing fetal and adult brain tissue samples. (**B**) Z-score accessibility values for regions defined as differentially-accessible comparing fetal and adult heart tissue samples. Red-blue colour scale indicates increased/decreased accessibility, z-score normalized per-column.

Supplementary Figure 2. Autosome distribution of accessibility-altered regions. Genomic distribution of regions changing accessibility in fetal/adult comparison. Red/blue: density of defined differentially-accessible regions. Line: relative proportion of regions more accessible in adult (top) or fetal (bottom) tissues.

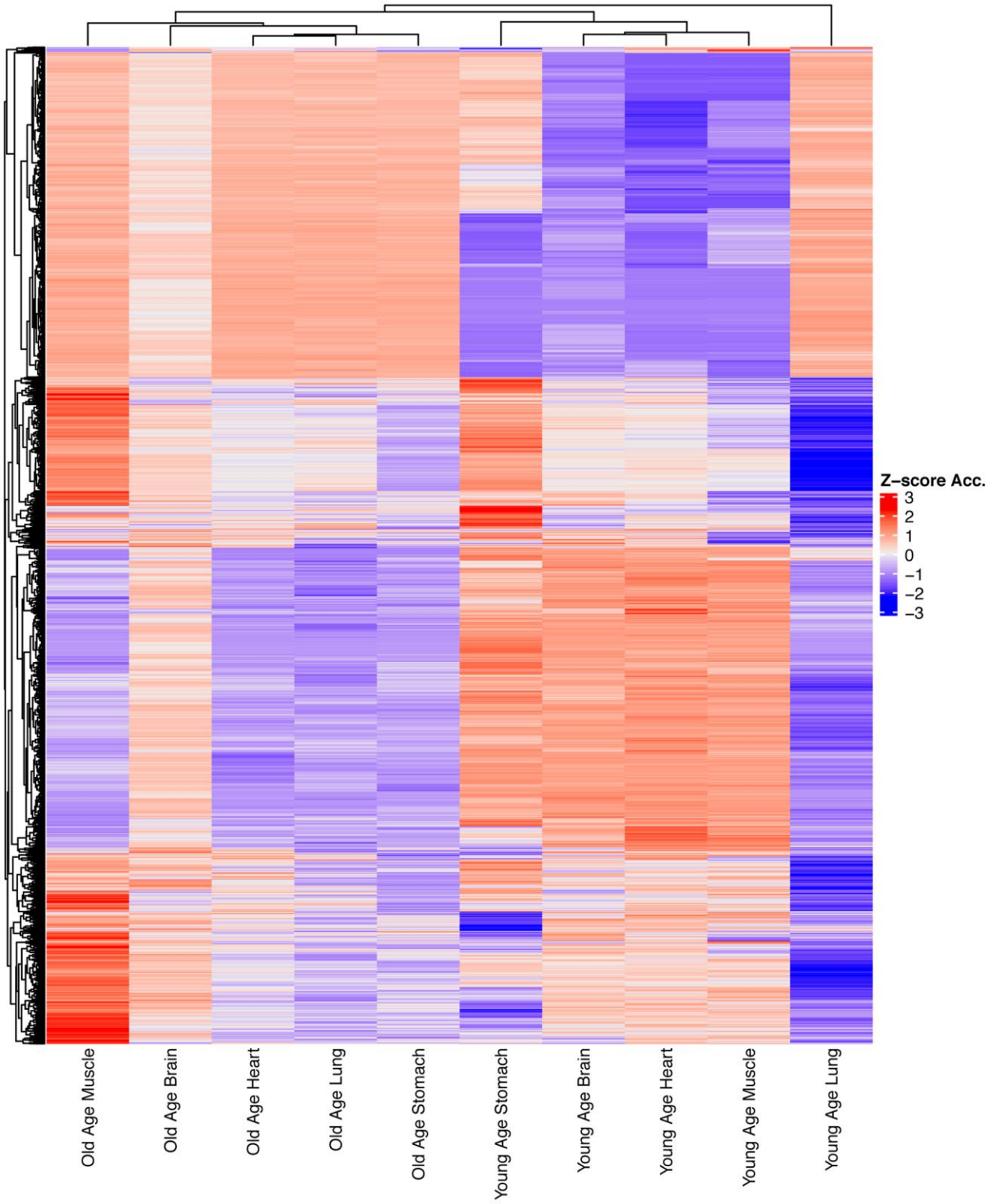

Supplementary Figure 3. Changes in regional accessibility across young-age and old-age adult tissue samples. Equivalent to Figure 1A. Red-blue colour scale indicates increased/decreased accessibility, z-score normalized per-column.

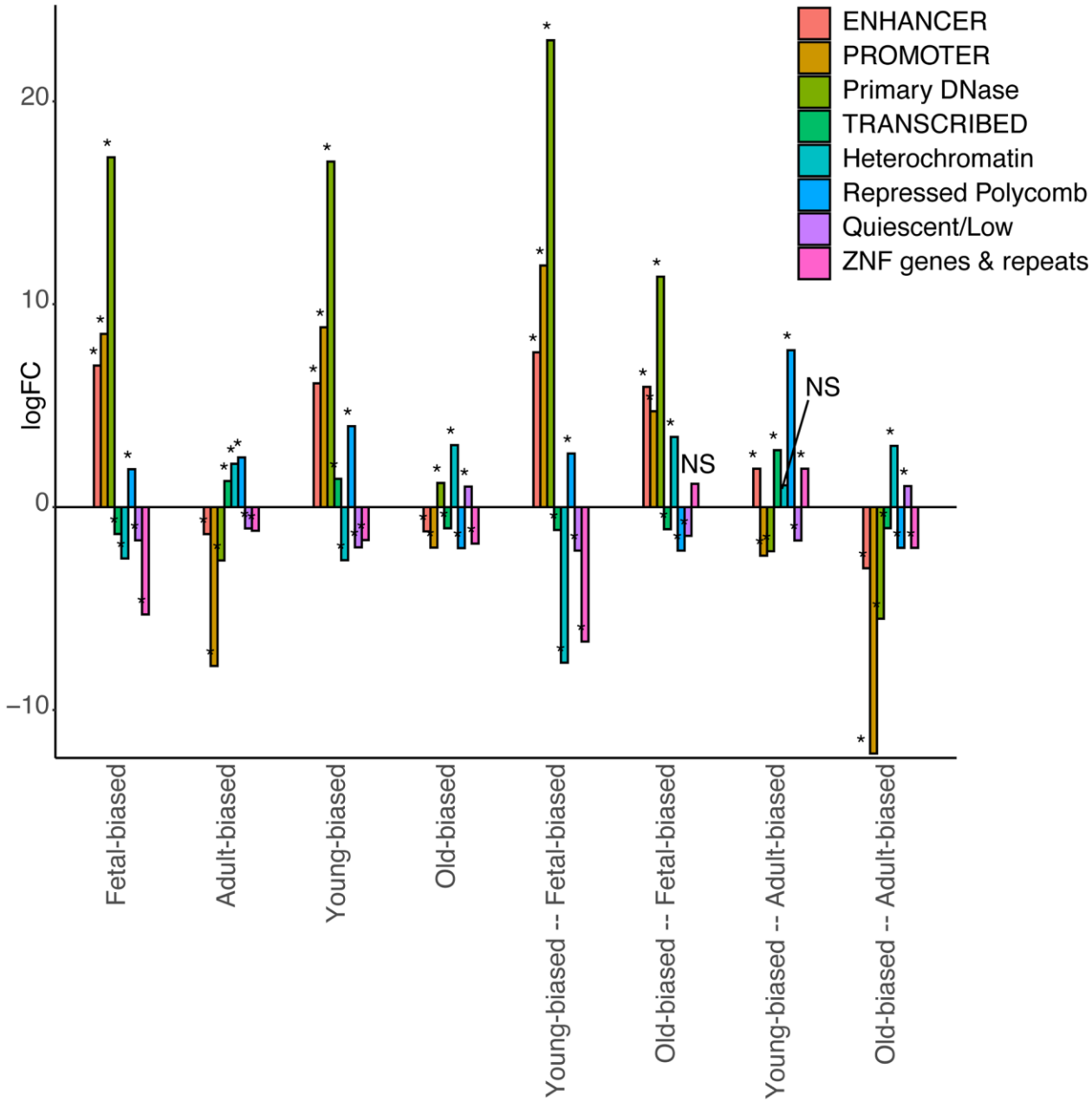

Supplementary Figure 4. Enrichment for epigenetic states. Bar plots indicate log10 logFC enrichment/depletion values for different region sets (e.g., young-biased regions) falling within different Roadmap HMM-annotated epigenetic states. Asterisk (*) indicates significant hypergeometric test for enrichment/depletion of an indicated region set for indicated epigenetic state ($p < 0.05$). Intersection sets (e.g., young-biased, fetal-biased intersected regions) are indicated with "—".

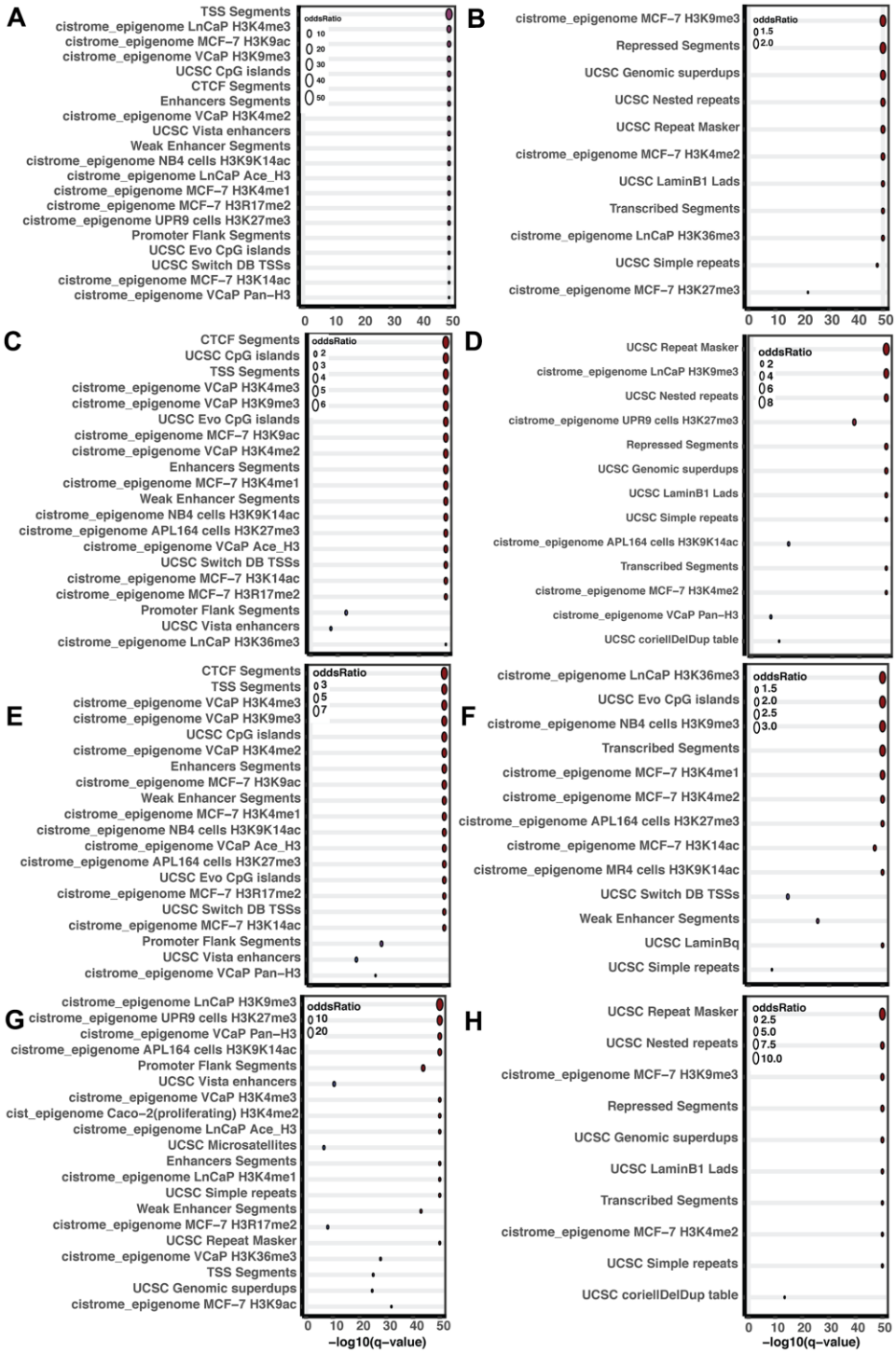

Supplementary Figure 5. LOLA enrichment plots. Enrichment q-values for top terms in the LOLA regional-enrichment analyses. (**A**) Fetal-biased Regions (**B**) Adult-biased Regions (**C**) Young-biased Regions (**D**) Old-biased Regions (**E**) Young-biased – Fetal-biased Regions (**F**) Young-biased– Adult-biased Regions (**G**) Old-biased – Fetal-biased Regions (**H**) Old-biased – Adult-biased Regions. All listed terms are significant, q-value < 0.05. See also Supplementary Table 2.

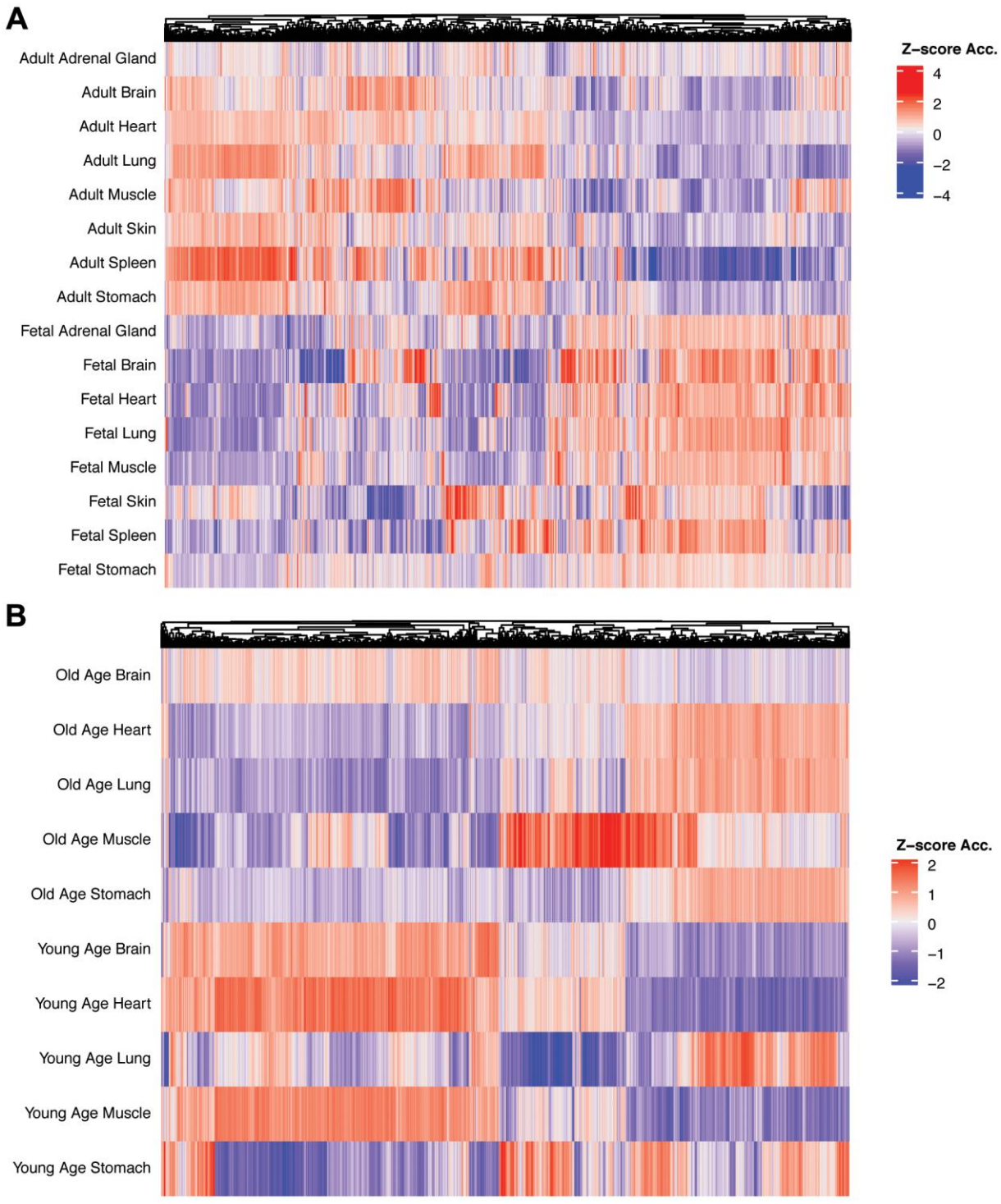

Supplementary Figure 6. Promoter accessibility heatmaps. Red-blue colour scale indicates increased/decreased accessibility, z-score normalized per-column. (**A**) Promoter accessibility differences between fetal and adult tissue samples, for significantly-altered promoters (adj. p-val < 0.05). (**B**) Promoter accessibility differences between young-age and old-age adult tissue samples, for significantly-altered promoters (adj. p-val < 0.05).

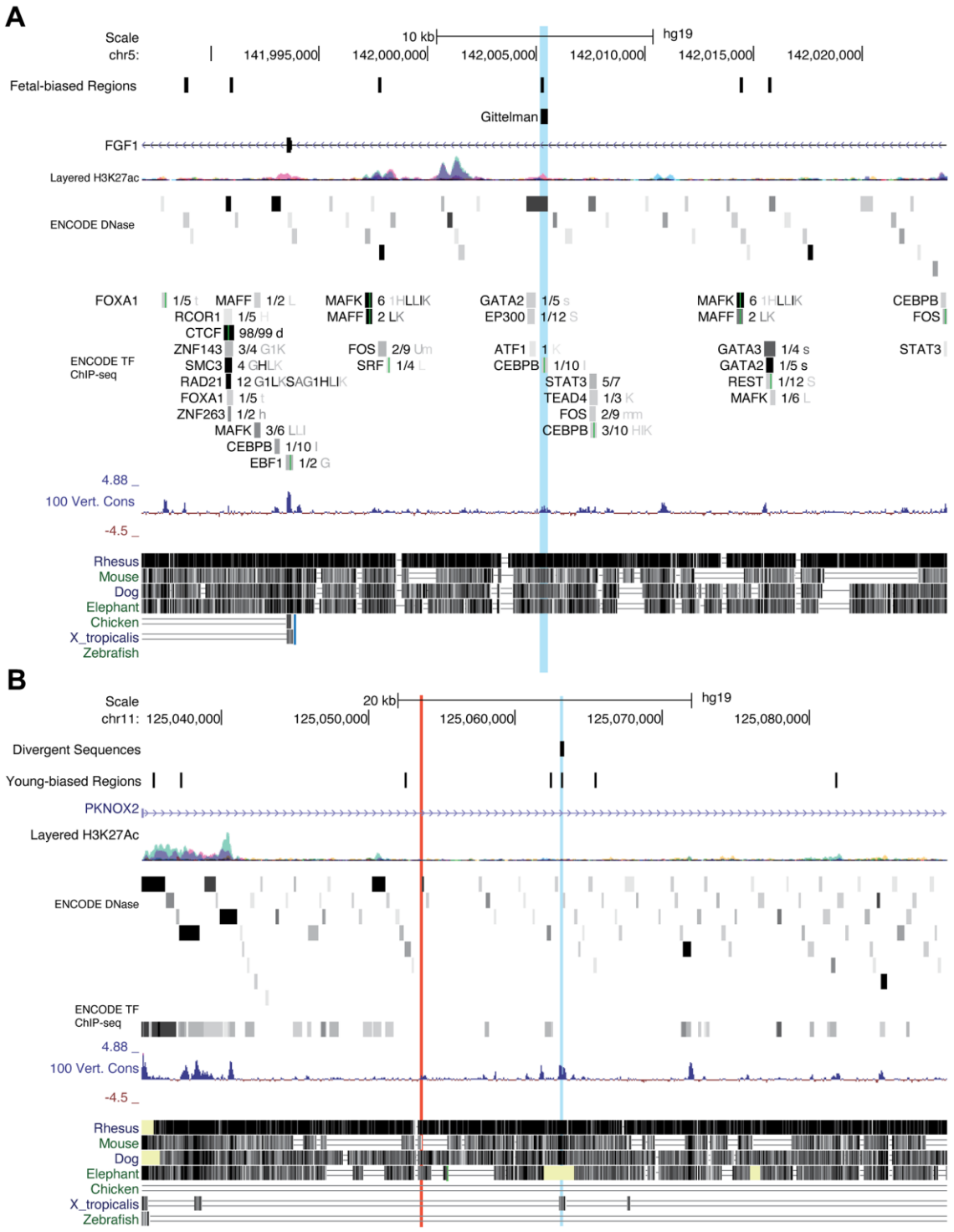

Supplementary Figure 7. UCSC genome screenshots for two representative human divergent-sequence loci. Additional tracks (top to bottom): Layered H3K27ac signal from ENCODE datasets, layered DNase-I hypersensitivity sites from ENCODE datasets, aggregated ENCODE transcription-factor ChIP-seq data, phyloP100ways conservation track (per-bp), multiple-sequence alignment to human reference sequence. (**A**) A human-accelerated region [20] (top track – highlighted in light blue) intersects a region losing accessibility in adult tissue (bottom track) intronic to the *FGF1 gene* (and which also has promoter-capture data to suggest promoter contact). Also intersects a possible CEBPB binding site (ENCODE TF-ChIP-seq track). (**B**) A human-accelerated region [20] (top track - highlighted in light blue) intersects a region losing accessibility in old-age adult tissue (bottom track) intronic to the *PKNOX2 gene* (and which also has promoter-capture data to suggest promoter contact). Upstream of this region lies the variant rs590211(highlighted in red), which has been associated with human-longevity via GWAS studies [25, 26].

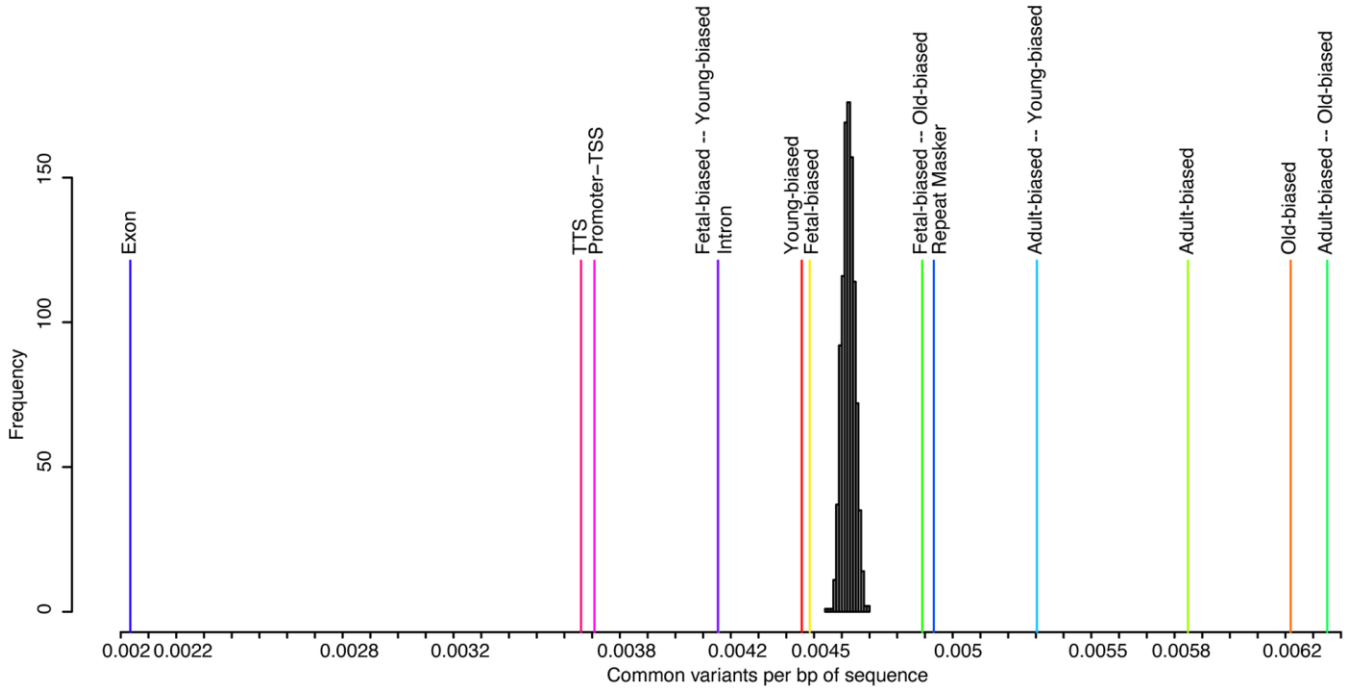

Supplementary Figure 8. Chimpanzee genomic distribution plot. Counts of chimpanzee common variants per bp of sequence for region sets were compared to random region sets along with other genomic features; labels correspond to results in Supplementary Table 3.

Supplementary Tables

Please browse Full Text version to see the data of Supplementary Tables 1–4.

Supplementary Table 1. Region set characterization.

Supplementary Table 2. Regulatory gene associations and expression data.

Supplementary Table 3. Evolutionary sequence analyses.

Supplementary Table 4. Disease associations.